

LIBRARY COPY 2
(XEROX PAPER)

**A STUDY OF A GENERAL 1-D
TWO-FLUID CRITICAL FLOW MODEL**

A STUDY OF A GENERAL ONE DIMENSIONAL TWO-FLUID CRITICAL FLOW
MODEL

CARL F. SCHWELLNUS

B.A.Sc. University of Toronto, Toronto

A Thesis submitted to the School of Graduate Studies in
partial fulfillment of the requirements for the degree of:

MASTER OF ENGINEERING

McMASTER UNIVERSITY

Copyright Carl F. Schwellnus November 1988

McMASTER UNIVERSITY LIBRARY

MASTER OF ENGINEERING (1988)
(Mechanical)

McMASTER UNIVERSITY
Hamilton, Ontario

TITLE: A Study of a General One-Dimensional
Two-Fluid Critical Flow Model

AUTHOR: Carl Schwellnus, B.A.Sc. (University of
Toronto)

SUPERVISOR: Dr. M. Shoukri

NUMBER OF PAGES: (xiii) 128

ABSTRACT

Accurate modelling of critical two-phase flow is important for the simulation of Loss-of-Coolant-Accidents in the nuclear industry and for the sizing of emergency relief valve systems in the chemical industry. A large body of experimental and theoretical work including the development of many models has been done over the last twenty-five years but as yet there is no one model which can accurately predict flow over a wide range of conditions which has found general acceptance. The purpose of this work is to examine the existing models, and using a general one-dimensional two-fluid model, investigate the various possible forms of the terms and their effects on the predicted results.

The resulting computer model has six conservation equations plus a seventh for bubble growth in bubble flow. It allows for hydrodynamic as well as thermodynamic non-equilibrium and considers three flow regimes; bubble flow, churn flow, and annular flow. The model has improvements in the equations, interfacial terms, and interfacial constitutive relations.

The best forms of the equations with some new developments were then used to predict the experimental results from several tests with a variety of inlet conditions and experimental setups. The range of conditions tested were inlet stagnation pressures of .2 to 6.6 MPa slightly subcooled or saturated, with diameters from .00125 to .0127 m. and lengths from .001 to 3.6 m. The length to diameter ratios varied from .8 to 287. Comparison against

pressure profiles shows good agreement and with one exception, the predicted mass fluxes are within -9 to +13 % of the experimental values.

ACKNOWLEDGEMENTS

The author would like to thank Dr. Mamdouh Shoukri for his guidance, suggestions and support during this investigation. The constructive discussions with John Balyck, Dave Johnson, Greg Nurnberg and Amad Abdul-Razzak are gratefully acknowledged and the assistance and information provided by Dr. W. Garland, Dr. B. Donevski and Dr. R. Judd are also gratefully appreciated.

TABLE OF CONTENTS

LIST OF FIGURES	viii
LIST OF TABLES	x
NOMENCLATURE	xi
CHAPTER 1 INTRODUCTION	1
CHAPTER 2 LITERATURE REVIEW OF CRITICAL FLOW MODELS	3
2.1 SINGLE PHASE FLOW	3
2.2 TWO-PHASE FLOW	4
2.2.1 Homogeneous Equilibrium Model	5
2.2.2 Equilibrium Non-Homogeneous Flow Models	6
2.2.3 Thermal Non-Equilibrium Models	9
2.2.4 Multi-Equation Models	11
2.3 TWO-FLUID MODELS	14
CHAPTER 3 TWO-FLUID MODELLING	15
3.1 LOCAL INSTANTANEOUS EQUATIONS	15
3.2 AVERAGING	16
3.3 CONSTITUTIVE RELATIONS	21
3.3.1 Pressure Drop	22
3.3.2 Interfacial Terms	22
CHAPTER 4 A GENERAL TWO-FLUID MODEL FOR CRITICAL FLOW IN PIPES	26
4.1 MODEL EQUATIONS AND ASSUMPTIONS	26
4.1.1 Assumptions	26
4.1.2 Model Equations	26
4.1.3 Interfacial Momentum Transfer	30
4.1.4 Other Constitutive Relationships	30
4.2 SUBCOOLED FLOW	31
4.3 METHOD OF SOLUTION	32
4.4 CHOKING LOCATION	34
4.5 CRITICAL CONDITIONS	34
4.6 SOLUTION ALGORITHM	35
4.7 TOLERANCE	39
4.8 THERMODYNAMIC PROPERTY CORRELATIONS	40
4.9 TRANSITIONS	40
4.10 CAPABILITY	41
4.11 PROGRAM FLOW CHART	43

CHAPTER 5	RESULTS AND DISCUSSION	44
5.1	EFFECT OF MODEL EQUATIONS AND PARAMETERS	44
5.1.1	Correlations and Equation Forms Tested	44
5.1.2	Stability	46
5.1.2.1	Gradient of Liquid Density	46
5.1.2.2	Virtual Mass	47
5.1.3	Vapour Energy Equation	50
5.1.4	Bubble Diameter Equation	56
5.1.5	Momentum Interfacial Transfer	58
5.1.6	Interfacial Parameters	60
5.1.6.1	Interfacial Area	60
5.1.6.2	Interfacial Drag Force	63
5.1.6.3	Interfacial Heat Transfer	66
5.1.7	Effect of η in Momentum Transfer	71
5.1.8	Effect of Initial Bubble Diameter	72
5.1.9	Effect of Initial Bubble Density	73
5.1.10	Summary of Comparisons	75
5.2	COMPARISON WITH EXPERIMENTAL DATA	80
5.2.1	Al Sahan Data	81
5.2.2	Dobran Data	94
5.2.3	Richter Test Case	101
5.2.4	Celata et al Orifice Data	103
5.2.5	Mass Flux Data	106
CHAPTER 6	CONCLUSIONS	109
CHAPTER 7	FUTURE WORK	110
CHAPTER 8	BIBLIOGRAPHY	111
APPENDIX A	DEVELOPMENT STAGES	119
APPENDIX B	TEST SECTION GEOMETRY	123
B.1	AL SAHAN PIPE GEOMETRY	123
B.2	DOBRAN PIPE GEOMETRY	124
B.3	RICHTER TEST CASE GEOMETRY	126
B.4	CELATA EXPERIMENTAL ORIFICE GEOMETRY	127

List of Figures

Fig. 2.1: Predictions of Slip Flow Models For Initially Saturated Water:	8
Fig. 4.1: Program Flow Chart:	43
Fig. 5.1: Effects of the Virtual Mass Term in Different Flow Regimes:	50
Fig. 5.2: Comparison of Two Vapour Energy Equations: Pressure	52
Fig. 5.3: Effect of Terms in the Bubble Diameter Equation:	57
Fig. 5.4: Diagram of Interfacial Momentum Conditions:	58
Fig. 5.5: Effect of Interfacial Momentum Term:	60
Fig. 5.6: Comparison of Linear and Exponential Interpolation:	62
Fig. 5.7: Interfacial Area: Different Interpolation Schemes:	63
Fig. 5.8: Interpolation of Cfi: Comparison of Ffg:	65
Fig. 5.9: Interfacial Heat Transfer Coefficient with Recovery at Annular Flow	68
Fig. 5.10: Comparison of Interpolation of Heat Transfer Coefficient:	70
Fig. 5.11: Comparison of Interfacial Heat Transfer Coefficient:	71
Fig. 5.12: Effect of Momentum Sink Proportion:	72
Fig. 5.13: Effect of Initial Bubble Diameter:	73
Fig. 5.14: Effect of Initial Bubble Number Density:	74
Fig. 5.15: Al-Sahan Simulation .196 MPa:	83
Fig. 5.16: Al-Sahan Data Simulations .300 MPa: Pressure:	85
Fig. 5.17: Al-Sahan Data Simulations .479 MPa: Pressure:	87
Fig. 5.18: Al-Sahan Data Simulations .703 MPa: Pressure:	89
Fig. 5.19: Al-Sahan Data Simulations 1.000 MPa: Pressure:	91
Fig. 5.20: Comparison of Predicted Void Fractions:	94
Fig. 5.21: Dobran Simulation 2.23 MPa: Pressure:	95
Fig. 5.22: Dobran Simulation 2.58 MPa: Pressure:	97
Fig. 5.22: Dobran Simulation 3.49 MPa: Pressure:	99
Fig. 5.24: Richter Simulation 6.63 MPa: Pressure:	101
Fig. 5.25: Celata Orifice Simulation .950 MPa: Pressure:	104
Fig. 5.26: Comparison of Experimental Data:	107
Fig. A.1: Comparison of Errors in Simple Model Calculations:	120
Fig. B.1: Al-Sahan Test Section Geometry:	124
Fig. B.2: Dobran Test Section Geometry:	126

Fig. B.3: Richter Test Section Geometry:	127
Fig. B.4: Celata Test Section Geometry:	128

List of Tables

Table 3.1: Definition of Conservation Quantities:	16
Table 4.1: Chart of the Effect of Tolerance Size:	39
Table 5.1: Chart of Parameter Changes to Be Tried:	45
Table 5.2: Comparison of Models:	76
Table 5.3: Chart of Experimental Data Used:	81
Table 5.4: Chart of Mass Flux Data:	106
Table B.1: Al-Sahan Test Mass Flux Data:	124
Table B.2: Dobran Test Mass Flux Data:	125

NOMENCLATURE

<u>VARIABLE</u>	<u>REPRESENTS</u>	<u>UNITS</u>
a_i	-interfacial area	m^2/m^3
A	-cross sectional area	m^2
c	-speed of sound	m/s
C_D	-drag coefficient	
C_{fi}	-interfacial drag coefficient	
C_p	-spec. heat at const. press.	J/kgK
C_{vm}	-coeff. of virtual mass	
d	-bubble diameter	m
D	-diameter of pipe	m
e_k	-specific energy	J/kg
F_D	-drag force	N/m^3
F_{LG}	-interfacial force	N/m^3
F_{Wk}	-force from wall to phase k	N/m^3
g	-gravitational acceleration	m/s^2
G	-mass flux	kg/sm^2
h	-specific enthalpy	J/kg
\bar{h}	-heat transfer coefficient	W/m^2K
k	-slip	
k_t	-thermal conductivity	W/mK
L	-length of pipe	m
m	-mass transfer rate per unit vol.	kg/sm^3
M	-mass	kg
M_k	-interfacial momentum	kgm/s
\bar{n}	-normal vector	
N	-non-equilibrium parameter	
N	-bubble density	$1/m^3$
Nu	-Nusselt number	
P	-pressure	Pa
Pr	-Prandtl number	

<u>VARIABLE</u>	<u>REPRESENTS</u>	<u>UNITS</u>
q	-heat generation rate per unit vol.	W/m ³
Re	-Reynolds number	
s	-specific entropy	J/kgK
t	-time	s
T	-temperature	K
\bar{u}	-velocity vector	m/s
u	-velocity	m/s
v	-specific volume	m ³ /kg
W	-mass flow rate	kg/s
x	-quality	
z	-distance along pipe axis	m

<u>VARIABLE</u>	<u>REPRESENTS</u>	<u>UNITS</u>
α	-void fraction	
γ	-isentropic exponent	
Γ	-vapour generation rate	kg/sm ³
η	-exit pressure ratio	
η	-coefficient for interfacial momentum sink proportion	
θ	-angle of inclination	deg.
λ	-eigenvalue	
μ	-dynamic viscosity	Ns/m ²
ϕ	-Martinelli-Nelson parameter	
ρ	-density	kg/m ³
σ	-surface tension	N/m
$\bar{\tau}$	-viscous stress tensor	N/m ²

SUBSCRIPT**REPRESENTS**

b	-bubble
c	-critical
CR	-critical
e	-exit
eq	-equilibrium
fi	-interfacial friction factor
G	-gas phase
HEM	-Homogeneous Equilibrium Model
i	-interfacial
k	-k th phase
L	-liquid phase
max	-maximum
min	-minimum
o	-stagnation
p	-constant pressure
s	-constant entropy
sat	-saturation
thr	-throat
vm	-virtual mass
W	-wall
z	-exit plane

CHAPTER 1
INTRODUCTION

Critical flow or choked flow is a fluid mechanical maximum on the flow rate in pipes and nozzles for a given upstream or starting pressure. As one decreases the downstream or exit pressure, the flow rate will increase to a certain point and then remain constant no matter how much the downstream pressure is reduced. This maximum is the critical mass flow rate occurring when the flow is "choked". In the nuclear industry, the prediction of coolant loss rate during simulated Loss Of Coolant Accidents (LOCA's) is important. Since the coolant is undergoing a depressurization, flashing takes place and the flow is generally two phase choked flow. For design of Emergency Cooling Injection systems and prediction of core behavior, estimation of the coolant critical flow rate must be accurate. In the chemical industry, the safety relief systems on chemical reactors must be designed so that in the event of a runaway reaction, the emergency venting system can relieve the pressure safely. Sizing of these systems is again dependent upon the expected critical flow rate through the piping.

In the single phase case, the fluid flow rate is limited by the fluid velocity. The speed of the rarefaction wave that is carrying the downstream pressure "information" travelling upstream against the flow is the speed of sound. If the fluid velocity is the same or higher, then the "information" will no longer be passed upstream and the flow will be choked. Critical flow rate is therefore calculated using the speed of sound in the fluid.

In two phase or multi-phase flow, the situation is not that simple. Because of different flow regimes and phase

velocities, temperatures, and distributions, there is no similar effective analogy to the speed of sound in multi-phase cases. Theoretical and experimental studies of two phase critical flow have been done from the late nineteen fifties and early nineteen sixties to the present. As of this point, there seems to be no one model which is generally accepted for all conditions.

The purpose of this thesis is to briefly describe the progress in two phase flow modelling up to the present time and then, using a general two fluid model with six conservation equations, investigate the various forms of the terms in the equations and the effect of these terms on the calculated results. The end result is not intended to be a new model but rather a combination of the best methods of several models and new developments.

CHAPTER 2

LITERATURE REVIEW OF CRITICAL FLOW MODELS

A survey of the literature in the subject of choked flow models indicates that, at the present time, there isn't an accepted, universally applicable model for critical flow prediction with the necessary accuracy. Since there have been many reviews of critical flow models over the years; for example Saha (1978), Isbin (1980), Wallis (1980), and Abdollahian et al. (1982), it is not necessary nor is it within the scope of this project to conduct a full review of choked flow models and experiments. The intention is to give a quick background into the development of major models and those with relevance to this work.

2.1 SINGLE PHASE FLOW:

In single phase flow, the theory is quite well documented in almost any Fluid Mechanics text, e.g. Streeter and Wylie (1979). For isentropic flow through a varying cross section, the energy equation is:

$$dh = -d\left(\frac{du^2}{2}\right) \quad (2.1)$$

The isentropic flow condition is:

$$T dS = 0 = dh - \frac{dP}{\rho} \quad (2.2)$$

which implies that:

$$dh = \left(\frac{dP}{\rho}\right)_s \quad (2.3)$$

The continuity equation is:

$$\frac{d\rho}{\rho} + \frac{dA}{A} + \frac{du}{u} = 0 \quad (2.4)$$

The mass flux G is defined as:

$$G = u\rho \quad (2.5)$$

Combining (2.1), (2.2), (2.3), (2.4), and (2.5):

$$\frac{dG}{G} = \rho dP \left[\frac{1}{G^2} - \frac{1}{\rho^2} \left(\frac{\partial \rho}{\partial P} \right)_s \right] \quad (2.6)$$

The maximum flow rate occurs when the mass flux is independent of pressure, i.e. when:

$$\frac{\partial G}{\partial P} = 0 \quad (2.7)$$

which implies that:

$$G_{\max} = \rho \sqrt{\left(\frac{\partial P}{\partial \rho} \right)_s} \quad (2.8)$$

The velocity of sound with which pressure waves travel through the fluid is given by:

$$c = \sqrt{\left(\frac{\partial P}{\partial \rho} \right)_s} \quad (2.9)$$

Equation (2.8) and (2.9) show clearly that the speed of sound is the limiting or maximum velocity corresponding to the choked flow condition.

2.2 TWO PHASE FLOW:

As mentioned earlier, the concept of the speed of sound in two phase flow is not as clearly understood as in single phase. The assumptions in the single phase theory are that the flow is homogeneous and isentropic, neither of which is necessarily true in two-phase flow. Therefore, different critical flow conditions were developed.

In two phase flow there are two cases. The simpler of the two is two component flow mixture with no vapour generation such as air-water flows. A more complex case is one component mixtures such as steam-water flows. This thesis will concentrate on the latter.

2.2.1 HOMOGENEOUS EQUILIBRIUM MODEL:

The first important model was the Homogeneous Equilibrium Model (HEM) (Saha (1978), Hsu (1976), Wallis (1969)). Assumptions for the model are:

- flow is adiabatic and frictionless
- there is no heat transfer between phases
- liquid and vapour velocities are equal
- the flow is in thermal equilibrium at saturation conditions
- the mixture is homogeneous

Applying the energy and continuity equations and assuming incompressible liquid, the mass flux is given by:

$$G = \sqrt{\frac{2g(h_0 - (1-x)h_L - xh_C)}{(1-x)v_L + xv_C}} \quad (2.10)$$

where h_0 is the stagnation enthalpy and x is the exit quality. The critical mass flux is found by decreasing the exit pressure, calculating the exit conditions based on the isentropic flow assumption and calculating the mass flux using equation (2.10) until a maximum is reached.

As with most of the simple models, an equation can be derived in terms of the properties at the exit location of choking, but, since in almost all instances these conditions will not be known, these forms will not be listed here. The comparison with experimental data as shown by Saha (1978) and Wallis (1980) shows that the HEM gives relatively good results for long pipes where sufficient length is available to reach thermal equilibrium and when the flow regimes have almost equal phase velocities. However, the HEM underpredicts the critical discharge by up to a factor

of ten when the flow is not in thermal equilibrium. This usually occurs in short tubes where the fluid mixture does not have time to come to equilibrium.

2.2.2 EQUILIBRIUM NON-HOMOGENEOUS FLOW MODELS:

Because the HEM seriously underpredicted the mass fluxes in some cases, researchers tried to improve accuracy by including the ratio of the motion between phases, i.e. slip ratio k in the equations. Most were based on a general derivation of the critical mass flux equation with further conditions imposed in order to determine the slip at the exit. The general equation as given by Hsu (1976) is:

$$G_c^2 = -\frac{\partial}{\partial P_0} \left[\frac{[k(1-x)v_L + xv_G][xk + 1 - x]}{k} \right]_z^{-1} \quad (2.11)$$

The above equation can be derived from the mixture momentum equation allowing different phase velocities and by imposing the critical discharge criterion of equation (2.7). If an expression for the slip ratio k for critical flow can be determined, it is possible to calculate the critical mass flux.

One of the first conditions for slip was by Fauske (1961) and (1962) in which he basically defines a momentum-weighted specific volume using the momentum equation:

$$v_{mom} = \frac{[k(1-x)v_L + xv_G][xk + 1 - x]}{k} \quad (2.12)$$

It was argued that critical discharge corresponds to:

$$\frac{\partial v_{mom}}{\partial k} = 0 \Rightarrow k = \sqrt{\frac{v_G}{v_L}} \quad (2.16)$$

Moody (1965) and (1966) developed a different idea by using the continuity and energy equations to determine an equation for the mass fluxes in terms of the enthalpy, entropy, slip ratio and pressure. Both the derivatives of mass flux with respect to pressure and slip were set to zero and the result was a maximum flow rate corresponding to the slip ratio:

$$k = \left(\frac{v_G}{v_L} \right)^{1/3} \quad (2.14)$$

Fauske's model predicts higher flow rates than the HEM and agrees well with some data. Moody's model predicted similar results but underpredicted the experimental results for qualities between .5 and 1 and overpredicted for qualities between .01 and .5.

Levy (1965) used two momentum equations and the mixture continuity to derive an expression between quality and void fraction and used the derivative of mass flux with respect to momentum specific volume as defined by Fauske. An approximation for the critical slip was given by:

$$k = \sqrt{\frac{v_G}{v_L} 2\alpha} \quad (2.15)$$

There was not much improvement in the comparisons with experimental data.

Work done by Wallis (1980) demonstrates the difference between the three methods as shown in Fig. (2.1).

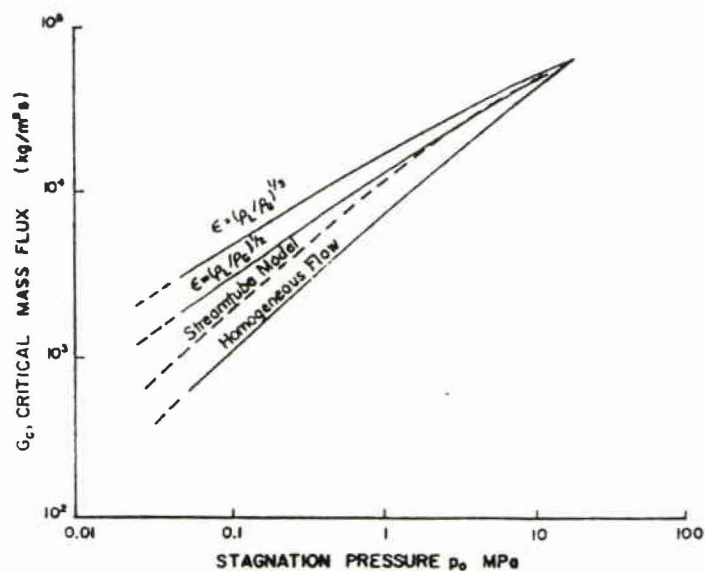


Fig. 2.1 Prediction of Slip Flow Models For Initially Saturated Water:

Measurements near the exit section have shown that the actual slip is lower than those predicted by the above equations. This suggests that overestimating k tends to counter balance the neglected effect of thermal non-equilibrium.

The Homogeneous Frozen Model, Saha (1978) and Wallis (1980), was another attempt at a slightly non-equilibrium model. The assumptions were:

- the average velocities of the two phases are equal
- there is no heat and mass transfer between phases
- the vapour expands isentropically as an ideal gas
- the critical flow is defined by the gas
- the quality is constant along the tube

The result is obtained by integrating the Bernoulli equation which leads to an expression for the critical pressure ratio:

$$\frac{P}{P_o} = \eta = \left[\frac{2}{\gamma + 1} \right]^{\frac{\gamma}{\gamma - 1}} \quad (2.16)$$

This gives the critical flow rate as:

$$G = \frac{x}{x_o v_{c_o} \eta^{-1/\gamma} + (1 - x_o) v_{L_o}} \sqrt{2g x_o v_{c_o} P_o \frac{\gamma}{\gamma - 1} \left[1 - \eta^{\frac{\gamma - 1}{\gamma}} \right]} \quad (2.17)$$

This model is not generally used as the results are not even as good as the HEM.

2.2.3 THERMAL NON-EQUILIBRIUM MODELS:

The next group of models attempted to quantify the deviation from thermal equilibrium in an empirical fashion. Three papers by Henry and Henry and Fauske et al. (1970a), (1970b) and (1971) started by defining an empirical parameter N representing the deviation of the exit quality from the equilibrium exit value. The non-equilibrium parameter N is defined as:

$$N = \frac{x}{k x_{eq}} \quad (2.18)$$

Since in general, x is less than x_{eq} and k is equal to or larger than one, the value of N is expected to be less than or equal to unity. $N=1$ will therefore correspond to homogeneous equilibrium flow. Henry (1970a) calculated the value of N using available data as:

$$N = 20 x_{aq}, 0 < x_{aq} < .05$$

$$= 1, x_{aq} \geq .05 \quad (2.19)$$

The first paper by Henry et al. (1970a) describes an equation for pipes:

$$G_{CR} = \frac{G_{HEM}}{\sqrt{N}} \quad (2.20)$$

where G_{HEM} is the HEM calculated mass flux. Henry et al. (1970(b)) also investigated the effect of length to diameter ratio L/D . For long pipes, two different entrance effects were taken into account. Pipes with sharp entrances had been observed to have flow separation for a distance of up to twelve diameters. Therefore two equations were developed to describe the effect of L/D on the equilibrium quality:

$$x_{thr} = N x_{aq} \left[1 - \exp \left(-B \left(\frac{L}{D} - 12 \right) \right) \right] \quad (2.24)$$

where B was experimentally determined to be .0253. The second entrance effect equation for smooth entrance regions had no initial twelve diameter term. Two expressions for critical mass flux and critical pressure ratio were derived:

$$G_c^2 = \frac{1}{\left[x_{thr} \frac{v_G}{P} - (v_G - v_{Lo}) N \frac{dx_{eq}}{dP} \right]_0} \quad (2.25)$$

$$\frac{P_c}{P_0} = \eta = 1 - \frac{G_c^2}{P_0} \left[\frac{v_{Lo}}{2C^2} + x_{aq} (v_G - v_{Lo}) \right] \quad (2.26)$$

where:

$$\frac{dx_{aq}}{dP} = \frac{(1-x) \frac{ds_L}{dP} + x \frac{ds_C}{dP}}{s_L - s_C} \quad (2.27)$$

Iterative improvement of an initial guess is used to solve simultaneously for mass flux and pressure ratio. For nozzles, orifices, and short tubes, the equations derived in a third paper, Henry et al. (1971) are similar but use different values for N that are corrected from data on nozzles etc. These equations are slightly more complicated numerically including polytropic expansion of the vapour, but have the same iterative improvement solution method. The third paper by Henry et al. (1971) also has modified solution forms for initially subcooled or saturated cases.

With the experimentally derived parameters and slightly more involved theory, the so-called Henry-Fauske models appear to be the most successful of the lumped models to date and are widely used.

2.2.4 MULTI-EQUATION MODELS:

The next group of models incorporates solutions to the conservation equations and usually attempts to consider either thermodynamic or hydrodynamic non-equilibrium or both. The complexity of the models ranges from three steady state mixture conservation equations of mass, momentum and energy to the models involving separate conservation equations for each phase for transient problems in two or three dimensions. In general, they are composed of experimentally derived correlations to some degree.

Development has been in many areas but mainly on the topics of initial nucleation, vapour generation, bubble growth, and mathematical solution methods. Edwards (1968) was among the first to work on bubble nucleation and growth as related to critical discharge. The major assumptions were:

- homogeneous flow
- vapour phase at saturation
- all bubble nuclei formed simultaneously with an arbitrary time delay for superheating
- for sharp edged orifices, flow separation and expansion takes place at constant pressure.

The Plesset and Zwick (1954) bubble growth correlations for conduction controlled heat transfer were used. Two arbitrary constants are used:

- a time delay for bubble nucleation
- the number of bubble nuclei per unit mass

A set of three mixture conservation equations was then formulated based on these assumptions and solved. The results compare well with data, however, a pressure correction was required for short tubes. The model showed promise for more advanced models.

Another effect that was shown to be important by Malnes (1975) was the amount of dissolved gases in the liquid. They are expected to provide other bubble nucleation sites. To agree with different experimental results, it was necessary to use widely varied values for the quantity of dissolved gases which indicates that the gases are not the only nucleation sites. Experimental studies since then have shown that the bubble nucleation takes place at the walls and not in the bulk of the fluid. This agrees with nucleate boiling theory.

A number of researchers worked on the development of models for vapour generation rate during depressurization. These models focused on different aspects of bubble nucleation theory and convective effects. Among these investigations are Rohatgi and Reshotko (1975), Ardron and Ackerman (1978), Rivard and Torrey (1975), Wolfert, Mather, Kroeger (1976), Elias and Chambré (1984) and Jackson and Davidson (1983).

In general it has been shown that bubble growth is not just conductive but that convective heat transfer predominates for even a relatively small difference in the phase velocities. Bubble nucleation is generally assumed to be initially driven by the difference in pressure within the bubble caused by surface tension. Thermal heat transfer effects contribute to growth after initial nucleation. This conforms with nucleate boiling theory.

The delay of nucleation has been modeled as due to pressure difference of superheat, as a finite time delay and also as a superheated temperature difference. There is no general agreement as to the form of the initial bubble density and initial bubble radius or void fraction. This will be discussed further later. Vapour generation expressions have not been successfully determined yet for models other than two fluid models (three full conservation equations for each phase).

In view of the large number of models that have been developed, it is difficult to determine how many conservation equations should be used. Bouré (1975) demonstrated that the six conservation equations with

appropriate forms for the interface transfers can be used to derive many forms of mixture models. Wallis (1980) commented, however, that in order to reduce the number of equations, additional empirical correlations must be used. This reduces the accuracy of the model to that which is little better than the empirically based models. Because of this, it is felt that probably the best model would be the full two fluid model.

2.3 TWO-FLUID MODELS:

The most advanced class of models used to date in terms of interpretation of actual phenomena in choking are the two fluid models which take different flow regimes into account. The interfacial transfer terms vary greatly from one flow regime to another. Among these models are those by Richter (1981, 1983), Dobran (1987), and Al-Sahan (1988). These will be examined in depth at a later point.

CHAPTER 3
TWO FLUID MODELLING

3.1 LOCAL INSTANTANEOUS EQUATIONS:

The development of general two fluid equations has been done in several works i.e. Bergles et al. (1981). The local instantaneous equations in their most general form are derived from integral balances within a control volume containing the two phases separated by an interface for mass, momentum and total energy. Using Leibnitz Rule and Gauss Theorem, the equations can be transformed from integral form to the so-called local instantaneous phase equations provided that the variables and their first derivatives are continuous and that the equations are applied to local regions of only one phase, i.e. each field is subdivided into subregions each occupied by a single phase separated by moving boundaries. They can then be written as:

$$\frac{\partial}{\partial t}(\rho_k \Psi_k) + \nabla \cdot (\rho_k \Psi_k \vec{u}_k) + \nabla \cdot \vec{J}_k - \rho_k \phi_k = 0 \quad (3.1)$$

There are also interfacial balance conditions, characteristic of two phase flow, which describe the interfacial transfer of the mass, momentum and energy between phases. They are commonly known as the interfacial jump conditions:

$$\sum_{k=1,2} (\dot{m}_k \Psi_k + \vec{n}_k \cdot \vec{J}_k) = 0 \quad (3.2)$$

where the quantities $\Psi_k, \vec{J}_k, \phi_k$ are given in Table 3.1.

Table 3.1: Definition of Conservation Quantities:

<u>Balance</u>	ψ_k	\vec{J}_k	ϕ_k
Mass	1	0	0
Momentum	\vec{u}_k	$P_k \delta_{ij} - \vec{\tau}_k$	\vec{g}_k
Energy	$e_k + \frac{1}{2} u_k^2$	$\vec{q}_k - (P_k \delta_{ij} - \vec{\tau}_k) \cdot \vec{u}_k$	$\vec{g}_k \cdot \vec{u}_k$

3.2 AVERAGING:

Although the above equations represent an exact mathematical model, they cannot be solved except in very simple cases. In order to derive a solvable set of equations appropriate for two-phase flow applications, averaging procedures are used as shown by Ishii (1975) and Bannerjee and Chan (1980).

Different methods of averaging can be used. Most commonly, space and time averaging are utilized. It has been shown by Delhaye in Bergles (1981) and Ishii (1975) that double averaging is required to ensure the continuity of the variables and their first derivatives. The operations are commutative and can be done in either order.

The volume averaging procedure can be applied by integrating each term over a control volume with the averaged value of any variable defined by:

$$\langle f_k \rangle = \frac{1}{V_k} \int_{V_k} f dv \quad (3.3)$$

where v_k is the volume of phase k within the integration region. The volume averaged phase volumetric concentration is defined as:

$$\langle \alpha_k \rangle = \frac{v_k}{v} \quad (3.4)$$

Time averaging should not be confused with steady state. It can be compared to a high frequency filtering of a signal or averaging over a sample period. The time derivatives still apply but are considered over time intervals larger than one period. Time averaging is defined as:

$$\bar{f} = \frac{1}{T} \int_0^T f dt \quad (3.5)$$

The averaging reduces the complexity of the equations dramatically but there is a loss of information in the process. The averaging operation for one variable eliminates the variations of the quantity within the volume of averaging but for two multiplied variables additional assumptions must be made regarding the average of a product. Distribution coefficients can be added to characterize the difference between the average of the product and the product of the averages, i.e.:

$$C = \frac{\langle \rho_k u_k \rangle}{\langle \rho_k \rangle \langle u_k \rangle} \quad (3.6)$$

Because of the lack of information about distribution coefficients, they are normally assumed to be 1.0.

The general volume and time averaged equations are:

Conservation of Mass:

$$\frac{\partial}{\partial t} \overline{\alpha_k \langle \rho_k \rangle} + \nabla \cdot \overline{\alpha_k \langle \rho_k \vec{U}_k \rangle} = -\overline{\langle \dot{m}_k \rangle}_i \quad (3.7)$$

where \dot{m}_{ki} is the interfacial mass transfer rate per unit volume:

$$-\overline{\langle \dot{m}_k \rangle}_i = \overline{\rho_k (\vec{U}_i - \vec{U}_k) \cdot \vec{n}_k} \quad (3.8)$$

Conservation of Momentum:

$$\begin{aligned} & \frac{\partial}{\partial t} \overline{\alpha_k \langle \rho_k \vec{U}_k \rangle} + \nabla \cdot \overline{(\alpha_k \langle \rho_k \vec{U}_k \vec{U}_k \rangle)} + \nabla \alpha_k \overline{P_k} - \nabla \cdot \overline{\alpha_k \langle \vec{\tau}_k \rangle} \\ & = \overline{\alpha_k \langle \rho_k \vec{g} \rangle} - \overline{\langle \dot{m}_k \vec{U}_{ki} \rangle} + \overline{\langle \vec{n}_k \cdot \vec{\tau}_k \rangle}_i + \overline{\langle \vec{n}_k \cdot \vec{\tau}_k \rangle}_w \end{aligned} \quad (3.9)$$

Conservation of Energy:

$$\begin{aligned} & \frac{\partial}{\partial t} \overline{\alpha_k \left\langle \rho_k \left(h_k + \frac{\vec{U}_k \cdot \vec{U}_k}{2} \right) \right\rangle} + \nabla \cdot \overline{\alpha_k \left\langle \rho_k \vec{U}_k \cdot \left(h_k + \frac{\vec{U}_k \cdot \vec{U}_k}{2} \right) \right\rangle} \\ & - \alpha_k \frac{\partial}{\partial t} \overline{\langle P_k \rangle} + \nabla \cdot \overline{\alpha_k \langle \vec{q}_k \rangle} - \nabla \cdot \overline{\alpha_k \langle \vec{n}_k \cdot (\vec{\tau}_k \cdot \vec{U}_k) \rangle} \\ & = - \overline{\left\langle \left[\dot{m}_k \left(h_k + \frac{\vec{U}_k \cdot \vec{U}_k}{2} \right) + \vec{n}_k \cdot \vec{q}_k - \vec{n}_k \cdot \vec{U}_k \cdot \vec{\tau}_k \right] \right\rangle}_i - \overline{\langle \vec{n}_k \cdot \vec{q}_k \rangle}_w + \overline{\alpha_k \langle \rho_k \vec{u}_k \cdot \vec{g} \rangle} \end{aligned} \quad (3.10)$$

Interfacial Jump Conditions:

$$\sum_{k=1,2} \overline{\langle \dot{m} \rangle}_{ki} = 0 \quad (3.11)$$

$$\sum_{k=1,2} \overline{\langle \dot{m}_k \vec{U}_k - \vec{n}_k \cdot \vec{\sigma}_k \rangle} = 0 \quad (3.12)$$

$$\sum_{k=1,2} \overline{\left\langle \dot{m}_k \left(e_k + \frac{1}{2} \vec{U}_k \cdot \vec{U}_k \right) + \vec{n}_k \cdot (\vec{q}_k - \vec{\sigma}_k \cdot \vec{U}_k) \right\rangle} = 0 \quad (3.13)$$

These equations are transient and in three dimensions. In order to simplify the model it will be assumed that, for the purpose of calculating critical discharge, the variations in the properties such as phase volumetric fraction, velocity, and pressure are not significant across the cross section of the pipe or

conduit. This is not totally valid. As mentioned previously, two dimensional effects have been noted by several investigators. To reduce the number of parameters that must be characterized and the complexity of the solution, the model equations are one-dimensional.

A steady-state one-dimensional model can be derived from the above equations. The interphase transfer terms are characterized by terms representing vapour generation, and interfacial and wall drag forces. For example, in the Conservation of Mass equation, $\langle \dot{m}_k \rangle_i$ is the rate of mass transfer out of phase k per unit volume represented by the rate of vapour generation Γ . In the following equations: $\alpha_c = \alpha$ and $\alpha_l = (1 - \alpha)$. The revised steady-state averaged one-dimensional conservation equations are:

Conservation of Mass for the Liquid:

$$\frac{d}{dz} \overline{(1 - \alpha) \langle \rho_l u_l \rangle} = \overline{\langle \dot{m}_l \rangle} = -\Gamma \quad (3.14)$$

Conservation of Mass for the Gas:

$$\frac{d}{dz} \overline{\alpha \langle \rho_c u_c \rangle} = \overline{\langle \dot{m}_c \rangle} = \Gamma \quad (3.15)$$

In the one-dimensional phase momentum equation, it is assumed that the axial gradient of the axial component of the shear stress tensor is negligible. Also the interfacial viscous stress term is denoted by an interfacial force term F_{LG} and the wall shear stress term is denoted by a wall friction expression F_{Wk} . The momentum equations are:

Conservation of Momentum for the Liquid:

$$\frac{d}{dz} \overline{(1 - \alpha) \langle \rho_l u_l^2 \rangle} + (1 - \alpha) \frac{d}{dz} \overline{\langle P_l \rangle} = \overline{(1 - \alpha) \langle g_z \rho_l \rangle} - \overline{\langle \dot{m}_l u_l \rangle}_i + \overline{F_{LG}} - \overline{F_{WL}} \quad (3.16)$$

Conservation of Momentum for the Gas:

$$\frac{d}{dz} \overline{\alpha \langle \rho_c u_c^2 \rangle} + \alpha \frac{d}{dz} \langle P_c \rangle = \overline{\alpha \langle g_z \rho_c \rangle} - \langle \dot{m}_c u_c \rangle_i - \overline{F_{LC}} - \overline{F_{WC}} \quad (3.17)$$

Because the heat transfer conditions at the wall are not generally known and likely are small compared to the rates of transfer within the fluid, the wall is considered adiabatic. In the energy equation, as a result, the wall heat transfer is zero. Another assumption is that the viscous dissipation is negligible. The interfacial heat transfer term is denoted by a heat transfer rate per unit volume:

$$\langle q_k \rangle_i = Q_{LC}$$

Using these approximations and substitutions, the result is:

Conservation of Energy for the Liquid:

$$\frac{d}{dz} (1 - \alpha) \left\langle \rho_l u_l \left(h_l + \frac{u_l^2}{2} \right) \right\rangle = - \left\langle \left(\dot{m}_l \left(h_l + \frac{u_l^2}{2} \right) + Q_{LC} \right) \right\rangle_i + (1 - \alpha) \langle \rho_l u_l g_z \rangle \quad (3.18)$$

Conservation of Energy for the Gas:

$$\frac{d}{dz} \alpha \left\langle \rho_c u_c \left(h_c + \frac{u_c^2}{2} \right) \right\rangle = - \left\langle \left(W_c \left(h_c + \frac{u_c^2}{2} \right) + Q_{LC} \right) \right\rangle_i + \alpha \langle \rho_c u_c g_z \rangle \quad (3.19)$$

The interfacial jump conditions are used to relate the interfacial terms for each phase.

Interfacial Jump Conditions:

$$\langle \dot{m}_l \rangle_i = - \langle \dot{m}_c \rangle_i \quad (3.20)$$

$$\left[\langle P_l \rangle - \langle P_c \rangle \right] \frac{\partial \alpha}{\partial z} = \langle \dot{m}_l (u_l - u_c) - n_l \cdot (\tau_{Lz} - \tau_{Cz}) \rangle_i \quad (3.21)$$

$$\left\langle (q_L - q_C) - \dot{m}_L \left[\left(h_L + \frac{u_L^2}{2} \right) - \left(h_C + \frac{u_C^2}{2} \right) \right] \right\rangle_i = 0 \quad (3.22)$$

From this point, the averaged notation will not be used and all variables will be assumed to be time and space averaged.

3.3 CONSTITUTIVE RELATIONS:

In order to solve the six equations, it is obvious that expressions for some of the unknown variables must be found. The equation of state can be used to correlate the thermodynamic properties of the liquid and the gas. This aids in the reduction of the number of variables but, as will be shown later, there are necessary requirements for the range and accuracy of the correlations. The other expressions are known as constitutive relationships. They are generally empirically based correlations for quantities which can be measured from some simpler experiments. Relations for the following must be found:

- frictional pressure drop for both single and two phase conditions,
- interfacial area,
- interfacial force including constant velocity drag force and virtual mass force,
- interfacial heat transfer.

These constitutive relations have a very significant effect upon the final model's predictions, and therefore, careful selection or derivation of these terms is essential. A very much more intensive discussion of the choices will follow.

It is also important to note that the forms of the conservation equations can be considerably altered by addition of equations or by using balances at the interface instead of full conservation equations. In addition this derivation is for constant cross sectional area. The variable area and the change in area along the tube must be included especially in the conservation of mass equations. The final form of the expressions will take this into account.

3.3.1 Pressure Drop:

There are several correlations available for frictional pressure drop. Most take the form similar to that of the single phase Fanning or Moody friction factor equations such as McAdams or use modifiers for the entire single phase friction pressure drop such as Martinelli-Nelson. The most commonly used correlations appear to be curve fits for the friction factor using the Fanning or Moody expressions in single phase. In two phase, correlations for the ϕ_{lo}^2 Martinelli-Nelson parameter are based on curve fits of data or linear interpolation of a lookup table.

3.3.2 Interfacial Terms:

It has been demonstrated experimentally that fluid mixture passes through several different flow regimes before choking from bubbly flow to churn flow to annular flow to dispersed droplet flow. The interfacial terms of force and heat transfer are very strong functions of flow regime and, in one dimensional models, usually take the form of an area times a driving force. Since simple relations that would be useful for the whole range of flow regime transitions

do not exist, it is necessary to use individual correlations for each flow regime or approximations for them.

The interfacial area is the surface area of the interface usually per unit volume. In order to derive an interfacial area for bubble flow, correlations generally assume spherical bubbles and approximations for size and numbers. This can be modified for void fraction to estimate agglomeration and change of shape of the bubbles as they grow larger. For annular flow, the assumption is usually a gas core with a perfectly cylindrical interface with a liquid annulus. There are additional modifications that can take into account the ragged or wavy interface and dispersed droplets. It is important to note that increasing complexity beyond a certain point is useless if the rest of the terms in the equations are not as accurately portrayed. For churn flow no correlation has yet been found for interfacial area nor interfacial heat transfer. They are calculated from interpolation between the two "known" states of bubble and annular flow. There is one correlation for interfacial drag force by Ishii (1979). It has been used but has limitations which will be discussed later. The interfacial heat transfer in the first separated critical flow models assumed only conductive heat transfer. It was shown that convective heat transfer was the dominant mode. Because of this the general form of the heat transfer term is:

$$q_i = h_i \alpha_i (T_L - T_C) + \Gamma (h_C - h_L) \quad (3.24)$$

where h_i is the convective heat transfer coefficient which is a function of the velocity differences between

the two phases and the fluid properties. Again correlations for bubble spheres and for the assumed cylindrical annular interface are used.

The interfacial force represents the force applied from one phase to another across the interface due to the relative motion of the two phases. Ideally it should be possible to describe this term using one expression, however, no such expression exists since it would have to take into account relative velocity and relative acceleration between the fluids. Initially the force was modeled as a steady state drag force but, due to instabilities in the flow calculations, another term referred to as the virtual mass term was added. In the beginning, it was assumed that it was necessary for stable calculations but did not represent any physical phenomenon. Further work has shown clearly since then that it does indeed simulate the virtual force caused by relative acceleration. The terms' form has changed considerably due to mathematical and experimental analysis from a relatively simple difference in accelerations to the mathematically "objective" form derived by Drew et al. (1979). The coefficients of the expression vary with the geometry of the interface. The applicability of the virtual mass term to all flow regimes is also in question. Although there are much larger relative accelerations in churn and annular flow, the changing interface geometry appears to limit the magnitude of the term for those flow regimes. The virtual mass term and its effects will be discussed later.

Extensive comparison will be made between the models by Richter (1981) and (1983), Dobran (1987) and Al-Sahan (1988) and the general model developed here because they appear to be the only one dimensional steady state models yet found with the exception of the large scale codes developed by the public utilities such as TRAC etc. These models differ from the general form in the constitutive relations used and in the form of the equations used. All three models used a total energy equation which is formed by the addition of the two energy equations. The second energy expression used is an energy balance at the interface similar to the interfacial jump condition. Both energy balance at the interface and the true vapour energy equation have been investigated and will be discussed further. Use of certain terms in the momentum equations will also be discussed.

It must be again emphasized that the purpose of this work was to compare the use of different equations and constitutive relations in order to determine, if possible, the best available form of the model based on comparisons with results from several varied experiments.

CHAPTER 4

A GENERAL TWO-FLUID MODEL FOR CRITICAL FLOW IN PIPES

4.1 MODEL EQUATIONS AND ASSUMPTIONS:

4.1.1 Assumptions:

The main assumptions of the model are:

- the flow is steady;
- the flow is one dimensional and in the direction along the pipe axis;
- there is uniform pressure across the pipe cross section;
- the viscous dissipation terms are negligible;
- there is negligible heat loss or gain from the pipe walls;

4.1.2 Model Equations:

Before listing the equations, a few variables should be expanded. The first is the vapour generation:

$$\Gamma = \frac{1}{A} \frac{dW_c}{dz} = \frac{W dx}{A dz} = - \frac{1}{A} \frac{dW_l}{dz} \quad (4.1)$$

where W is the mass flow rate across the pipe cross section. M_{Li} and M_{Gi} are the interfacial momentum transfer terms. There is some discussion in the literature as to what should be included in this expression so several forms were tried. The effect of gravity is taken into account by using the component of gravitational acceleration in the direction of flow: $g_z = g \sin(\theta)$ where θ is the angle of inclination from the horizontal.

The conservation equations taking into account the variable pipe cross section are:

Conservation of Mass for the Liquid:

$$\begin{aligned}
 & -\rho_L u_L A \frac{d\alpha}{dz} + \rho_L A(1-\alpha) \frac{du_L}{dz} + \rho_L(1-\alpha)u_L \frac{dA}{dz} + \\
 & u_L(1-\alpha)A \left(\frac{\partial \rho_L}{\partial P} \right)_{sat} \frac{dP}{dz} = -W \frac{dx}{dz}
 \end{aligned} \quad (4.2)$$

Conservation of Mass for the Gas:

$$\rho_C u_C A \frac{d\alpha}{dz} + \rho_C \alpha A \frac{du_C}{dz} + \rho_C \alpha u_C \frac{dA}{dz} + u_C A \alpha \left(\frac{\partial \rho_C}{\partial P} \right)_{sat} \frac{dP}{dz} = W \frac{dx}{dz} \quad (4.3)$$

Conservation of Momentum for the Liquid:

$$\begin{aligned}
 & \rho_L u_L(1-\alpha)A \frac{du_L}{dz} + A(1-\alpha) \frac{dP}{dz} = F_{wL}A + F_{LC}A \\
 & -M_{Li} - (1-\alpha)A\rho_L g \sin(\theta)
 \end{aligned} \quad (4.4)$$

Conservation of Momentum for the Gas:

$$\rho_C U_C \alpha A \frac{du_C}{dz} + A \alpha \frac{dP}{dz} = -F_{wC}A - F_{LC}A - M_{Ci} - \alpha \rho_C A g \sin(\theta) \quad (4.5)$$

Conservation of Total Energy (formed by addition of the two energy conservation equations):

$$\begin{aligned}
 & W \frac{dx}{dz} \left[(h_C - h_L) + \frac{u_C^2 - u_L^2}{2} \right] + W_C \left[\left(\frac{\partial h_C}{\partial P} \right)_{sat} \frac{dP}{dz} + u_C \frac{du_C}{dz} \right] + W_L \left[\frac{dh_L}{dz} + U_L \frac{du_L}{dz} \right] \\
 & + W g \sin(\theta) = 0
 \end{aligned} \quad (4.6)$$

Conservation of Vapour Energy:

The conservation equation for the vapour phase is:

$$W_C \left(\frac{\partial h_C}{\partial P} \right)_{sat} \frac{dP}{dz} + W_C u_C \frac{du_C}{dz} + W \frac{dx}{dz} \left(h_C + \frac{u_C^2}{2} \right) = q_i A \quad (4.7)$$

where:

$$q_i = \alpha_i h_i (T_L - T_C) + \frac{W}{A} \frac{dx}{dz} (h_C - h_L) \quad (4.8)$$

The vapour phase is considered saturated, i.e.

$$T_G = T_{sat}(P)$$

$$\begin{aligned} \frac{dh_c}{dz} &= \left(\frac{\partial h_c}{\partial P} \right)_{sat} \cdot \frac{dP}{dz} \\ \frac{d\rho_c}{dz} &= \left(\frac{\partial \rho_c}{\partial P} \right)_{sat} \cdot \frac{dP}{dz} \end{aligned} \quad (4.9)$$

The model developed by Richter (1981) and those recently published by Dobran (1987) and developed by Al-Sahan (1988) replace the complete vapour energy equation with an energy balance at the interface in the form:

$$W \frac{dx}{dz} (h_c - h_L) + W_c \left(\frac{\partial h_c}{\partial P} \right)_{sat} \frac{dP}{dz} = \bar{h}_i a_i A (T_L - T_c) \quad (4.10)$$

The differences between the results for the full vapour energy equation and the interfacial energy balance will be discussed later.

There is another equation for bubble growth which is applicable only in the bubble flow regime to account for the change in bubble diameter. After bubble nucleation occurs, the bubbles will grow at a rate related to the changes in void fraction and quality. Starting with the rate of change of vapour axial flow along the pipe given by:

$$W \frac{dx}{dz} = \frac{dW_c}{dz} \quad (4.11)$$

but

$$W_c = \alpha \rho_c u_c \quad (4.12)$$

and in bubble flow

$$\alpha = \frac{N \pi d_b^3}{6} \quad (4.13)$$

Substituting:

$$W \frac{dx}{dz} = \frac{d}{dz} \left(\frac{N \pi d_b^3}{6} \rho_c u_c \right) \quad (4.14)$$

and assuming that N is constant for this step:

$$W \frac{dx}{dz} = \frac{N\pi}{6} \left[3d_b^2 \frac{dd_b}{dz} u_c \rho_c + d_b^3 u_c \frac{d\rho_c}{dz} + d_b^3 \rho_c \frac{du_c}{dz} \right] \quad (4.15)$$

Collecting terms:

$$W \frac{dx}{dz} = N \frac{\pi}{6} d_b^3 \rho_c u_c \left[\frac{3}{d_b} \frac{dd_b}{dz} + \frac{1}{\rho_c} \frac{d\rho_c}{dz} + \frac{1}{u_c} \frac{du_c}{dz} \right] \quad (4.16)$$

this simplifies to the final equation:

$$\frac{dx}{dz} = x \left[\frac{3}{d_b} \frac{dd_b}{dz} + \frac{1}{\rho_c} \left(\frac{\partial \rho_c}{\partial P} \right)_{sat} \frac{dP}{dz} + \frac{1}{u_c} \frac{du_c}{dz} \right] \quad (4.17)$$

This expression is used to solve for the bubble diameter and N is recalculated using the new void fraction and bubble diameter. This seventh equation is included in the numerical calculations up to the transition point from bubble to churn flow. The change in N is calculated in a mathematically fictitious manner, however, it allows for change in N which is not included in most other models. Richter (1981) also used a seventh equation for bubble diameter, however, in deriving this equation which is equivalent to 4.17, he neglected the gradients of density and velocity. This proved to be incorrect and a comparison of the effects of the various terms in the equation will be discussed later in the thesis.

The use of equation (4.17) and the updating of the bubble number density is somewhat unique to this general model. The Richter model uses an interface balance based on the bubble diameter rate equation with only the change in bubble diameter term. The full equation has not been found in any of the literature. Dobran and Al-Sahan used a constant value for N and the relationship for void fraction in terms of bubble diameter.

4.1.3 Interfacial Momentum Transfer:

Only a small number of terms are not explicitly formulated in the equations. The two which do have an effect on the primary variables are the interfacial momentum transfer terms: M_{Li} and M_{Gi} . When there is vapour generation there is mass, momentum and energy transfer across the interface. Technically, the parameter values at the interface such as velocity are different from those in the bulk of each phase so the calculation should use the interfacial velocities; however, these are not often known so the assumption that the parameters are those in the bulk of each phase is reasonable. There is some dispute over what is actually involved in the transfer. The newly formed gas has momentum that it transfers to the gas phase but its velocity will not be that of the bulk gas. There should be some additional momentum from somewhere which will raise the newly formed gas to the bulk gas velocity. According to Wallis (1969) this momentum will come from each of the phases in the proportion η to $1-\eta$. The value of η was determined by Wallis (1969) to be .5. Interfacial momentum interchange can be represented in any one of three combinations of these terms from none to the use of both components. The full terms are as follows:

$$M_{Li} = -W u_L \frac{dx}{dz} - (1-\eta)(u_c - u_L)W \frac{dx}{dz} \quad (4.19)$$

$$M_{Gi} = W u_L \frac{dx}{dz} - \eta(u_c - u_L)W \frac{dx}{dz} \quad (4.19)$$

4.1.4 Other Constitutive Relationships:

Other terms which are represented by constitutive relations are for:

- interfacial area;
- interfacial force;
- interfacial heat transfer;

Each is different for different flow regimes.

The interfacial force, as mentioned previously, is modelled as a constant relative velocity drag force and a relative acceleration based virtual mass force. The heat transfer is proportional to the interfacial area and heat transfer coefficients. These will be discussed later.

4.2 SUBCOOLED FLOW:

The model for single phase subcooled flow is to calculate pressure drop using single phase friction factor and change in cross sectional area until saturation pressure is reached. According to nucleation theory, the conditions for nucleation during depressurization are not so much a temperature difference as a pressure difference between the superheated liquid and the saturated vapour. The pressure difference is due to the surface tension of the curved interface at a nucleation site. The bubble will nucleate when the surrounding pressure drops to the point where the difference between the saturated vapour pressure in the bubble nuclei and the liquid pressure is greater than four times the surface tension over the bubble diameter.

The initial size and number of nucleation sites are two of the most inadequately verified quantities in the entire model. In quite a few models, they are adjustable parameters to match experimental results. Until a recognized theoretical correlation is developed, this amounts in my opinion to fitting the simulations to the

data. It is always nice to be able to say that the model fits the data if a parameter is modified but a model is of limited use for prediction unless the modification is effective over the full range of experimental data. In this work, the values for initial bubble diameter and bubble density are set to values suggested by Richter (1981). These are 2.5×10^{-5} m. and 10^{11} sites/m³. respectively. These numbers will be kept constant except to investigate the effect since the intention is to find the best possible model by using general correlations and not by adjusting parameters. The quantities are only used initially as both variables are changed by the solution of the equations.

The growth of the bubble is dependent upon relative velocity and the difference between phase temperatures. The temperature differential is driven by the drop in pressure and vapour generation.

4.3 METHOD OF SOLUTION:

The program solution method requires entry of three sets initial conditions. The first set is pressure and temperature in the subcooled case or pressure and stagnation quality for saturation conditions. The second is the pipe geometry with diameter as a function of distance along the tube and the third is an initial guess for mass flux. If the liquid is subcooled or just saturated, the program steps along the tube until the frictional pressure drop lowers the pressure enough to start nucleation and generate an initial void fraction. At this point, the slip is assumed to be approximately one so the quality can be calculated from the

relationship:

$$x = \left[1 + \frac{\rho_o(1-\alpha)l}{\rho_c \alpha k} \right]^{-1} \quad (4.20)$$

where k is the slip. The gas velocity can be found by definition:

$$u_c = \frac{xW}{\alpha \rho_c A} \quad (4.21)$$

and the liquid velocity from the slip. If the initial conditions are saturated, the calculation proceeds as though nucleation just began with the given stagnation quality. With initial values for all the variables, the solution to the system of equations can be found by stepping along the axial direction until reaching critical conditions or the end of the test section.

The primary variables solved for in the equations are liquid pressure, quality, void fraction, liquid temperature, liquid velocity, and gas velocity:

$$P_L, x, \alpha, T_L, u_L, u_c$$

and in bubble flow, the additional variable, bubble diameter d . The vapour pressure is assumed to be equal to the liquid pressure except in the bubble flow regime where it is related by the surface tension. The vapour is assumed to be saturated with the saturation temperature corresponding to the vapour pressure.

The method of solution is to integrate with respect to the distance along the pipe using a guess for mass flux until a critical condition is reached. If this location does not coincide with a point of narrowest cross section furthest from the entrance to the pipe, then the mass flux is adjusted up to shorten the distance

to the choking point or decrease the mass flux to increase the distance to choking point. The process is iterated until the correct mass flux is found.

4.4 CHOKING LOCATION:

The location of the choking plane will be at the end of the pipe or at a point of minimum cross section closest to the end. This stands to reason since the velocities at the smallest diameter will be the highest and choking occurs at a velocity limit.

4.5 CRITICAL CONDITIONS:

Critical conditions are characterized mainly in two different ways. It has been theoretically and experimentally observed that at the location of critical flow, there is a very large but finite pressure drop. This makes sense intuitively, and it is the most physically understandable condition. The other commonly used criteria involves the determinants of the matrices. The matrices are; [A], formed from the coefficients of the derivative terms in the equations, [X], a derivative vector of the primary variables, and [B], a constant vector of the constant terms in the conservation equations. The criteria requires that the determinant of the coefficient matrix and the determinants of the same matrix with a column replaced by the column vector [B] are zero.

$$[A] \frac{d}{dz} [X] = [B]$$

$$\det(A) = 0, \det(A_i) = 0 \quad (4.22)$$

where the i^{th} column is replaced by [B].

The large magnitude negative pressure gradient was chosen because it made more sense physically than the

mathematically derived determinant condition and it was simpler and faster numerically to implement. The minimum value for choking is almost arbitrary. It must be high enough to allow for huge decrease in pressure as the step in the z direction is made but not too high so as to be impossible to reach due to numerical calculation error. Richter chose:

$$\frac{dP}{dz} < -2 \times 10^{12} Pa/m. \quad (4.23)$$

Since his numerical algorithm had a fixed step size, this condition was acceptable. Because of the use of a more sophisticated algorithm with variable step size, the magnitude of the critical pressure drop can be decreased. As a result of the fact that the algorithm decreases the step size as the magnitude of the gradients increases, the size of the step at high pressure gradients is very small (on the order of 10^{-9} m. or less). Therefore, the increased iteration to find the critical plane location is not justified because of the extremely small changes in z . The value of:

$$\frac{dP}{dz} < -2 \times 10^{10} Pa/m. \quad (4.24)$$

was chosen to reduce iteration and numerical computation time. It should be noted, however, that although this condition has little effect on the calculation of critical plane location, it does have a very great effect on the critical pressure calculated at the exit.

4.6 SOLUTION ALGORITHM:

A system of nonlinear equations can be formed into a matrix equation of the form:

$$[A] \frac{d}{dz} [X] = [B] \quad (4.25)$$

where $[X]^T = [P_L, x, \alpha, T_L, u_L, u_C]$ (4.26)

This system can be reduced to the form of:

$$\frac{d}{dz}[X] = [C] \quad (4.27)$$

by Gaussian elimination and back substitution. One is left with a set of derivatives equated to a set of very mathematically complicated nonlinear expressions. It would require a prohibitive amount of work to solve this algebraically but there are many library packages with subroutines specifically designed for reduction of these equations and solution of the reduced form of the equation. The two main algorithms for the numerical integration problem are:

- the fourth order Runge-Kutta method;
- the Predictor-Corrector or Adams-Moulton method;

Since both are easily found in almost any numerical methods text, i.e., Gerald (1980), only a quick description will be given here.

The Runge-Kutta methods are based on a Taylor Series approximation for each step in the function. The method is explicit and involves only information for a single distance step. It has good accuracy when used with fourth order or higher approximation but it is costly if the evaluation of [B] is numerically complex. The equation set in this model is very mathematically involved, so the requirement of a minimum of four functional evaluations for each step is a great disadvantage of this method. Exact estimation of the error is also somewhat uncertain.

Adams-Moulton is a semi-implicit multi-step method, meaning it involves the use of the past distance step information and it uses an equation for a prediction of the next step value and then a second equation to correct

the values used. This is done iteratively to a point where the error is less than a given tolerance. Because of this, the error can be determined relatively easily. More important is the fact that since it uses previously calculated values, it requires only one new [B] matrix evaluation per step. This reduces computation time significantly. Predictor-Corrector methods apparently have better stability properties. Due to the smaller computation time and better stability and error estimation, the Predictor-Corrector algorithm was used.

It is important to make the correct choice of the tolerance. In most software packages, the tolerance is actually two quantities; the relative tolerance and the absolute tolerance. The former is roughly equivalent to the percent error but not in percent. The latter is an absolute minimum value for the difference between the calculated value and the "true" value. It is normally set to a value that is larger than the uncertainty of the numerical precision of the computer. The selection of the relative tolerance will be discussed later.

The numerical package to be used was determined largely by two criteria. The first was the ability of the routine to stop when a given condition was reached called root finding ability as opposed to a given interval of distance. The second was the ability of the software to be transferred to a microcomputer from a VAX 8600. This implies that the source code be available and be "public domain" software.

The solver routines from the IMSL package have the capability of solving matrix derivative and vector system, i.e. the matrix [A] can be full or the identity

matrix. It does not, however, have root finding ability built in, and even though that can be overcome, it is also a licensed software package that is non-transferable.

The LSODE ordinary differential equation solvers from Lawrence Livermore National Laboratory have a routine called LSODAR which solves only vector systems but has the root finding capability built in, and is in public domain. Another nice feature is that the routine can automatically switch to a "stiff" method if required.

A stiff system of equations is defined in Carey and Oden (1984) as when the real part of the smallest eigenvalue of the coefficient matrix is very much smaller than the real part of the largest eigenvalue. In solvers for systems of the ordinary differential equations, this translates to a condition that the step size must be prohibitively small in order to satisfy stability criteria for the matrix equation. Both IMSL and LSODAR routines have automatic step size adjustment, and two methods of solution for non-stiff and stiff systems. The first is very important for reducing computation time since it allows for an increase in step size up to a point where the error is still within a specified tolerance. Since the steps can be larger, the amount of computation is less. This also reduces the error at the choking location since it is kept within tolerance when the gradients are changing very rapidly at the exit. There are also stability criteria for step size. These are theoretical mathematical restrictions on the maximum step size in order to ensure a stable solution.

Due to the root finding ability and availability for transfer, the Livermore routine was chosen for the program. An IMSL routine for matrix decomposition was used initially for simplicity but a later version uses a LINPACK routine for this task. The program calculates the coefficients of the [A] and [B] matrices, decomposes and back substitutes the [A] matrix and substitutes in the ordinary differential equation solver.

4.7 TOLERANCE:

The relative tolerance for the initial work was .0001. This seemed to strike a reasonable balance between computation efficiency and accuracy. Since tolerances are normally lower than the expected error, .01% seemed reasonable. The absolute tolerance was set close to the numerical uncertainty of double precision arithmetic. A check of the effect of tolerance was made after the program was debugged. It was found that a tolerance of 10^{-5} represented the best accuracy before greatly increasing computer time. Al-Sahan (1988) also found this and therefore it was used as the tolerance for all final runs.

Table 4.1: Chart of the Effect of Tolerance Size:

RICHTER TEST CASE: $G = 37000 \text{ kg/m}^2/\text{s}$

<u>TOLERANCE</u>	<u>CHOKING AT $z \equiv$ (m.)</u>	<u>CPU TIME (s.)</u>
10^{-3}	.2732	20.33
10^{-4}	.2703	30.77
10^{-5}	.2600	58.47
10^{-6}	.2591	177.95

4.8 THERMODYNAMIC PROPERTY CORRELATIONS:

Obviously, thermodynamic property correlations are required for pressure, temperature, density, enthalpy, entropy, specific heat, thermal conductivity, dynamic viscosity, and surface tension. The independent variables are pressure and temperature or both. The correlations, used by Richter from International Steam Tables with superheat, were implemented.

4.9 TRANSITIONS:

Only three flow regimes were used in the general model for simplicity, although as many as five have been used by Al-Sahan (1988). Since the dispersed and homogeneous regimes are involved only at the highest void fractions after annular flow, they would only be used in calculations for the last very small portion of the simulation. Obviously, this would not substantially effect the location of choking along the z axis, and therefore, would have little effect on the mass flux calculation. The other variables such as exit pressure and void fraction would be affected, but, since the magnitude of the critical pressure drop at the exit also affects these parameters, the inclusion of these flow regimes would not likely have much of an effect at all. In view of the fact that the transition points are not clearly defined nor are all the equations for the dispersed and homogeneous regimes, only three flow regimes were used; bubble, churn, and annular. Considering the velocities involved, slug flow would not likely be encountered.

Since the transition from bubbly flow to churn is generally accepted to be at a void fraction of

approximately .3, it was used as the first transition point. Richter used a void fraction of .8 for the churn to annular flow transition as did Dobran. This value was selected for lack of a better point. The transitions occurred at constant void fraction independent of velocity and pressure. This is not a very realistic assumption; however, the only other way to determine transition point would be to use flow regime maps. The only general map available for pressures and fluids is the semi-theoretical map by Taitel and Dukler (1976). Some transition lines are clearly defined, but from churn to annular, although defined by an equation, is stated to be an approximation only. This would be little better than the constant void fraction value. For lack of a better flow regime map, the constant transition points were used. One would expect that, if for lower velocities, the transition to annular occurs at a lower void fraction, adjusting it in that direction would improve the accuracy for lower velocity and hence lower mass flux cases.

4.10 CAPABILITY:

This program can calculate the location of choking and critical mass flux for circular cross section variable diameter test situations. The assumption of steady-state does not necessarily limit the use of the equations to steady state simulations only. Transient cases can be simulated by using different runs to simulate intervals in time history each of which is approximately steady state. If the variations in the primary transient variable, pressure, are small over the interval of time for the fluid to pass through the pipe, the assumption is valid. This is usually the case.

As a by-product of the computation, a data file is formed for the primary variables: distance, pressure, liquid and gas temperature, liquid and gas velocity, quality and void fraction. Another data file has interfacial parameters of heat transfer, drag coefficient and area, and frictional pressure drop, but only for the two phase section. In this way almost every major value used in the calculations can be stored for comparison, plotting etc. The program requires a subroutine for the geometry of the pipe but every other parameter is prompted for on the screen. The program is intended to be in two versions for the VAX 8600 and for an IBM compatible microcomputer.

4.11 PROGRAM FLOW CHART:

A flow chart of the program with subroutines used is shown below:

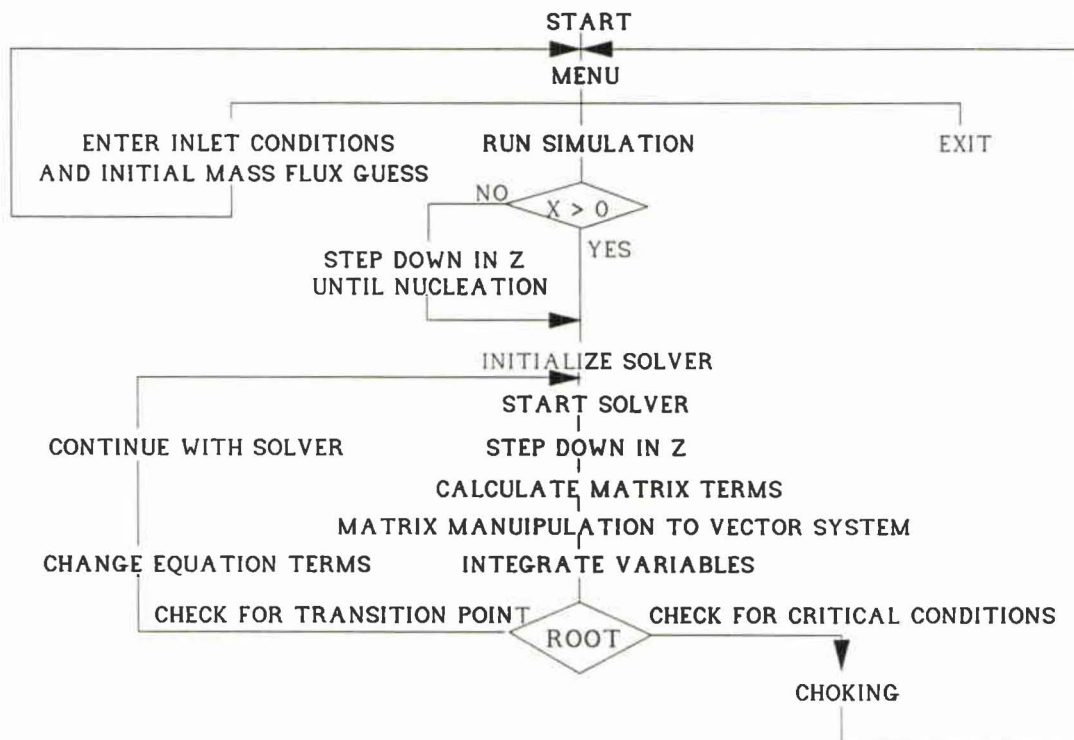


Fig. 4.1 Program Flow Chart:

CHAPTER 5

RESULTS AND DISCUSSION

The results and discussion are divided into two parts. The first is the comparison of the different forms and correlations required for closure in the general model. A large number of parameters can be altered and the best form resulting from this will be discussed. The second part will be a comparison of the general model with existing experimental data. The effectiveness of the simulations can be determined by checking against the mass flux and pressure information from several experimental systems.

5.1 EFFECT OF MODEL EQUATIONS AND PARAMETERS:

During the development of the model a test case was needed as an example for comparison purposes. Almost all the work was done using the experimental result from Sozzi and Sutherland (1975) which was also used as an example by Richter (1981), for his work. The responses were well known as was the exact test geometry. For a complete description of the experimental test cases and their dimensions, see Table 5.3 and APPENDIX B.

5.1.1 CORRELATIONS AND EQUATION FORMS TESTED:

Since this work was intended to test the effects of changing parameters in the general model, comparison against other models is very important. The variations in the program used are as follows:

Table 5.1 (a): Chart of Parameter Changes to Be Tried:

<u>PARAMETER</u>	<u>CHANGES TO BE TRIED</u>	<u>FROM</u>
-deriv. of dens. wrt. to press. at sat.	-off saturation line -P, T(Psat) -T, P(Tsat)	
-7th eqn. for bubble diam.	-Richter formulation -Simplified formulation -full eqn. formulation	-Richter -New -New
-Vapour Energy eqn.	-energy bal. at the interface -cons. of vapour energy	-Richter -New
-Interfacial Momentum trans.	-none -momentum interchange -momentum sinks for vel. diff. -both	-Al-Sahan -New -Richter -New
-Fric. Press. drop	-constant value for f -Moody factor func. of Re#	-Richter -Al-Sahan
-Virtual Mass	-Wallis form -Drew et al. form -No and Kazimi coefs. -Al-Sahan coefficients	-Richter -Al-Sahan -New -Al-Sahan
-Virtual mass applied in flow regimes	-bubble flow only -bubble and churn flow -all three flow regimes	-Richter -New -New
-Interfacial area in churn flow	-linear interpolation -exponential interp.	-Richter -New
-Interfacial Drag force	-linear interp. of C_{fi} -Ishii correlation -Al-Sahan method -exponential interp.	-Richter -Al-Sahan -Al-Sahan -New
-Interfacial Heat transfer in churn flow	-lin. interp. of h -lin. with estim. of gas vel. -exp. with estim. of gas vel. -exp. with heat transfer parameter	-Richter -New -New -New

5.1.2 STABILITY:

In control, unstable can refer to an oscillation which grows and computation problems when the matrices are ill-conditioned. The former did not occur, but some results were numerically calculable up to some point after which the matrices were too ill-conditioned for the routines to continue. There were also several instances where calculations proceeded very well numerically, but in physical terms, the answers calculated were meaningless. An example of this was the deceleration of the gas phase as it moved down the pipe. The word stability will be used to refer to both physically impossible circumstances and numerical results which cannot be computed further.

5.1.2.1 Gradient of Liquid Density:

The first of the two terms that have an effect on the stability of the solution is the derivative of liquid density with respect to distance. The gas is assumed to be saturated, but the liquid starts out at saturation and almost immediately becomes superheated due to the decrease in pressure. If saturated, the derivative can be expressed using the chain rule, as mentioned previously. Only the density is affected by the superheating since the change in enthalpy is determined as a separate variable and is converted to a change in temperature using the specific heat at constant pressure.

There is a problem with stability if an attempt is made to take the derivative off the saturation

line, so the liquid derivative must be approximated at saturation conditions. The question is which saturation point.

If the pressure is assumed saturated and the temperature calculated accordingly, the use of that derivative causes instability. The only other possibility is to use the superheated temperature and its saturated pressure. This works well and makes sense intuitively since the properties at a higher temperature will drive the equations towards non-equilibrium.

5.1.2.2 Virtual Mass:

The second term which has an effect on the stability is the virtual mass. Starting with the known expression for the virtual mass of a sphere:

$$F_{vm} = C \rho_L u_G \alpha \frac{d}{dz} (u_G - u_L) \quad (5.1)$$

where $C=0.5$, the equation for the virtual mass term has evolved substantially. The constant will vary significantly if the geometry of the interface is non-spherical. The form of the virtual mass term was described by Wallis (1969) as a constant times the derivative of the relative velocity. This was used by Richter (1981, 1983) and was first tried here and proved to be satisfactory for the high mass flux case of Sozzi and Sutherland (1975). For the low mass flux cases of Al-Sahan (1988), the equations became unstable and results were unsatisfactory. In these test cases, a longer distance is required to reach choking conditions. The gradients of the primary variables with respect to the axial distance are lower in magnitude. This results in a smaller virtual

mass term with respect to the other terms in the equations, which has a destabilizing effect on the calculations.

A literature survey demonstrated the lack of general consensus on the form and the constants of the virtual mass term. Dobran (1987) used the expression:

$$F_{vm} = \alpha \rho_L C_{vm} \left(u_C \frac{du_C}{dz} - u_L \frac{du_L}{dz} \right) \quad (5.2)$$

where

$$C_{vm} = .3 \tanh(4\alpha). \quad (5.3)$$

Drew et al. (1979) discussed mathematically the reasons for a specific form based on the property of objectivity. The calculation of the two constants introduced was left to future researchers. The form is:

$$F_{vm} = C_{vm} \rho_L \left[\frac{D_C(\bar{u}_C - \bar{u}_L)}{Dt} + (\bar{u}_C - \bar{u}_L) \cdot [(\lambda - 2)\bar{\nabla} u_C + (1 - \lambda)\bar{\nabla} u_L] \right] \quad (5.4)$$

The arguments expressed in the paper and subsequent discussions with other researchers indicated that this was the best form available. The constants were considered by Kazimi and No (1985, 1986) who calculated mathematical limits on the value of the constants C and λ . Through the use of eigenvalue analysis, they derived two expressions for the constants:

$$C_{vm} \geq \frac{1}{\lambda} \sqrt{4\alpha(1-\alpha)^3 \frac{\rho_C}{\rho_L}} \quad (5.5)$$

$$\lambda > 1 - \frac{k}{(k-1)((1-\alpha)k + \alpha)} \quad (5.6)$$

They recommended using $\lambda = 1.0$ and adjusting C_{vm} accordingly. This was tried with values just higher than the limit and the results were not satisfactory. In particular, if the value of λ was calculated using the inequality, the stability was worse since the inequality allows for negative values at high void fraction. The coefficients used by Al-Sahan (1988) from Ishii and Chawla (1979) were:

$$C_{vm} = \frac{1 + 2\alpha}{2(1 - \alpha)} \quad (5.7)$$

$$\lambda = 2(1 - \alpha) \quad (5.8)$$

This was tried and found to be successful. It should be noted that the values in these equations satisfy the Kazimi and No (1986) inequalities.

A comparison of the effects of changing the coefficient of virtual mass force was done using the Kazimi and No (1986) correlations. It demonstrated that lower axial gradients of the primary variables were predicted resulting in a longer distance required to reach choking if the constant C_{vm} was increased.

Despite the fact that higher relative accelerations occur in churn and annular flow, Richter (1981), Al-Sahan (1988), and Dobran (1987) considered the term only for bubble flow. No information could be found in the literature to explain why this was the case. The assumption appeared to be that the different gas surface geometries reduce the relative magnitude of the term. To check this effect, runs were made incorporating the virtual mass term in churn and bubble flow as well as in all three regimes. The result was to stabilize the calculations

and to reduce the computation time but also to require a longer distance to choking for the same mass flux. Both the degree of non-equilibrium, which drives the vapour generation, and the velocity differences were lower with the incorporation of the virtual mass effect in flow regimes other than bubble flow.

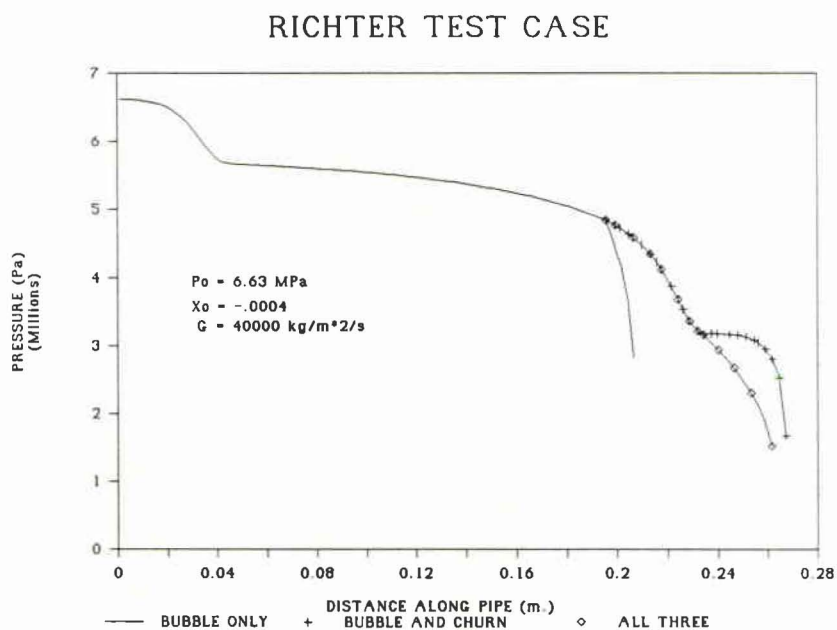


Fig. 5.1: Effects of the Virtual Mass Term in Different Flow Regimes:

Because of the unrealistic changes at the transition from churn to annular flow and better comparisons with experimental results, it was decided that the virtual mass term should be used only in bubble flow equations.

5.1.3 VAPOUR ENERGY EQUATION:

In the three previous two-fluid one-dimensional models, the vapour energy equation was replaced with an energy balance at the interface as shown by equation

4.10. The conservation of energy across the interface shows that the total energy convected across the interface defined by an overall heat transfer coefficient \bar{h}_i is equal to the energy lost due to the formation of vapour and the change in enthalpy of the gas. Although this makes sense intuitively, the overall convective heat transfer coefficient used was obtained from empirical Nu versus Re number relations originally developed for sensible heat transport. The conservation of vapour energy equation for steady state is defined as follows:

$$\frac{d}{dz} \left[W_c \left(h_c + \frac{u_c^2}{2} \right) \right] = q_i A + q_{wc} A + \alpha \rho_c u_c g A \sin(\theta) \quad (5.9)$$

Expanded assuming adiabatic wall:

$$W_c \frac{dh_c}{dz} + u_c W_c \frac{du_c}{dz} + \left(h_c + \frac{u_c^2}{2} \right) W \frac{dx}{dz} = q_i A + \alpha \rho_c u_c g A \sin(\theta) \quad (5.10)$$

where;

$$q_i = a_i h_i (T_l - T_c) + \frac{W}{A} \frac{dx}{dz} h_{lc} \quad (5.11)$$

Translated the interfacial heat transfer is equal to the sensible heat transferred to it and the increase in energy due to vaporization. The walls are assumed to be adiabatic and for horizontal flow the gravitational term is zero. In equation (5.11), h_i is the sensible heat transfer coefficient which can be obtained from available empirical relationships. Expanded and collected, the equation becomes:

$$\begin{aligned} W_c \left(\frac{\partial h_c}{\partial P} \right)_{sat} \frac{dP}{dz} + W \left(h_l + \frac{u_c^2}{2} \right) \frac{dx}{dz} + W_c u_c \frac{du_c}{dz} \\ = h_i a_i A (T_l - T_c) + W_c g \sin(\theta). \end{aligned} \quad (5.12)$$

Equations (4.10) and (5.12) are both similar and both make sense physically depending on the definition of h_i , i.e. whether it is the sensible heat transfer

coefficient or the total heat transfer coefficient at the interface. For the same value of heat transfer coefficient, the vapour generation term in the conservation of energy equation is smaller, i.e. $h_i + \frac{u_i^2}{2} < h_c - h_i$ except for very high gas velocities. The coefficient is smaller so one would expect the vapour generation to be larger. This proves to be the case. Figure 5.2(a) to 5.2(g) show the results obtained by using the full vapour energy equation (5.12) and the interfacial energy balance equation (4.10) for Richter's test case. For this simulation, stagnation conditions were $P_0 = 6.63$ MPa and $x_0 = -.0004$. The critical mass flux was measured by Sozzi and Sutherland (1975) and found to be $33,930$ kg/m²s.

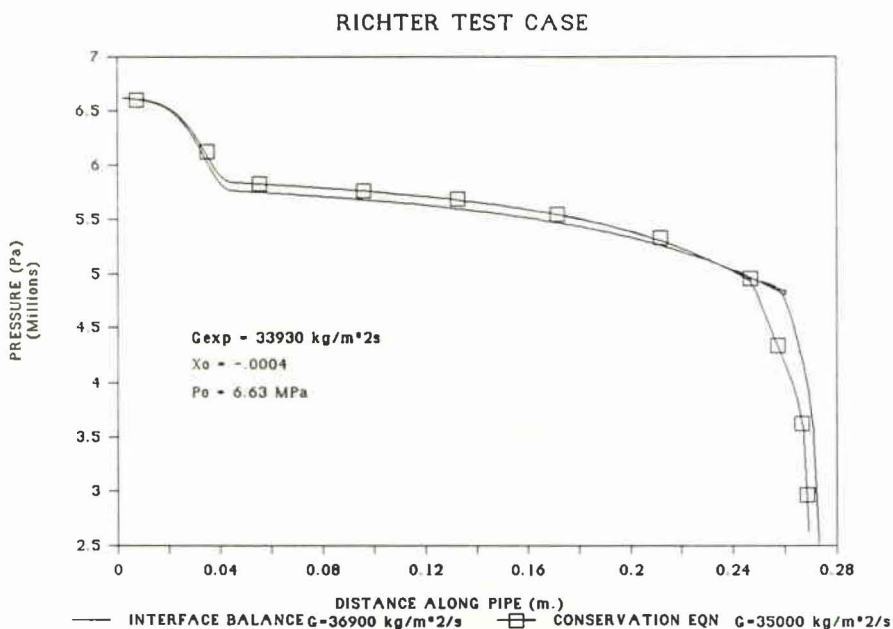


Fig. 5.2 (a): Comparison of Two Vapour Energy Equations: Pressure

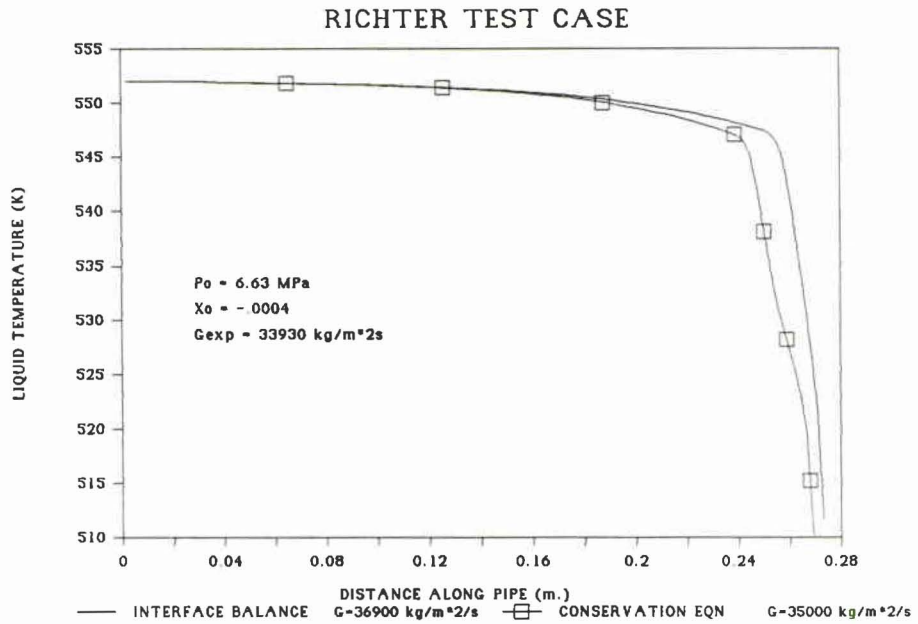


Fig. 5.2 (b): Comparison of Two Vapour Energy Equations: Liquid Temperature

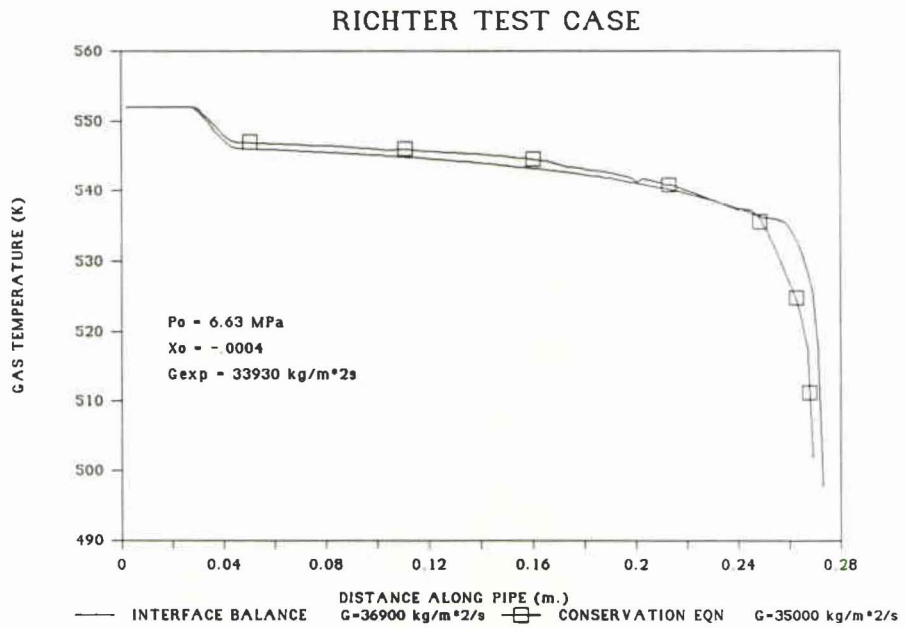


Fig. 5.2 (c): Comparison of Two Vapour Energy Equations: Gas Temperature

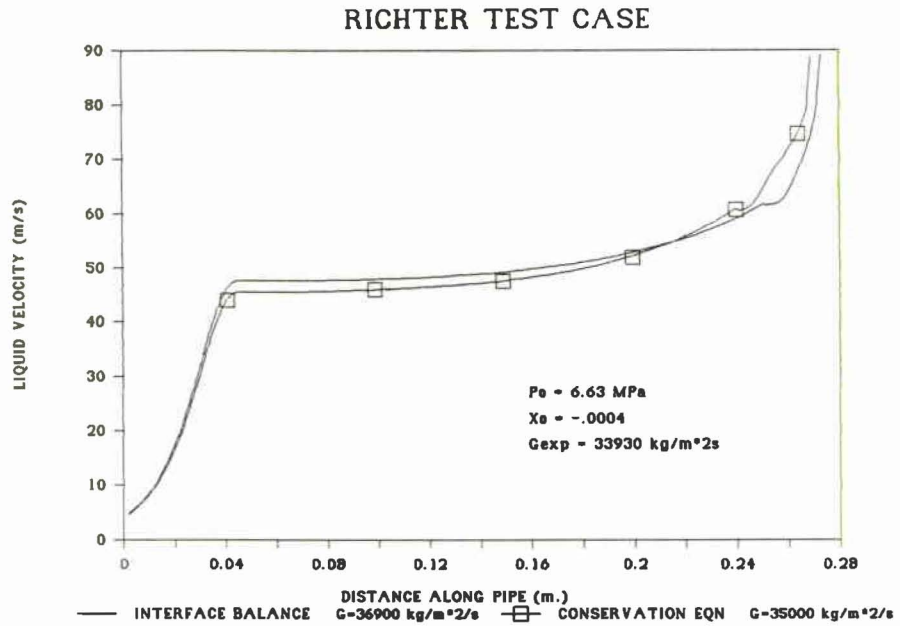


Fig. 5.2 (d): Comparison of Two Vapour Energy Equations: Liquid Velocity

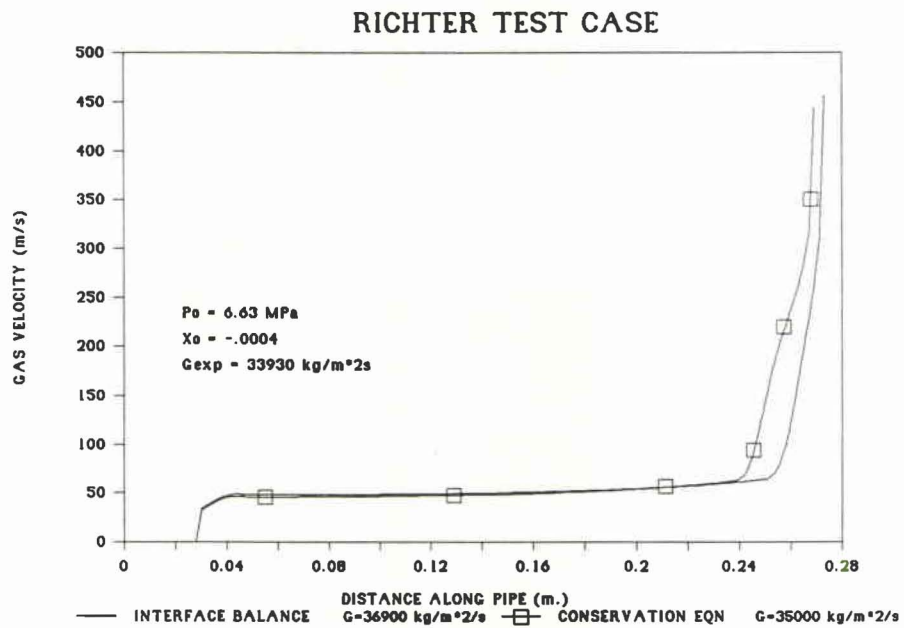


Fig. 5.2 (e): Comparison of Two Vapour Energy Equations: Gas Velocity

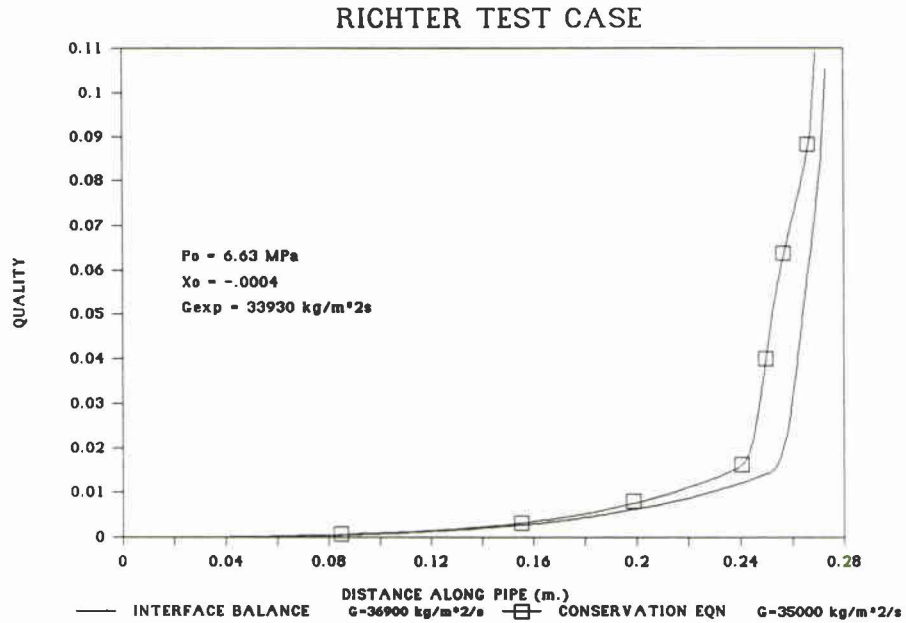


Fig. 5.2 (f): Comparison of Two Vapour Energy Equations: Quality

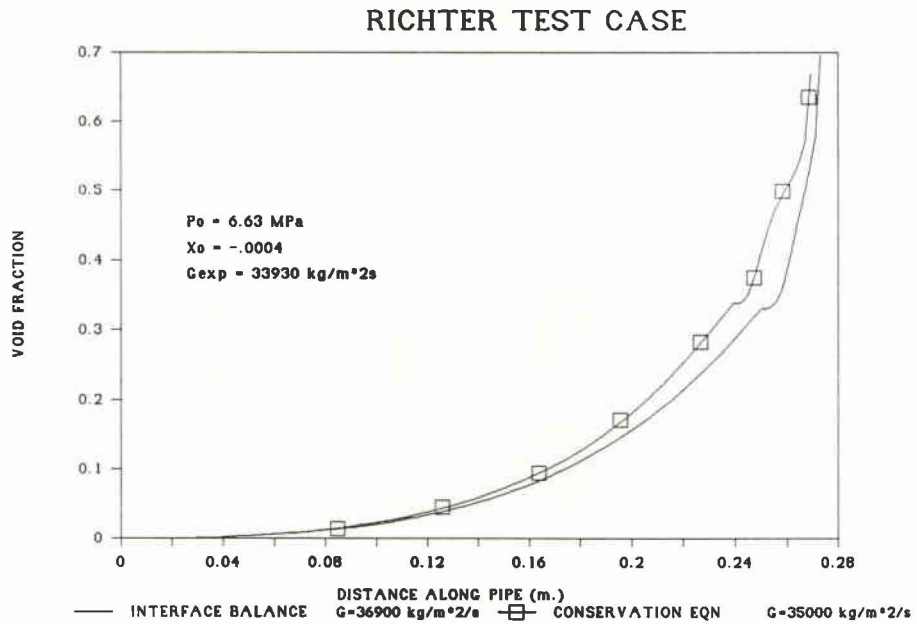


Fig. 5.2 (g): Comparison of Two Vapour Energy Equations: Void Fraction

The main noticeable difference appears to be a faster increase initially in the vapour generation, but that is made up later by the balance equation so the quality at the exit location is approximately the same. The mass fluxes predicted are slightly different; 35000 kg/m²s when the vapour energy equation was used and 36900 when the energy balance equation was used. Since the conservation equation is more comprehensive, and the available correlations for h_i are really for sensible heat and do not include the latent heat effect, it is suggested that the full conservation equation be used in the future. Also, a slight decrease in the predicted mass fluxes is in the right direction when compared against experimental results.

5.1.4 BUBBLE DIAMETER EQUATION:

The bubble diameter equation is the seventh equation used in bubble flow. The original simple form of the equation is from the Richter model but a more complete expansion leads to equation (4.17). A comparison of the effects of the various terms in the equation is shown in Figure 5.3:

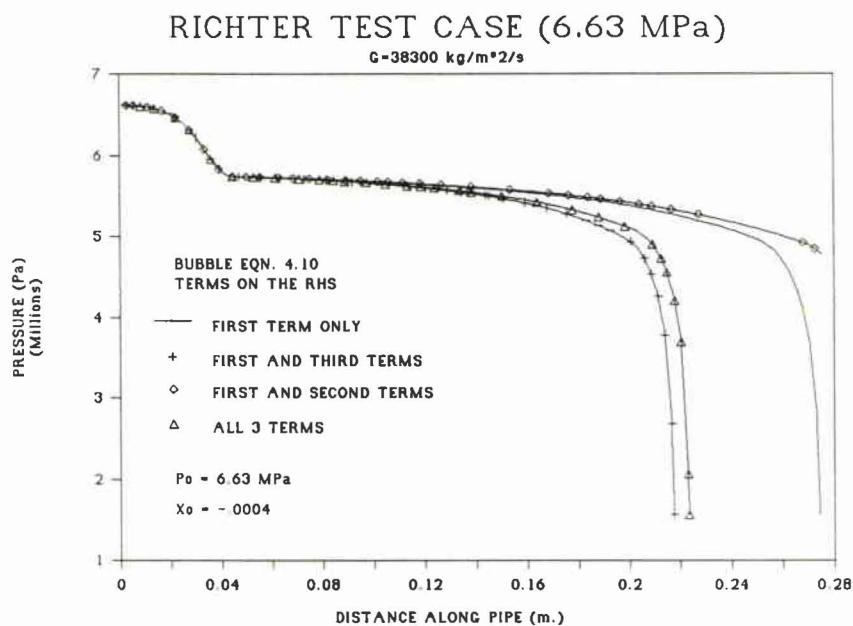


Fig. 5.3: Effect of Terms in the Bubble Diameter Equation:

The two terms involving change in pressure and change in velocity have opposite effects which counteract each other. When added, the pressure term increases the distance to choking or increases the predicted mass flux, while the velocity term does the opposite and seems to dominate when the two are both in the equation. Three test cases using the full bubble diameter equation were checked against the simpler form of the equation without the pressure and velocity terms; Richter 6.63 MPa, Dobran 3.49 MPa, and Al-Sahan .196 MPa. The results show almost no change in the Dobran cases but a small reduction in the predicted mass flux for the Al-Sahan case and a significant change in the predicted mass flux for the Richter case from 38300 kg/s/m² to 35900 kg/s/m² which is closer to the experimental value of 33900 kg/s/m². Since the effects of the terms on the simulations are only in the

bubble flow regime, these results make sense because the vast majority of the Richter case is simulated in this regime. The other two test cases have a larger percentage of the simulation in the other regimes. In view of the improvement in the Richter simulation, it would seem that the best equation to be used is the fully expanded bubble diameter equation. Figure 5.3 shows the effect of these terms on the required length to reach choking for a given mass flux of $38300 \text{ kg/m}^2\text{s}$.

5.1.5 MOMENTUM INTERFACIAL TRANSFER:

The interfacial momentum transfer term in the momentum equations has been the object of some debate. Intuitively there should be momentum exchange due to the vapour generation; however, if there is also a velocity difference between phases, the momentum needed to change the newly formed vapour from liquid to gas velocity should also be included. The following diagram shows the conditions at the interface.

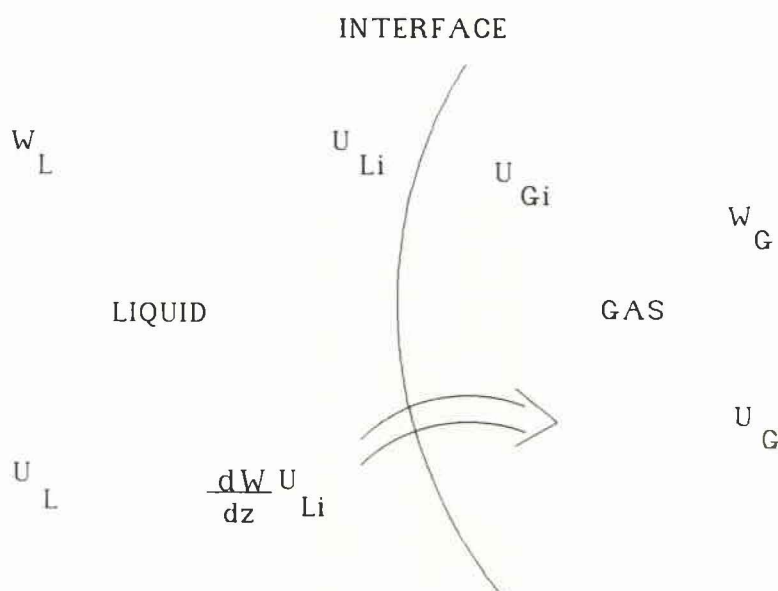


Fig 5.4: Diagram of Interfacial Momentum Conditions:

The recently generated gas is initially moving at the liquid velocity. It is necessary for the momentum required to raise the velocity to the gas velocity to come from somewhere. Wallis (1969) and Richter (1981) represented this as a momentum sink in each phase equation with a proportion of the required inertia coming from each phase. The full exchange terms should be of the form:

$$M_{Li} = -W u_{Li} \frac{dx}{dz} - (1 - \eta)(u_{Ci} - u_{Li})W \frac{dx}{dz} \quad (5.13)$$

$$M_{Ci} = +W u_{Li} \frac{dx}{dz} - \eta(u_{Ci} - u_{Li})W \frac{dx}{dz} \quad (5.14)$$

Wallis (1969) suggested a value of .5 for η which can be interpreted as half the momentum required being donated by each phase.

Strictly speaking, the calculation should be done using the velocity of the liquid and gas at the interface. These are generally not known to any accuracy and in the lumped control volume case, the lumped phase velocities should be used. Therefore, the average phase velocities are used.

There are obviously several ways of using this term, from neglecting it entirely to the use of the transfer part i.e. the first term in equations (5.13) and (5.14) or the sink part, i.e. the second term in the two equations or both. The quantity η is also not very well defined. In Figure 5.5, the effect of the term altogether is shown to be minor:

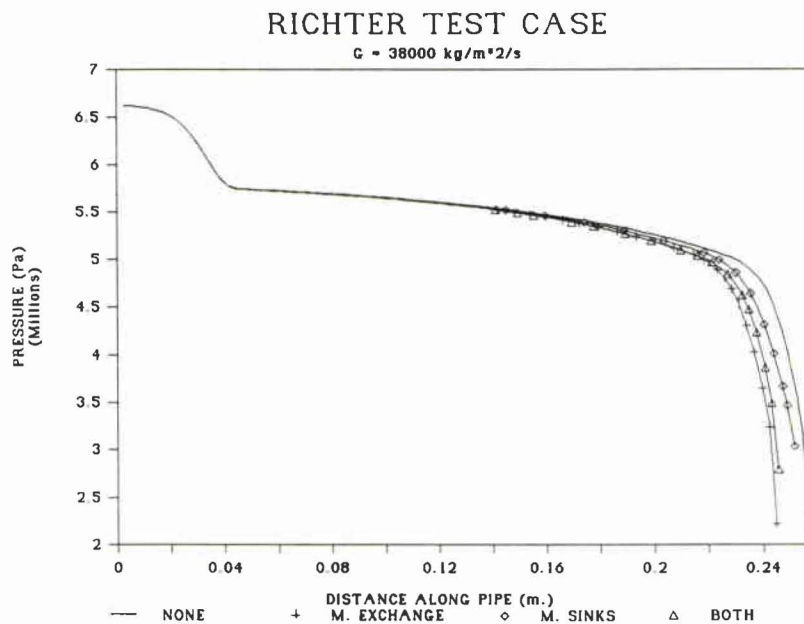


Fig. 5.5: Effect of Interfacial Momentum Term:

5.1.6 INTERFACIAL PARAMETERS:

Other than the interfacial momentum transfer and the virtual mass force, there are three interfacial parameters for which constitutive relations are required; interfacial area, interfacial drag force and interfacial heat transfer.

5.1.6.1 Interfacial Area:

The first of these is the interfacial area per unit volume. For bubble flow, the surface area is calculated from the given number of spheres of a given diameter using the surface area expression for a perfect sphere $N\pi d^2$. Since the two quantities are known for each calculation step, the value can be computed easily. For annular flow the correlation uses the void fraction to calculate the film thickness and compute interfacial area based on a gas cylinder. There is no allowance for wavy interface or

dispersed droplets. Other possible correlations for dispersed flow do exist; however, since they would be applied beyond annular flow, they would only affect the last few percent of the calculation. It was felt that the reasons mentioned previously for only having three flow regimes apply and the increase in complexity would not necessarily improve the accuracy due to the use of less accurate correlations elsewhere in the model.

For churn flow, the area is calculated in all the previously published models using a linear interpolation between the area at the transition point from bubble to churn and from churn to annular flow. This seems to be a standard method of computation, although it is not necessarily representative of the physical changes in the system. A possibly better method of interpolation would be "exponential" interpolation. Given any two points, an exponential curve can be defined between the two using only two constants. If the interpolation points are greater than an order of magnitude apart, it allows for an increasing rate of change which better matches the lower values. A diagram demonstrates the differences in Figure 5.6.

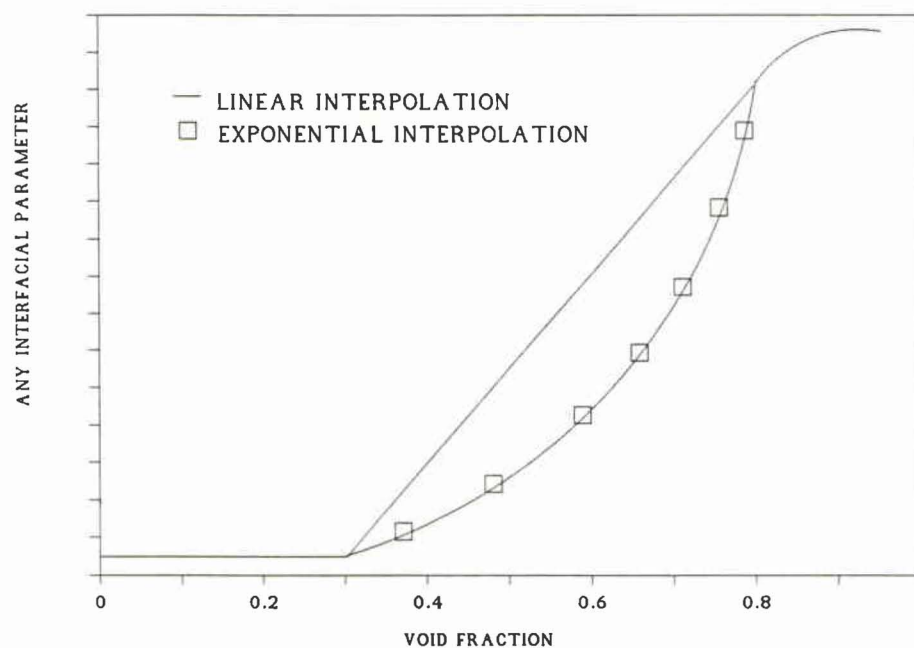


Fig. 5.6: Comparison of Linear and Exponential Interpolation:

Both exponential and linear interpolation have been tried and it was found that linear produced better results. The relationship between the void fraction and the interfacial area is shown in Figure 5.7. As the interfacial area decreases with increasing void fraction in the churn flow regime, using exponential interpolation results in an unrealistically high initial decrease in a_i at lower values of void fraction.

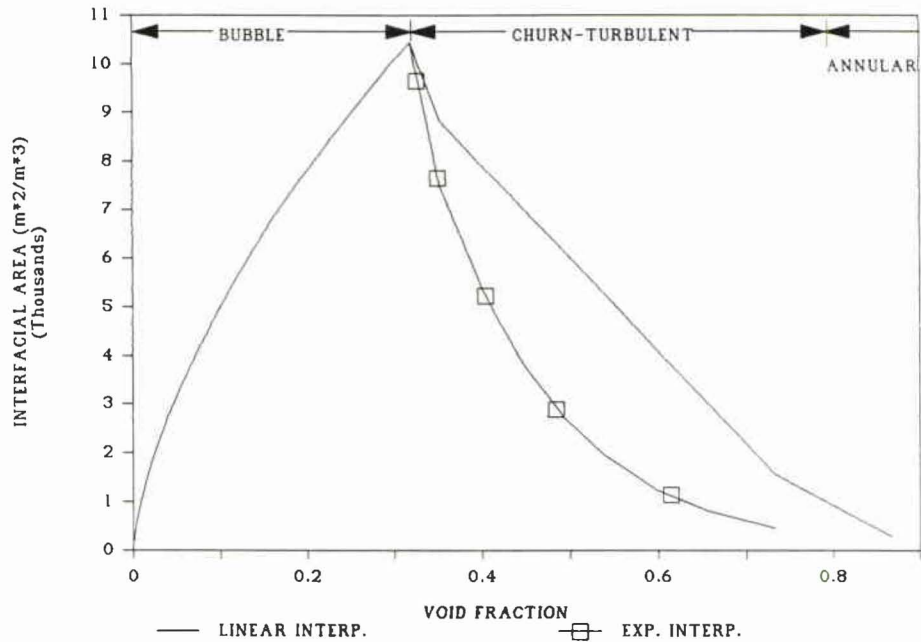


Fig. 5.7: Interfacial Area: Different Interpolation Schemes:

Linear interpolation was the best method tested for churn flow interfacial area given the correlations available.

5.1.6.2 Interfacial Drag Force:

The expression for constant velocity drag force on a spherical bubble is quite well known. A similar equation has been used in almost every two fluid model found:

$$F_D = \frac{1}{2} \frac{A_c}{\alpha} (C_D)_{1-\alpha} \alpha (1-\alpha)^3 \rho_L (u_c - u_L) |u_c - u_L| \quad (5.15)$$

where

$$A_c = \pi \frac{d^2}{4} \quad (5.16)$$

$$C_D = \frac{24}{Re_b} (1 + .15 Re_b^{.687}), Re_b \leq 1000$$

$$= .44, Re_b > 1000 \quad (5.17)$$

$$(C_D)_{1-\alpha} = C_D (1-\alpha)^{-2n} \quad (5.18)$$

The correlation for multi-bubble interaction effects comes from Rowe (1961) with Wallis (1969) suggesting a value of 2.35 for the exponent n .

Al-Sahan (1988) used a paper by Ishii and Zuber (1979) for the interfacial drag. The basic relationship is very similar but the drag coefficient has three forms for three flow sub-regimes. The first two are for bubbly flow and the third is for churn flow up to void fractions of .55. These constitute what would appear to be the state of the art correlations and they agree well with experimental data. At the present, time constraints prevent the use of these expressions. It should be noted that, although they cover churn flow, an expression for the drag force is still required for void fractions of .55 to .8.

For annular flow, the correlation chosen was used in Richter's and Al-Sahan's models from Wallis (1969).

$$a_i = 4\sqrt{\frac{\alpha}{D}} \quad (5.19)$$

$$F_D = \frac{C_{fi}}{2} \rho_c (u_c - u_L) |u_c - u_L| \quad (5.20)$$

where $C_{fi} = .005(1 + 75(1 - \alpha)) \quad (5.21)$

This expression appears to be quite often used. The correlation used by Dobran (1987) for C_{fi} was similar.

For churn flow, the only experimental correlation is from Ishii (1979) and is valid only to void fractions of .55. One could use it all the way to annular flow, but the discrepancy at the transition

point between annular and churn flow is great. It has been observed that, for stable, proper behavior of the solution, the junction at the transition points should be continuous and as smooth as possible.

An equation similar to equation 5.20 can be used for bubble flow for which C_{fi} can be defined as:

$$C_{fi} = \frac{3}{8} (C_D)_{1-\alpha} (1-\alpha)^3 \sqrt{\alpha} \frac{\rho_L D}{\rho_G d} \quad (5.22)$$

Calculating C_{fi} at the bubble to churn change location gives two known values with which to interpolate. The dependence of those known values is primarily on void fraction with slight dependence upon the ratio of densities. For drag coefficient, exponential interpolation proved to be the best. A comparison of the magnitudes of the value and Ishii's correlation follows.

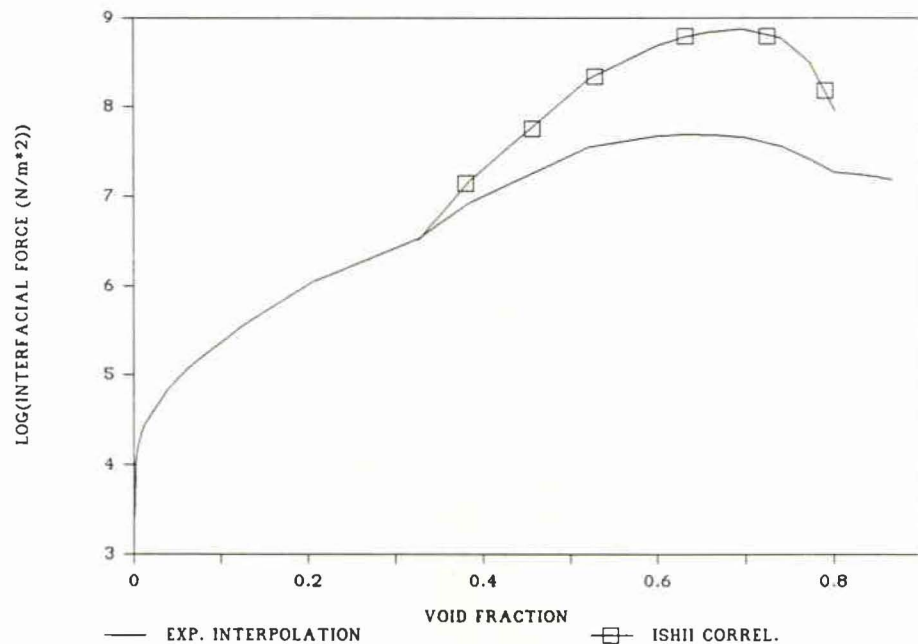


Fig. 5.8: Interpolation of C_{fi} : Comparison of F_{fg} :

This indicates that although exponential interpolation has no physical or experimental basis, the values calculated are similar for the range in which Ishii's correlation is valid.

5.1.6.3 Interfacial Heat Transfer:

The interfacial heat transfer term has the form:

$$q_i = h_i a_i (T_L - T_C) + \frac{W}{A} \frac{dx}{dz} h_{LG} \quad (5.23)$$

The parameters which affect it, for which correlations are needed, are the interfacial area and interfacial heat transfer coefficient. The surface area has been discussed already leaving the heat transfer coefficient.

The expression used for bubble flow is quite standardized:

$$Nu = \frac{h_i d}{k_L} = 2 + .15 Re_b^{1/2} Pr_L^{1/3} \quad (5.24)$$

where

$$Re_b = \frac{\rho_L (u_C - u_L) (1 - \alpha) d}{\mu_L} \quad (5.25)$$

Al-Sahan used slightly different numbers for the constant .15 and the exponent 1/2.

For annular flow, two expressions are used: In Richter and Al-Sahan, the so called Colburn analogy:

$$h_i = \frac{C_{fi}}{2} \rho_L C_{pL} (u_C - u_L) Pr^{-2/3} \quad (5.26)$$

and Dobran used the correlation from Solbrig et al. (1978):

$$Nu = \frac{h_i 2(R - \delta)}{k_C} = .023 Re_b^{.8} Pr^{.4} \quad (5.27)$$

It is important to note that the coefficient for annular flow depends on much more than just the void fraction. The correlation used by Richter and Al-Sahan was chosen.

The annular flow expression is dependent upon relative velocity. While the other variables do not vary much with the change in flow regime, the phase velocities vary greatly. This, and the fact that there are no churn flow heat transfer correlations, made the calculation of heat transfer coefficient in churn flow one of the bigger problems to be solved in the model.

Richter used equation (5.22) to calculate a modified value for C_{fi} at bubble flow and then calculated h_j from equation 5.26 and used linear interpolation with the values for the velocities at bubble flow transition. The other models use similar methods with linear interpolation. A large instantaneous jump in the value of the heat transfer coefficient at the transition point destabilizes the equations so that they predict changes of the primary variables in the wrong direction, i.e. a negative change in void fraction. The equations eventually stabilize and the gradients reverse to the expected direction but this occurs as the simulation is taking place and it lengthens the predicted distance to choking. In Figure 5.9 the interfacial heat transfer coefficient is plotted with respect to void fraction using linear interpolation of the heat transfer coefficient. The discrepancy at the annular transition point and the decrease and then increase in the void fraction demonstrates this underprediction of the coefficient

on the churn side and also the reverse of the void fraction and the recovery. This is not a realistic physical phenomenon either.

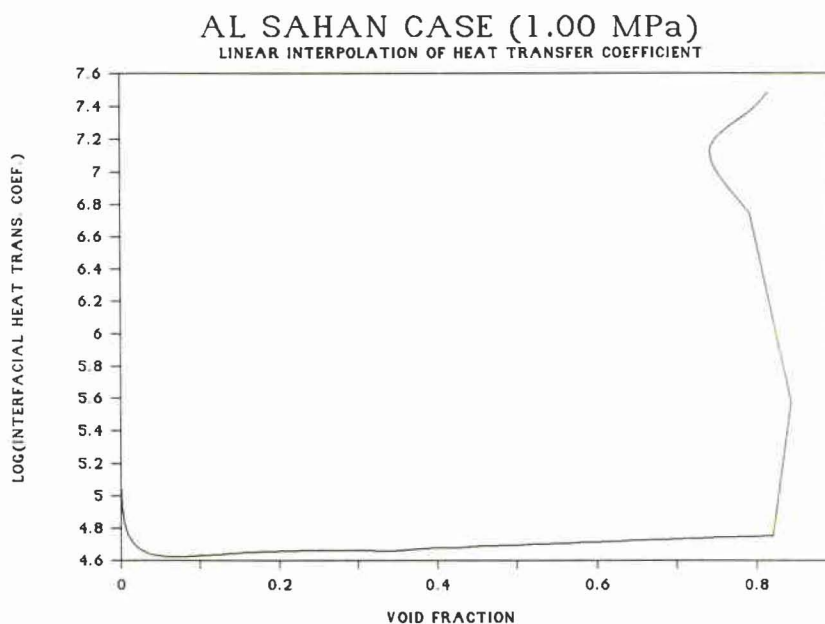


Fig. 5.9: Interfacial Heat Transfer Coefficient with Recovery at Annular Flow

In order to make a better estimate of the heat transfer coefficient at the annular transition, efforts were made to better estimate the gas velocity which accelerates dramatically through the churn flow regime. An attempt was made to estimate the gas velocity at void fraction of .8 using a void fraction-slip correlation. With Chisolm's expression and the definition equation for void fraction, it is possible to iteratively solve for the quality at the flow transition point:

$$k = \left[x \left(\frac{\rho_L}{\rho_G} \right) + 1 - x \right]^{1/2} \quad (5.28)$$

$$\alpha = \left[1 + \frac{W_L \rho_G}{W_G \rho_L k} \right]^{-1} \quad (5.29)$$

Equating the slip in the two equations results in an equation which can be iterated to find x at a void fraction of .8. The gas velocity is calculated using:

$$u_c = \frac{xW}{\rho_c \alpha A} \quad (5.30)$$

Assuming liquid velocity to be approximately the same, the velocity difference can be determined and used for an estimation of heat transfer coefficient at the annular flow transition point. In theory, this should work nicely, but, in practice, it depends on the accuracy of the void fraction correlation. As a result of this and the fact that the liquid velocity does not stay the same, the gas velocity estimate had to be halved for reasonable results and was still relatively unreliable. Instability also arose if the estimate over predicted the coefficient at the transition point by a significant amount. None of the methods so far were satisfactory.

A new simple method was developed which utilized a so-called Heat Transfer Parameter which was simply the heat transfer coefficient divided by the velocity difference. It is easy to get an estimate of this at the annular flow transition point since the correlation becomes independent of velocity. The already calculated bubble heat transfer coefficient is divided by velocity difference and interpolation, exponential or linear, is performed between two known points. This proved to work very well and is easily the best available solution to the problem. It also eliminated the destabilization of the equations. Even if more elaborate curve fits and correlations are developed, removing the velocity dependence is still the best way to get interpolation limits. It was

therefore chosen as the method used for the general model. A comparison sketch of the prediction and interpolation methods is shown in Figure 5.10.

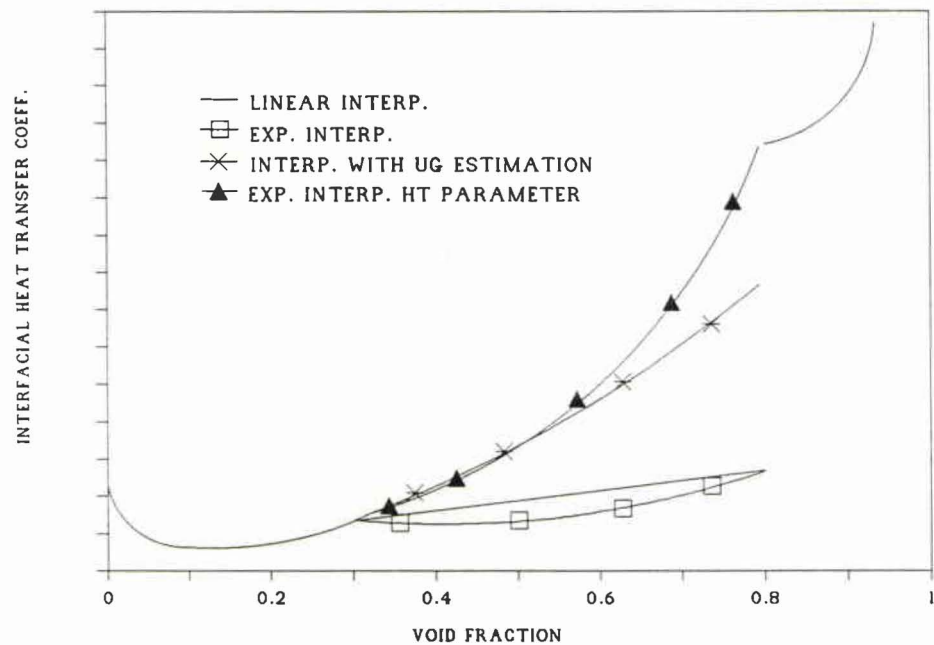


Fig. 5.10: Comparison of Interpolation of Heat Transfer Coefficient:

The effect of the discrepancy of values at the annular transition point results in a similar effect on the interfacial heat transfer as with the interfacial drag force. The superiority of the new method for interfacial heat transfer interpolation can be shown by a comparison of the present models results versus simulation results by Al-Sahan (1988) for the 1.00 MPa test case. A smoother plot and less violent transitions are more characteristic of physical changes in the real world. Figure 5.11 shows a comparison of heat transfer coefficient when calculated by exponential interpolation of the Heat

Transfer Parameter and data taken directly from Al-Sahan's thesis model's simulation. It demonstrates the superiority clearly:

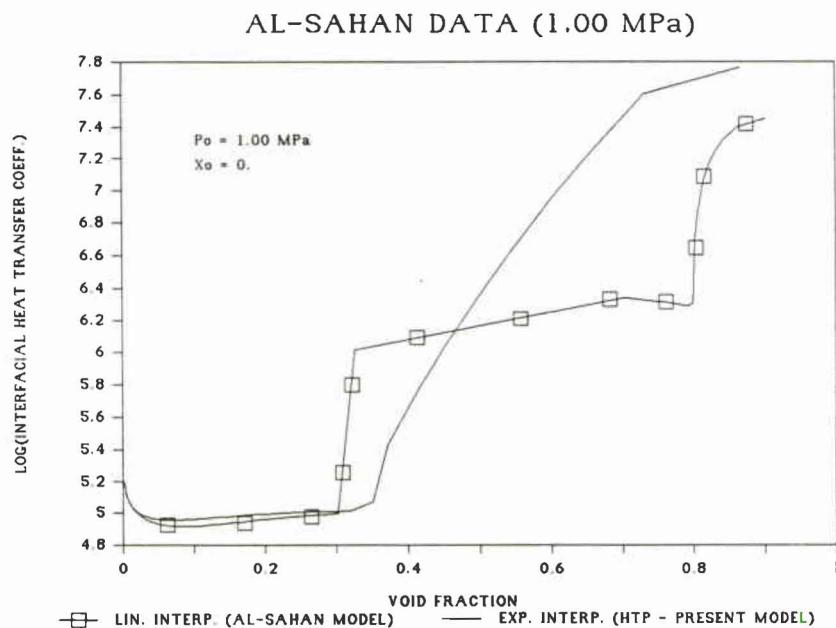


Fig. 5.11: Comparison of Interfacial Heat Transfer Coefficient:

5.1.7 EFFECT OF η IN MOMENTUM TRANSFER:

The effect of η , the proportion of the momentum sinks taken from the gas phase seems to be somewhat parabolic. From Figure 5.12, the results for η of .1 would have slightly lower mass flux than the middle range of values of .25 to .5, but would be quite similar to η of 1.0 which donates all the momentum from the gas. The effect is not dramatic and only affects the last portion of the simulation but further work could be done experimentally to verify the use of $\eta = .5$.

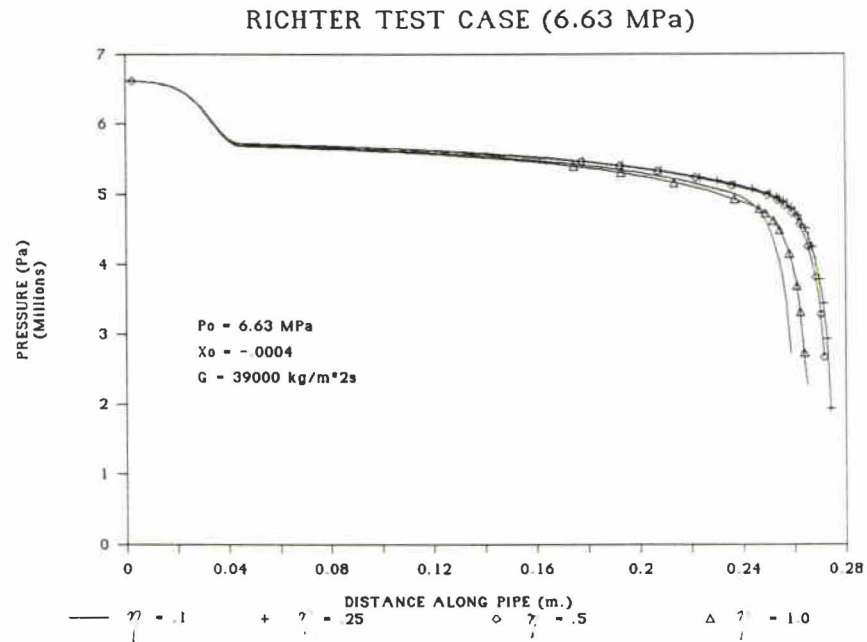


Fig. 5.12: Effect of Momentum Sink Proportion:

5.1.8 EFFECT OF INITIAL BUBBLE DIAMETER:

The effect of d_0 is somewhat interesting. One would expect that decreasing the initial bubble diameter by half would have as much effect in the opposite direction as increasing it. As shown below, this is not the case. It appears that decreasing d_0 below 2.5×10^{-5} m. has little effect; however, increasing it for the same bubble density would decrease the predicted mass flux. Since experimental data has shown that d_0 should perhaps be larger and N smaller, adjusting both might offset each other's consequences somewhat. This could explain why using the possibly "wrong" values could still give reasonable results.

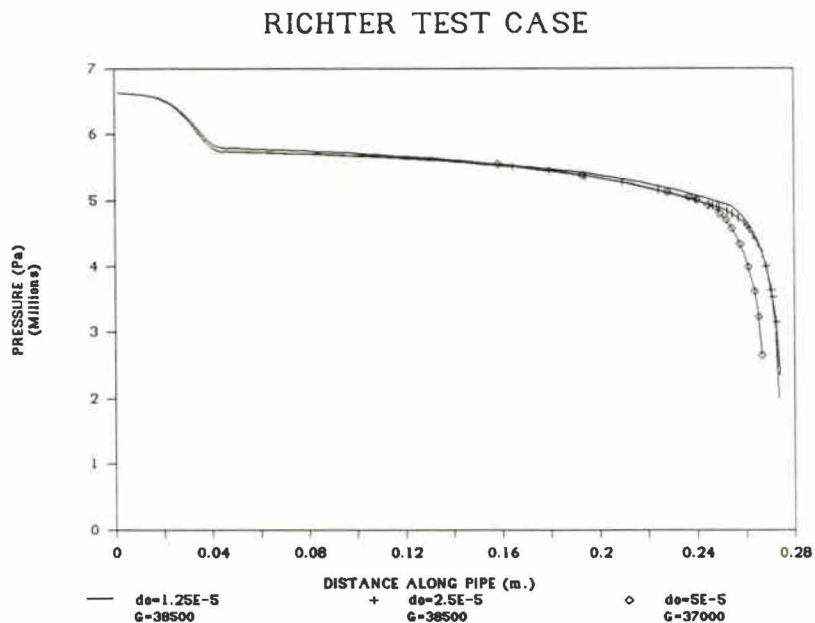


Fig. 5.13: Effect of Initial Bubble Diameter:

5.1.9 THE EFFECT OF INITIAL BUBBLE DENSITY:

The effect of initial bubble density, N , is more dramatic and is shown in Figure 5.14. In these simulations, the mass flux was varied to achieve choking at the same location for different values of N .

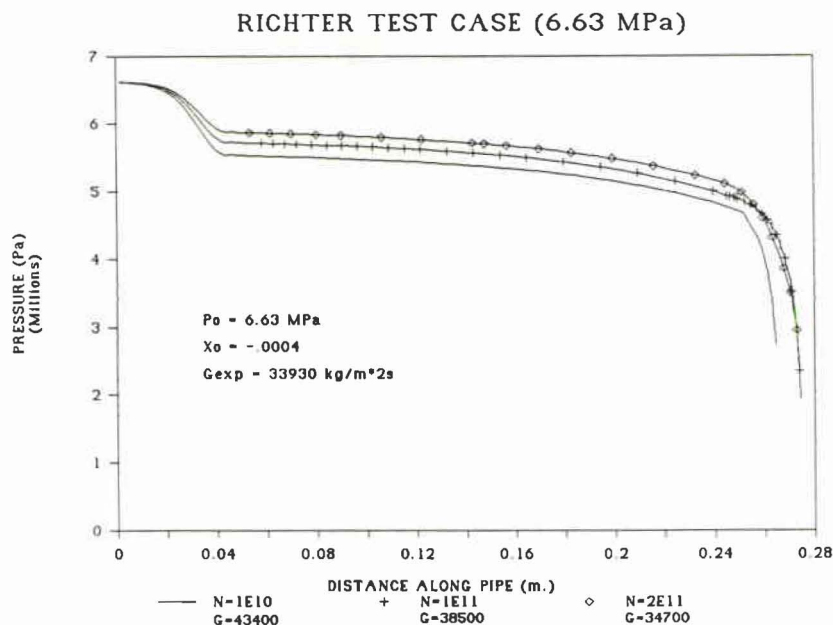


Fig. 5.14: Effect of Initial Bubble Number Density:

With slight differences in pressure drop in the bubble and churn flow regimes, the predicted mass fluxes are very different. If one decreases N , the vapour generation would be less and the choking would occur later in the pipe corresponding to higher mass flux for a given length of pipe. This is the case as demonstrated below. A decrease of a factor of ten changes the predicted mass flux from 38500 to 43400 kg/sm^2 . This is a considerable change. Increasing N by a factor of two decreases the mass flux to 34700 kg/sm^2 . Obviously this parameter has quite an effect. Although this observation differs from those of other researchers, it should be noted that, in the present work, the value is only used initially and it will slowly increase as vapour generation occurs, while in previous models N is a constant. Note that the relative error in experimental versus theoretical mass flux decreases from about 14% to about 2% leading to the use

of N as an empirically adjusted parameter in some models. It would be nice to determine experimentally the effect of pressure on N before using an empirically derived correlation.

5.1.10 SUMMARY OF COMPARISONS:

A chart of the different models demonstrates the main distinctions between them.

Table 5.2: Comparison of Models:

PARAMETER	RICHTER MODEL	DOBRAN MODEL	AL SAHAN MODEL	PRESENT MODEL
VAPOUR ENERGY EQUATION	BALANCE AT THE INTERFACE	SAME AS RICHTER	SAME AS RICHTER	CONSERVATION OF VAPOUR ENERGY
BUBBLE DIAMETER FOUND FROM:	A CHANGE IN BUBBLE DIAMETER EQUATION	THE EQUATION FOR VOID FRACTION	SAME AS DOBRAN	A CHANGE IN BUBBLE DIAMETER EQUATION
BUBBLE DIAMETER EQUATION	$(h_s - h_l) \frac{dd_b}{dz} = \frac{2\bar{h}(T_l - T_c)}{\rho_c u_c} - \frac{\partial h_c d P d_s}{\partial P dz 3}$	$\alpha = \frac{N \pi d^3}{6}$	$\alpha = \frac{N \pi d^3}{6}$	$\frac{dx}{dz} = \frac{3x dx}{d_b dz} + \frac{x du_c}{u_c dz} + \frac{x \partial \rho_c dP}{\rho_c \partial P dz}$
SINGLE PHASE PRESSURE DROP	$f = .02$	$f = \frac{16}{Re_l}; Re_l < 2000$ $f = .079 Re_l^{-.25}; Re_l \geq 2000$	$f = \frac{16}{Re_l}; Re_l \leq 2100$ $\frac{1}{\sqrt{f}} = 3.48 - 4.0 \log \left[\frac{2\epsilon}{D} + \frac{9.35}{Re_l \sqrt{f}} \right]$ $Re_l > 2100$	SAME AS DOBRAN
TWO-PHASE PRESSURE DROP	ϕ_{LO}^2 FROM TABLE INTERPOLATION	$\phi_{LO} = 1 + (\gamma^2 - 1) [B x^{\frac{(2-n)}{2}} (1-x)^{\frac{(2-n)}{2}} + x^{2-n}]$ $\gamma = \frac{f_{CO} \rho_L}{f_{LO} \rho_C}$ $B = B(Y, G)$	$\phi_{LO}^2 = \phi_{LO}^2(x_E, P)$	$\phi_{LO}^2 = \phi_{LO}^2(x_E, P)$ TABLE INTERPOLATION
BUBBLE DRAG FORCE	$F_D = \frac{3(C_D)}{4d} \alpha (1-\alpha)^2 \rho_l u_c - u_l (u_c - u_l)$ $C_D = \frac{24}{Re} (1 + .15 Re^{.687}); Re < 1000$ $= .44; Re \geq 1000$ $(C_D)_{1-\alpha} = C_D (1-\alpha)^{-4.7}$	SAME AS RICHTER	SAME AS RICHTER FOR BUBBLE FLOW BUT USED THE FOLLOWING FOR DISTORTED BUBBLE FLOW: $C_D = \frac{4}{3} f \sqrt{\left(\frac{g d \rho}{\sigma} \right) \left[\frac{1 + 17.67(1-\alpha)^{1.3}}{18.67(1-\alpha)^{1.8}} \right]}$	SAME AS RICHTER

ANNULAR DRAG FORCE	$F_D = \frac{2C_D}{D} \sqrt{\alpha} \rho_c u_c - u_l (u_c - u_l)$ $C_{fi} = .005(1 + 75(1 - \alpha))$	SAME AS RICHTER $C_{fi} = .079 Re_c^{.28} \left[1 + 24(1 - \sqrt{\alpha}) \left(\frac{\rho_l}{\rho_c} \right)^{1/3} \right]$	SAME AS RICHTER	SAME AS RICHTER
CHURN DRAG FORCE	LINEAR INTERPOLATION OF C_{fi}	LINEAR INTERPOLATION OF C_{fi}	$C_D = \frac{8}{3} (1 - \alpha)^2$	EXPONENTIAL INTERPOLATION OF C_{fi} : $C_{fi} = a \exp(b\alpha)$
VIRTUAL MASS FORCE TERM	$F_{vm} = .5 \rho_l u_c \alpha \frac{d}{dz} (u_c - u_l)$	$f_{vm} = \alpha \rho_l C_{vm} \left(u_c \frac{du_c}{dz} - u_l \frac{du_l}{dz} \right)$ $C_{vm} = .3 \tanh(4\sqrt{\alpha})$	$F_{vm} = \rho_l C_{vm} E$ $E = \left[u_c - (2 - \lambda)(u_c - u_l) \right] \frac{du_l}{dz}$ $- \left[u_c - (1 - \lambda)(u_c - u_l) \right] \frac{du_l}{dz}$ $C_{vm} = \frac{1}{2} \alpha \left[\frac{1 + 2\alpha}{1 - \alpha} \right]$ $\lambda = 2(1 - \alpha)$	SAME AS AL SAHAN $C_{vm} = \frac{1}{2} \left[\frac{1 + 2\alpha}{1 - \alpha} \right]$ $\lambda = 2(1 - \alpha)$
BUBBLE INTERFACIAL AREA	$a_i = N \pi d^2$	SAME AS RICHTER	SAME AS RICHTER	SAME AS RICHTER
ANNULAR INTERFACIAL AREA	$a_i = \frac{4\sqrt{\alpha}}{D}$	SAME AS RICHTER	SAME AS RICHTER	SAME AS RICHTER
CHURN FLOW INTERFACIAL AREA	LINEAR INTERPOLATION	LINEAR INTERPOLATION	LINEAR INTERPOLATION	LINEAR INTERPOLATION
BUBBLE INTERFACIAL HEAT TRANSFER	$N = 2 + .6 Re_b^{.55} Pr^{1/3}$ $Re_b = \frac{Re}{(1 - \alpha)}$	SAME AS RICHTER	$N = 2 + .46 Re_b^{.55} Pr^{1/3}$ $Re_b = \frac{Re}{(1 - \alpha)}$	SAME AS RICHTER

ANNULAR INTERFACIAL HEAT TRANSFER	$\bar{h} = \frac{C_{\mu}}{2} \rho_l C_{pl} (u_G - u_L) Pr^{-2/3}$	$N = .023 Re_c^{.8} Pr^{.4}$	SAME AS RICHTER	SAME AS RICHTER
CHURN FLOW INTERFACIAL HEAT TRANSFER	LINEAR INTERPOLATION OF HEAT TRANSFER COEFF. WITH MODIFICATIONS	LINEAR INTERPOLATION OF HEAT TRANSFER COEFF.	SAME AS DOBRAN	EXPONENTIAL INTERPOLATION OF HEAT TRANSFER PARAMETER
INITIAL BUBBLE NUCLEATION DENSITY	$N = 1 * 10^{11} m^{-3}$	SAME AS RICHTER	$N = 3.9 * 10^6 P_o^{4.53}$	$N = 1 * 10^{11} m^{-3}$
BUBBLE DENSITY	N DETERMINED FROM VOID FRACTION AND BUBBLE DIAMETER	N CONSTANT	N CONSTANT	N DETERMINED FROM VOID FRACTION AND BUBBLE DIAMETER
PRESSURE DIFFERENCE WITHIN BUBBLE	$P_G - P_L = \frac{4\sigma}{d}$	$P_G - P_L = \frac{C\sigma^{1.5}}{k_B T_{crit}} \left(\frac{T_o}{T_{crit}} \right)^{13.73}$ $C = .08$	SAME AS RICHTER	SAME AS RICHTER
SOLUTION PROCEDURE	MANUAL MATRIX DECOMPOSITION OF SIMPLE DIFFERENTIALS	MATRIX DECOMPOSITION AND RUNGE-KUTTA INTEGRATION	MATRIX DECOMPOSITION AND PREDICTOR-CORRECTOR IMSL ROUTINE DGEAR	MATRIX DECOMPOSITION AND PREDICTOR-CORRECTOR LIVERMORE ROUTINE LSODAR WITH ROOT FINDING AT TRANSITION POINTS AND CRITICAL PLANE LOCATION
CRITICAL CONDITION	$\left \frac{dp}{dz} \right > 2 * 10^{12} \frac{Pa}{m}$	$\det [A] = 0$ and $\det [A]_{q_1} = 0$ with columns replaced by [B]	$\frac{dP}{dz} < -10^9 \frac{Pa}{m}$	$\frac{dP}{dz} < -2 * 10^{10} \frac{Pa}{m}$

The best available equations and term forms appear to be the full vapour energy conservation equation, interfacial momentum transfer with momentum sinks and using the virtual mass term only in bubble flow with the form by Drew et al. and the coefficients from Ishii and Chawla (1979). A seventh fully expanded equation for bubble diameter and non-constant values for N appear to be useful. The bubble nucleation governed by superheat due to pressure difference across the curved bubble surface agrees well with nucleation theory and, although initial bubble diameter and density are within the range for boiling theory, they do not agree with the most recent experimental work. They are, however, the best available values at the moment.

In single phase, the consensus is to use Moody or Fanning friction factor and, in two-phase, correlations or lookup table interpolation of the Martinelli-Nelson parameter are generally used. In bubble flow, the drag coefficient, interfacial area and heat transfer coefficient are well correlated with generally used expressions. Some work has been done in the area of distorted bubble flow, but, until a larger body of work has been established, there are no generally accepted correlations.

The same is true in annular flow. A set of expressions for the three interfacial terms is commonly used. Although they are far from ideal, they are the best available. The reasons for not using the increased complexity of dispersed flow and homogeneous flow have been previously outlined. It is likely that, in future, better correlations will be developed and used.

The churn flow correlations are all forms of interpolation. The only churn flow expression available was for drag coefficient by Ishii and was only applicable for void fraction up to .5. A comparison of the values predicted shows the experimental correlation close to the interpolation. For interfacial area, because it is slowly decreasing towards annular flow, linear interpolation proved to be the best. For drag coefficient and interfacial heat transfer, the "exponential" interpolation was better due to the large differences in the values at the transition points. The heat transfer parameter proved to be very superior for interpolation compared to heat transfer coefficient.

The best method of solution is the Adams-Moulton method with root-finding. A tolerance of 10^{-5} and critical pressure gradient of $2 \cdot 10^{-12}$ have been found to be the most suitable values for computation.

5.2 COMPARISON WITH EXPERIMENTAL DATA:

There is an extremely large base of experimental data for critical flow, so to attempt to compare simulated results against all of it would be almost impossible. It is difficult to gain access to much of it however. It is important to have as large as possible a range of inlet pressures and pipe length to exit diameter ratios in order to compare for an accurate impression of the effectiveness of the model. What is required is not only mass flux but as many as possible of the physical parameters as well. In most cases, the measured critical mass flux is reported and in some cases the axial pressure variation is included. Four data sets were easily obtainable and quite wide ranging. They were the Sozzi and Sutherland (1975) experimental case used by

Richter as a code verification test, data by Al-Sahan along with model prediction data and results and computer runs from Dobran used in the Al-Sahan thesis and orifice test data done by Celata et al. (1983). These results cover the ranges listed in Table 5.3.

Table 5.3: Chart of Experimental Data Used:

<u>DATA BY</u>	<u>PRESS.</u> <u>(MPa)</u>	<u>DIAM.</u> <u>(m.)</u>	<u>LENGTH</u> <u>(m.)</u>	<u>L/D</u>	<u>SHAPE</u>
Al-Sahan	.20-1.0	.003175	.635	200	straight
Dobran	2.23- 3.49	.0125	1.21, 3.60	97, 288	rounded inlet
Sozzi- Sutherland	6.63	.0127	.2745	21.6	rounded nozzle
Celata	.95	.00125	.001 *	.8	orifice

* Length of orifice not including flow extension

Altogether they represent inlet pressure from .2 to 6.63 MPa and L/D ratios of .8 to 288 and diameters from .00125 to .127. The comparisons are shown in Fig. 5.14 to 5.24 with the experimental pressure data plotted as points if possible.

5.2.1 Al-Sahan Data:

It should be noted that Al-Sahan used the initial bubble density as a parameter which was varied to obtain the best fit with his data. He correlated these values of N_0 with initial pressure P_0 . This results in a closer fit to the data than is possible with constant N . Also, the final runs of this model could have been somewhat closer to the experimental points. When the calculation was done, the mass flux guess which produced choking at a point less than the length of the pipe was taken as the critical mass flux. This means

that the pressure profiles fall off at a shorter distance and do not match the experimental data as well as they could with further iteration of the mass flux guesses (see Fig 5.15-5.19). Also for a small change in the mass flux, a comparably larger change in the location of choking is predicted and this, therefore, lengthens the pressure profile significantly for an almost negligible change in mass flux. The test cases used from Al-Sahan were from a straight pipe with stagnation pressures of .196, .300, .479, .703, and 1.00 MPa. The data included critical discharge and axial pressure variation. Figure 5.15(a) compares the predictions of the present model and Al-Sahan's model with his experimental data for $P_0 = .196$ MPa. Figures 5.15(b) to .15(e) show the predictions of the present model for axial distribution of phase temperatures and velocities and the flow quality and void fraction. A comparison with the 196 kPa case shows that, even with the problems mentioned above, the model predictions are as good as those of Al-Sahan.

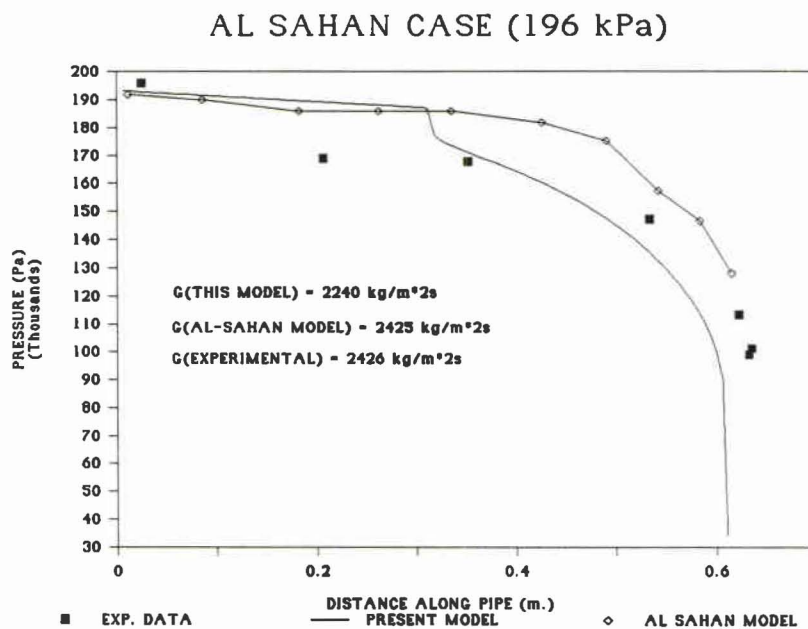


Fig. 5.15(a): Al-Sahan Data .196 MPa: Pressure:

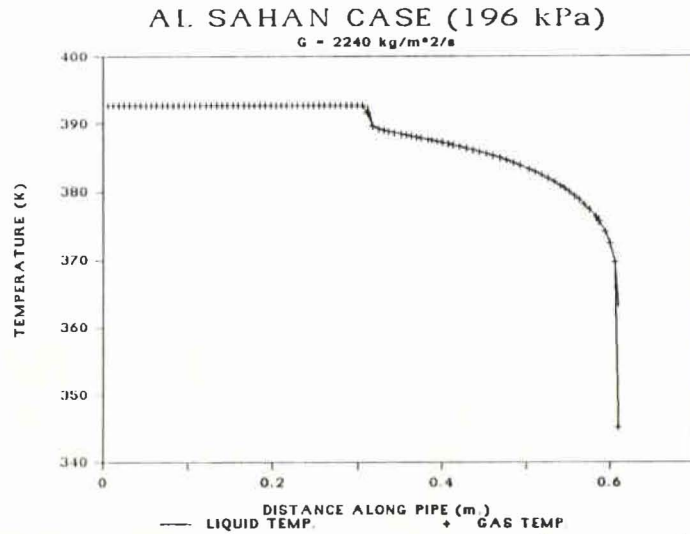


Fig. 5.15(b): Al Sahhan Simulation .196 MPa: Temperature:

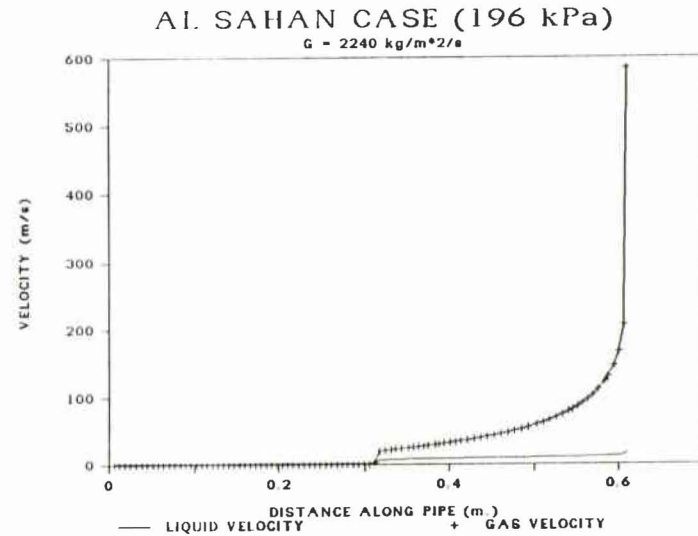


Fig. 5.15(c): Al Sahhan Simulation .196 MPa: Velocity:

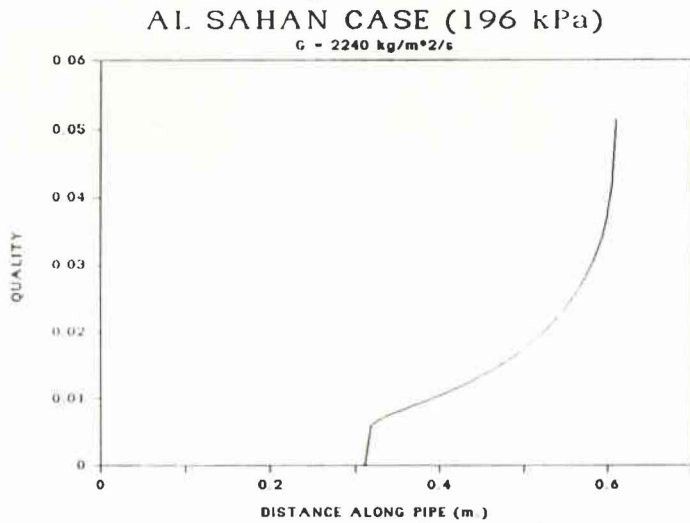


Fig. 5.15(d): Al Sahhan Simulation .196 MPa: Quality:

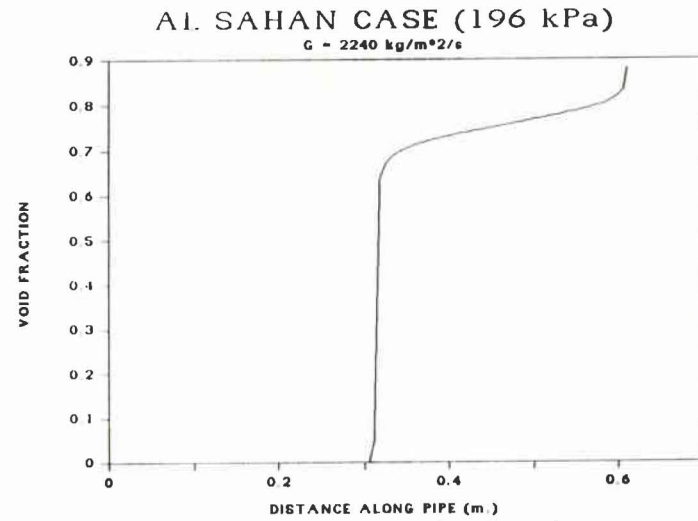
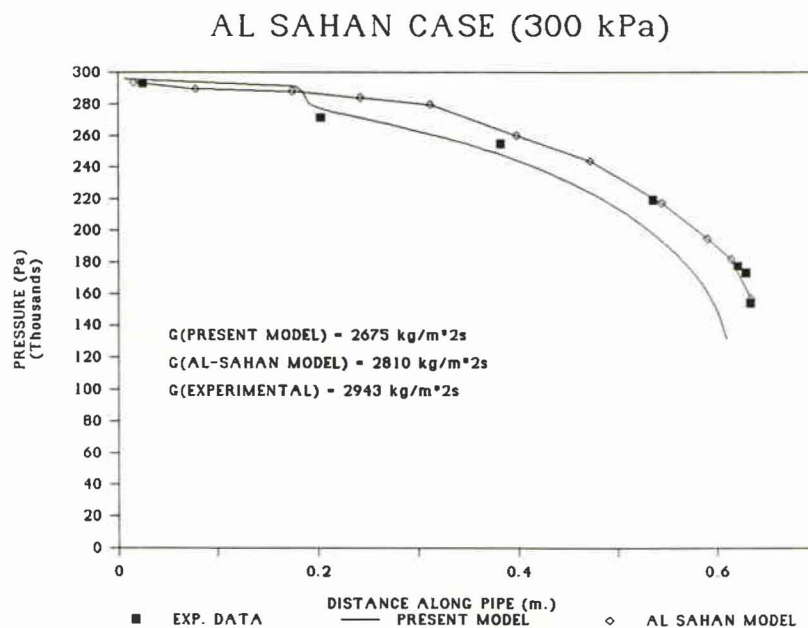


Fig. 5.15(e): Al Sahhan Simulation .196 MPa: Void Fraction:

The 300 kPa case in Figure 5.16 shows the Al-Sahan prediction is closer to the experimental pressure profile but, again for this simulation, closest choking was at .613 m. The initial pressure drop is followed better by the present model. It is interesting to note that, in both these cases, the single phase portions of the simulations appear to be "too long". If the initial bubble diameter was increased, the pressure difference required for nucleation would decrease and nucleation would occur slightly sooner.



**Fig. 5.16(a): Al-Sahan Data Simulations .300 MPa:
Pressure:**

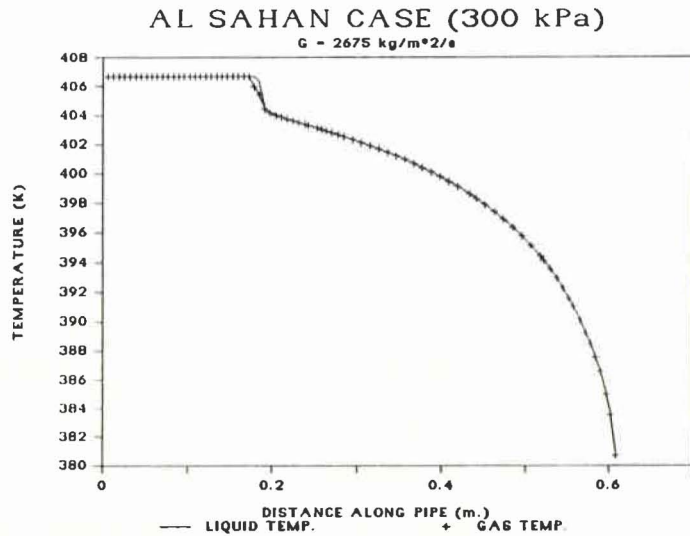


Fig. 5.16(b): Al Sahan Simulation .300 MPa: Temperature:

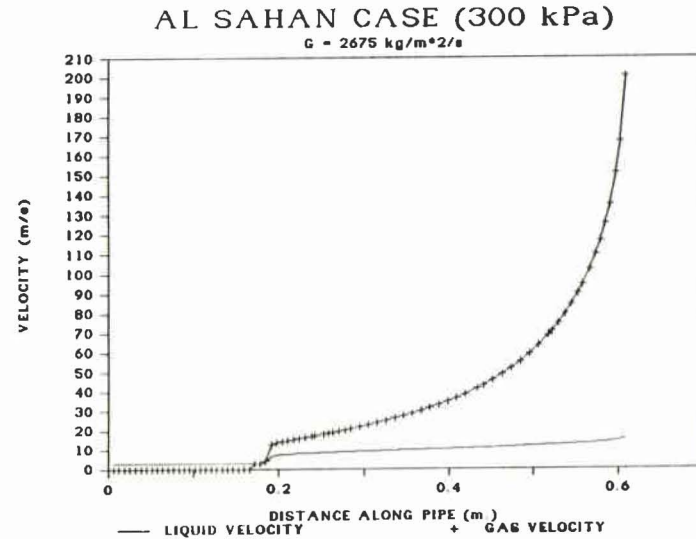


Fig. 5.16(c): Al Sahan Simulation .300 MPa: Velocity:

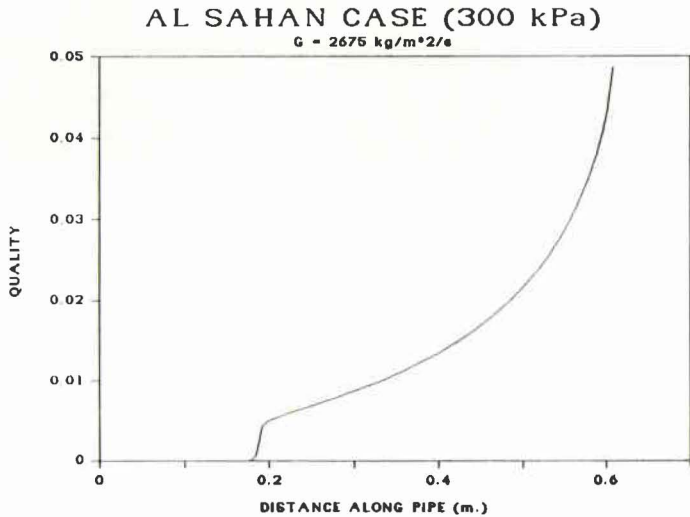


Fig. 5.16(d): Al Sahan Simulation .300 MPa: Quality:

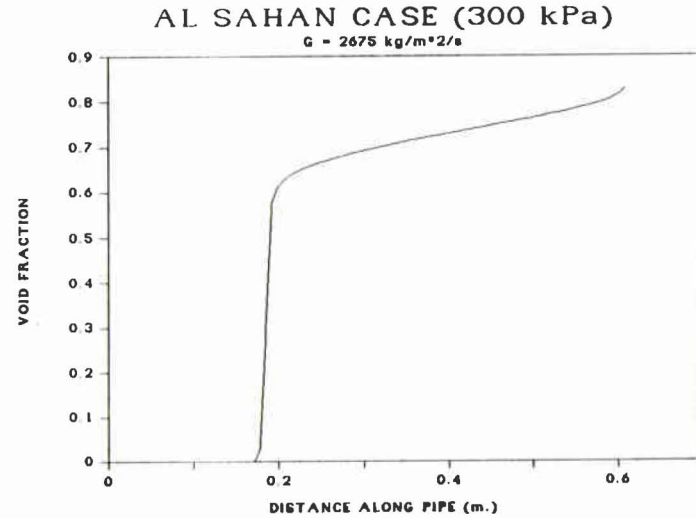
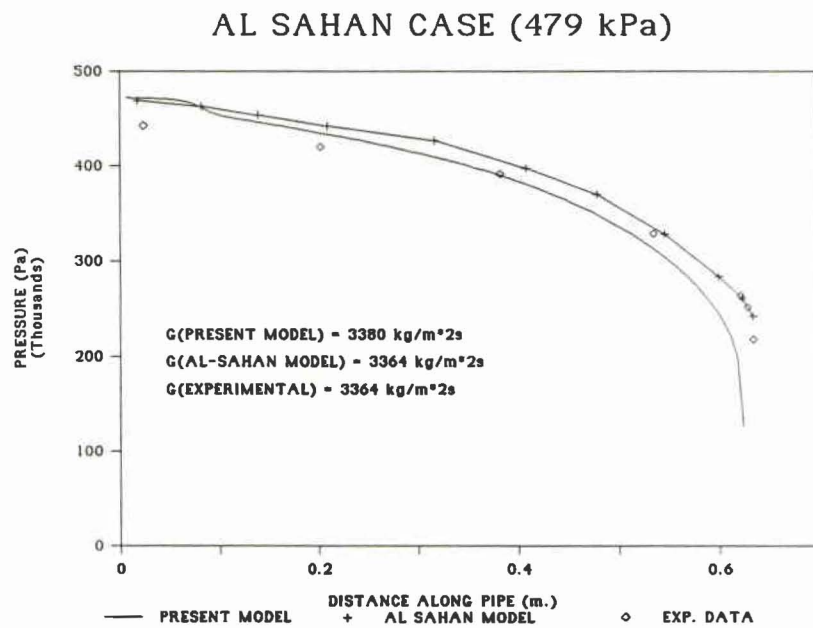


Fig. 5.16(e): Al Sahan Simulation .300 MPa: Void Fraction:

Figures 5.17, 5.18 and 5.19 show the simulation of Al-Sahan's tests for $P_0 = .479, .703,$ and 1.000 MPa respectively.



**Fig. 5.17(a): Al-Sahan Data Simulations .479 MPa:
Pressure:**

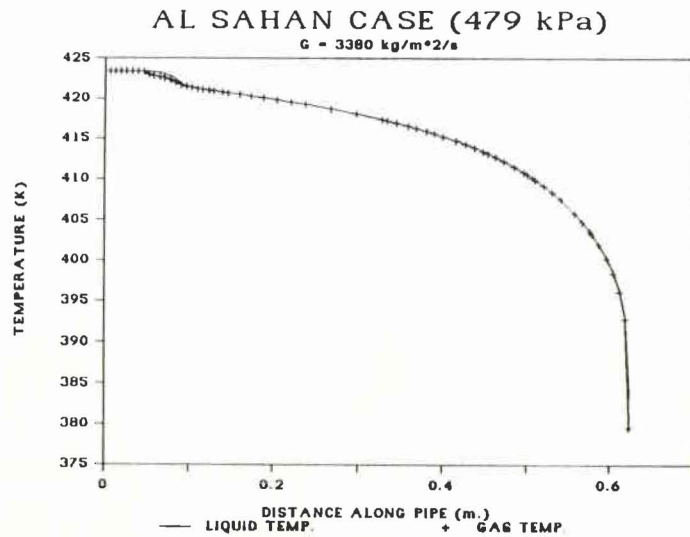


Fig. 5.17(b): Al Sahhan Simulation .479 MPa: Temperature:

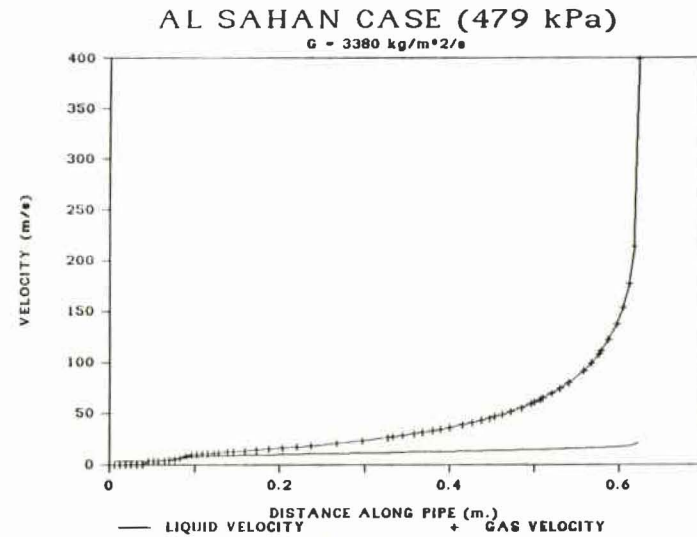


Fig. 5.17(c): Al Sahhan Simulation .479 MPa: Velocity:

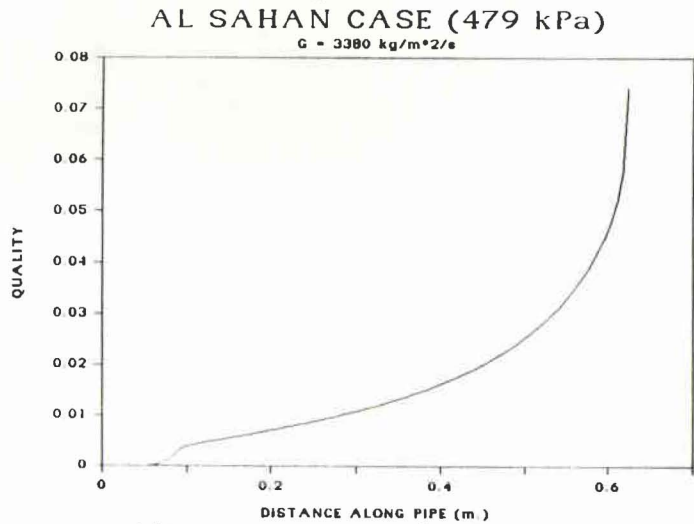


Fig. 5.17(d): Al Sahhan Simulation .479 MPa: Quality:

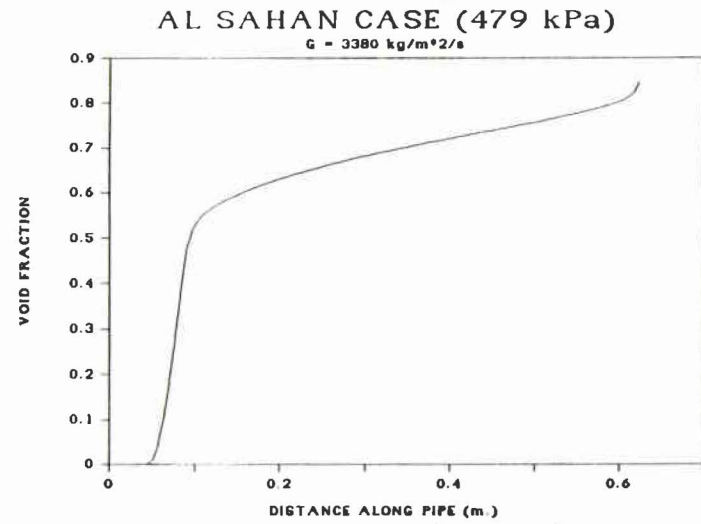
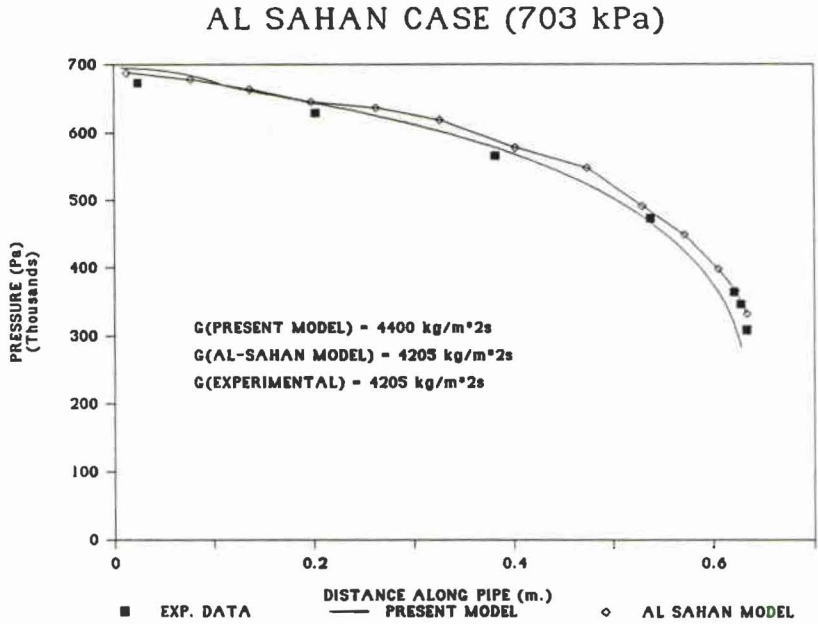


Fig. 5.17(e): Al Sahhan Simulation .479 MPa: Void Fraction:



**Fig. 5.18(a): Al-Sahan Data Simulations .703 MPa:
Pressure:**

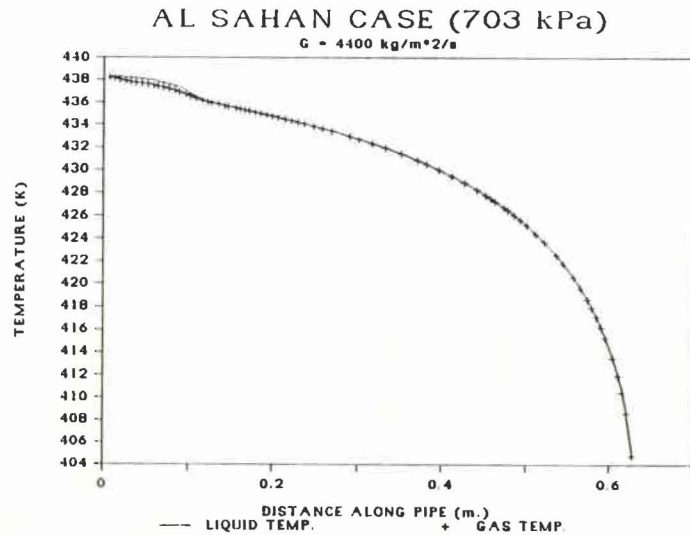


Fig. 5.18(b): Al Sahan Simulation .703 MPa: Temperature:

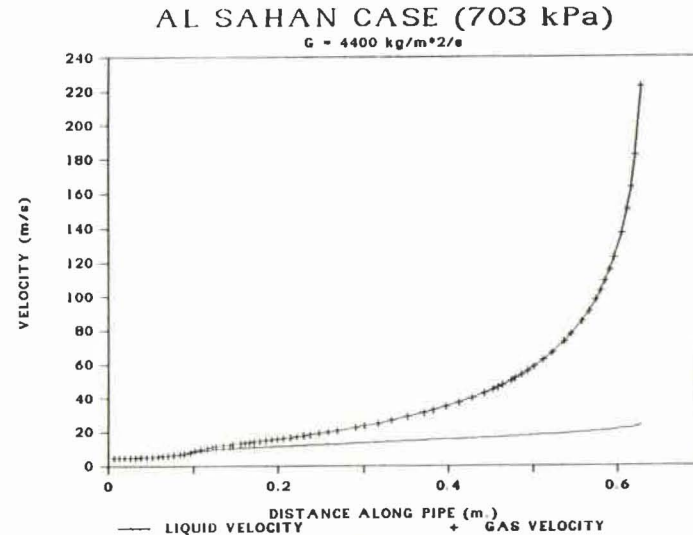


Fig. 5.18(c): Al Sahan Simulation .703 MPa: Velocity:

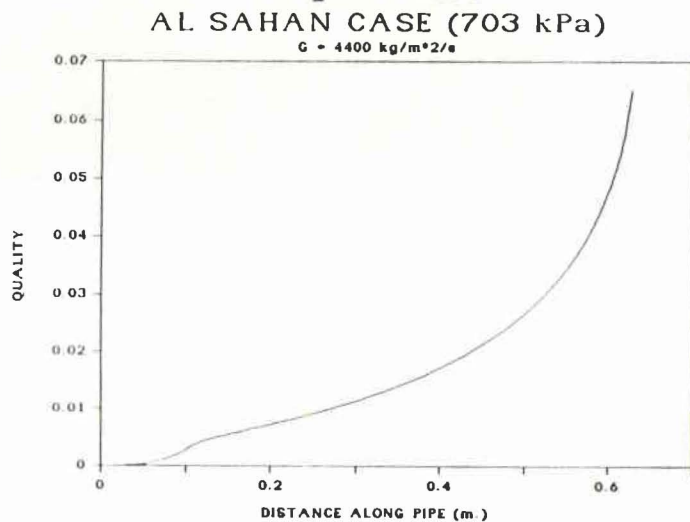


Fig. 5.18(d): Al Sahan Simulation .703 MPa: Quality:

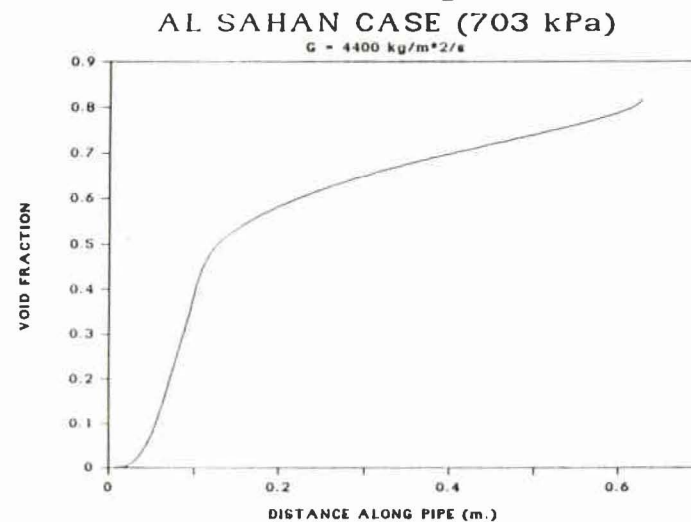
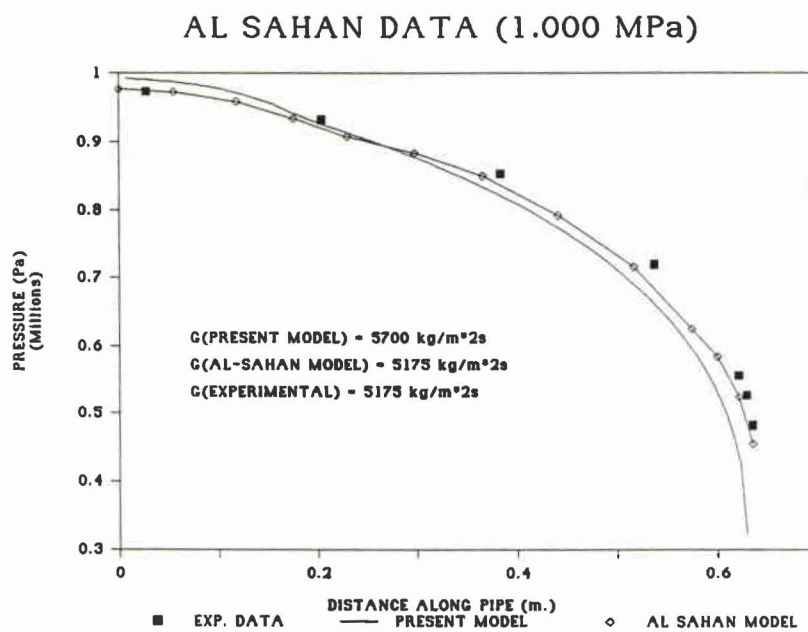


Fig. 5.18(e): Al Sahan Simulation .703 MPa: Void Fraction:



**Fig. 5.19(a): Al-Sahan Data Simulations 1.000 MPa:
Pressure:**

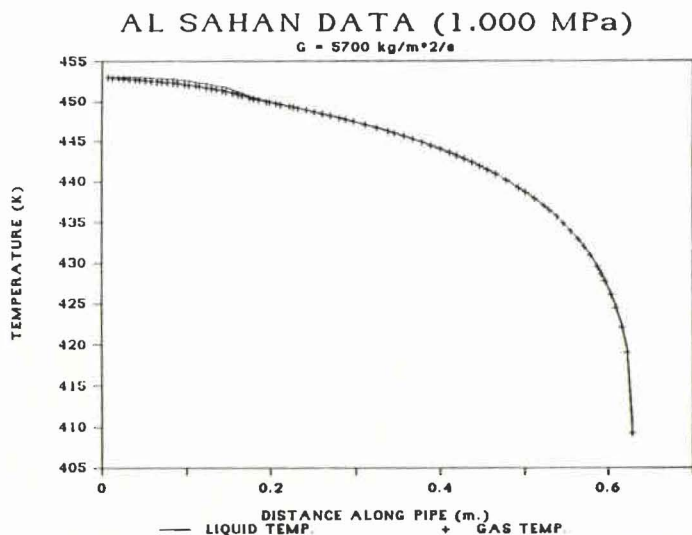


Fig. 5.19(b): Al Sahhan Simulation 1.00 MPa: Temperature:

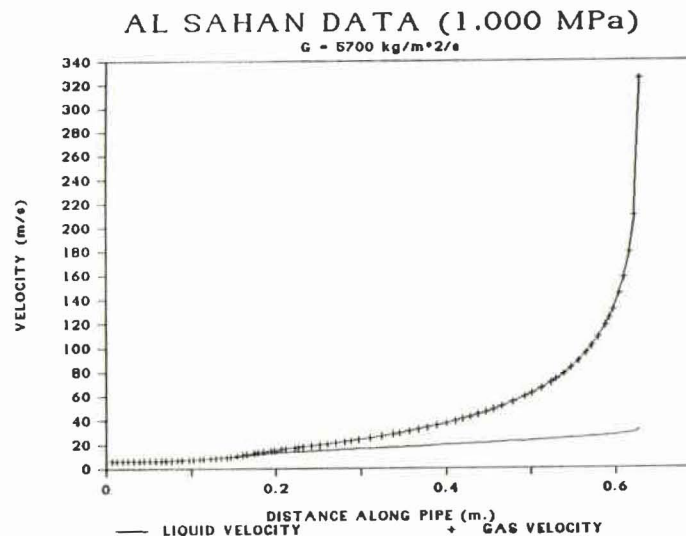


Fig. 5.19(c): Al Sahhan Simulation 1.00 MPa: Velocity:

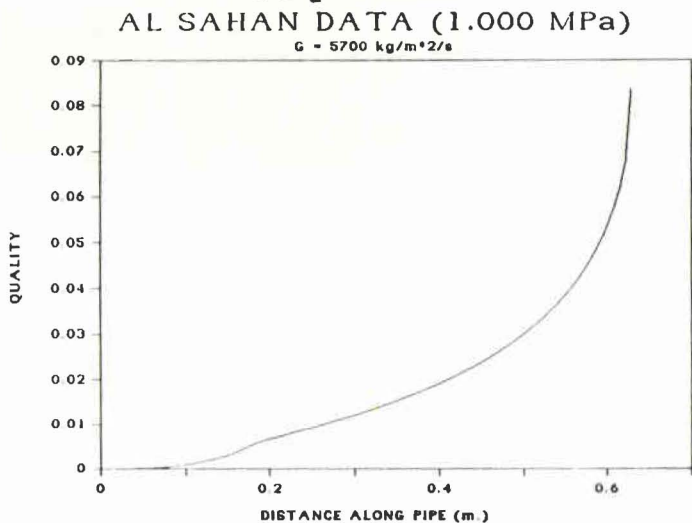


Fig. 5.19(d): Al Sahhan Simulation 1.00 MPa: Quality:

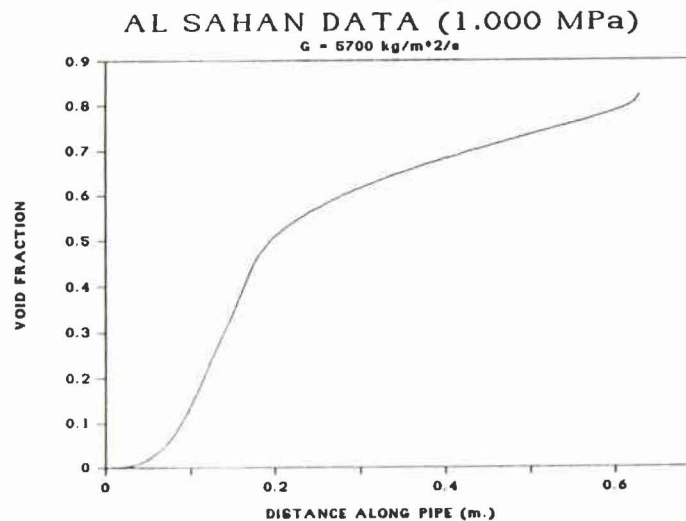


Fig. 5.19(e): Al Sahhan Simulation 1.00 MPa: Void Fraction:

The 479 kPa case demonstrates that initially the present model is closer and later it is worse. This is likely due to choking location. The 700 kPa and 1000 kPa cases demonstrate that the model is as good as Al-Sahan although it falls off a bit at the choking location of the 1000 kPa case. The data for comparison purposes was digitized from the thesis graphs using a graphics tablet and Autocad and plotted with Lotus 1-2-3. This allows for relatively accurate comparisons within 2-3 %. It is important to note that the pressure is not the only variable of interest and the other primary variables give an indication of the performance of the model. Intuitively, the variables should change smoothly and relatively continuously. A direct comparison of the 1000 kPa case for void fraction shown in Figure 5.20 demonstrates the superiority of the present model over Al-Sahan's. Note that the difference in the type of void fraction profile between this case and the Richter case is due to the different geometry and length of the test sections, and the different inlet conditions.

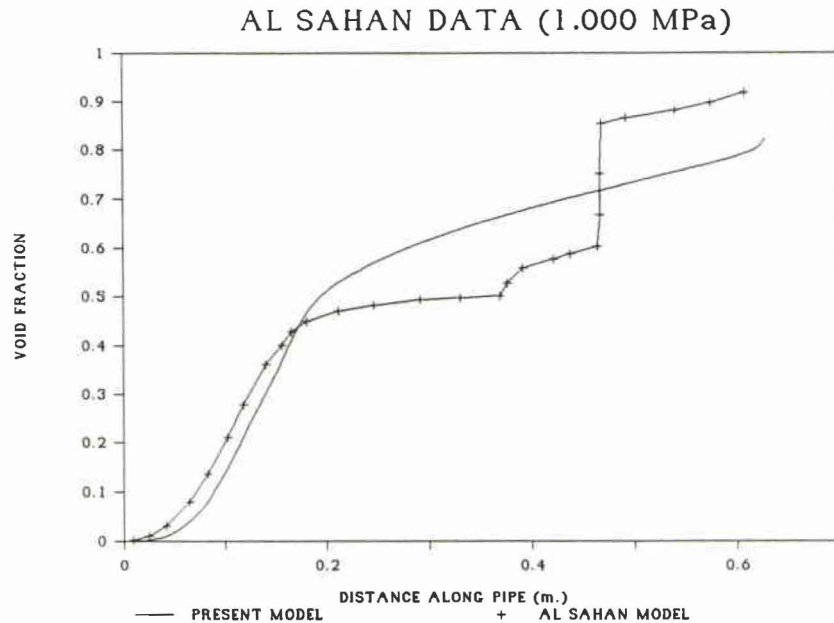


Fig. 5.20: Comparison of Predicted Void Fractions:

5.2.2 Dobran Data:

The Dobran data has been analyzed without exact pipe geometry. An estimate of the entrance shape was made but the exact pipe diameter function could not be found in the literature. Figure 5.21(a) shows the experimental axial pressure distribution together with simulations by Dobran, Al-Sahan and the present model. The plots demonstrated a considerable discrepancy in the pressure plots but the mass flux values predicted are closer to the experimental than Al-Sahan's (see Fig. 5.21-5.23). Although the 3.49 MPa case is not bad and could be improved slightly by decreasing the mass flux slightly, the pressure in all the cases is underpredicted by a considerable measure especially at the end of the pipe. At this time no explanation of this discrepancy can be offered. The worst error in the

prediction of all the mass fluxes occurs for the 3.49 MPa case with an error of 20%. This is still better than even Dobran's results.

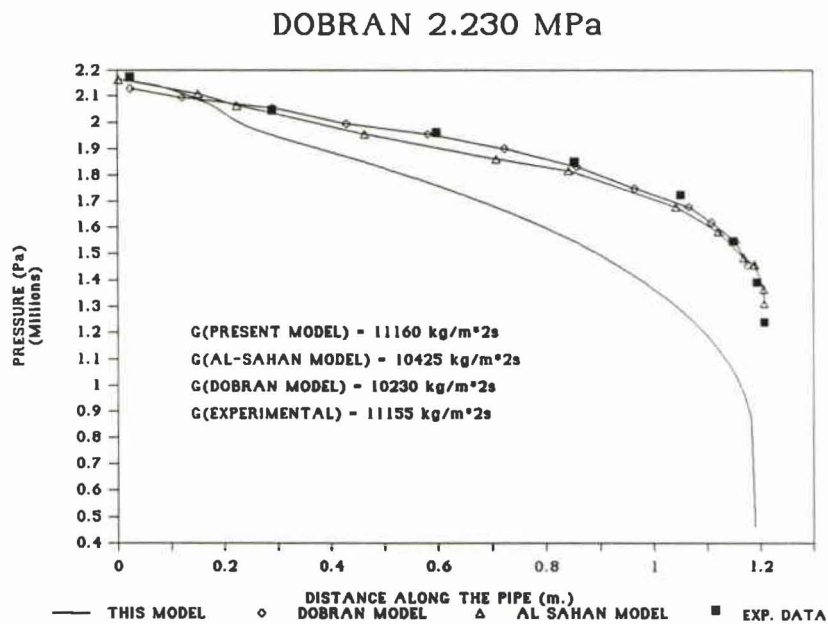


Fig. 5.21(a): Dobran Simulation 2.23 MPa: Pressure:

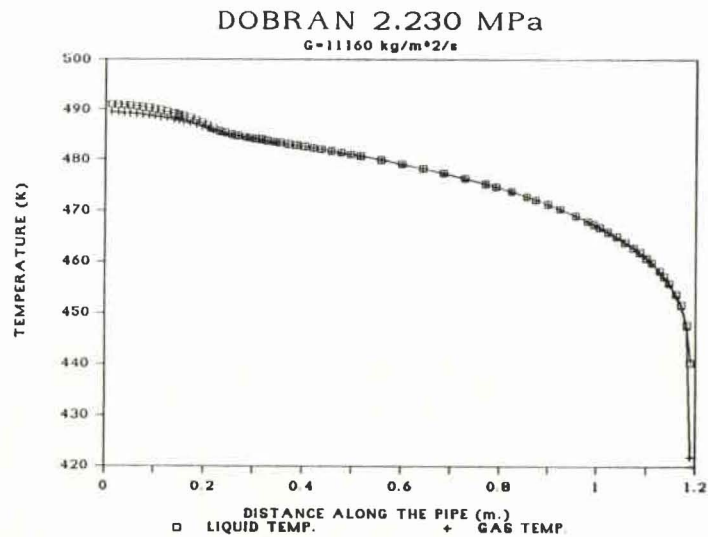


Fig. 5.21(b): Dobran Simulation 2.23 MPa: Temperature:

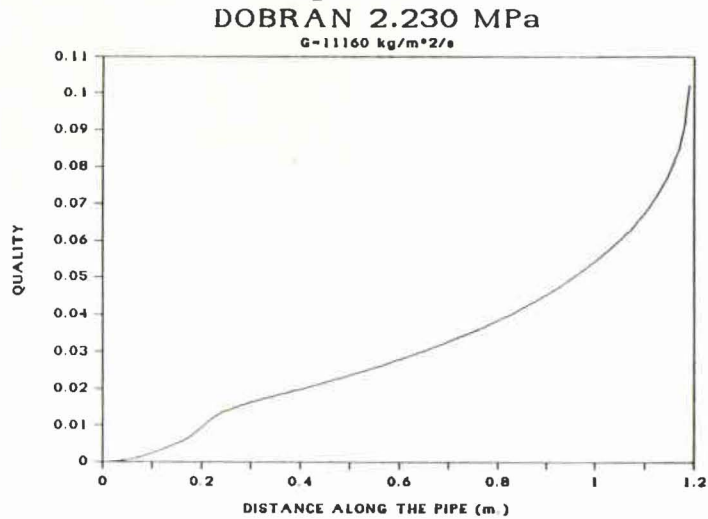


Fig. 5.21(d): Dobran Simulation 2.23 MPa: Quality:

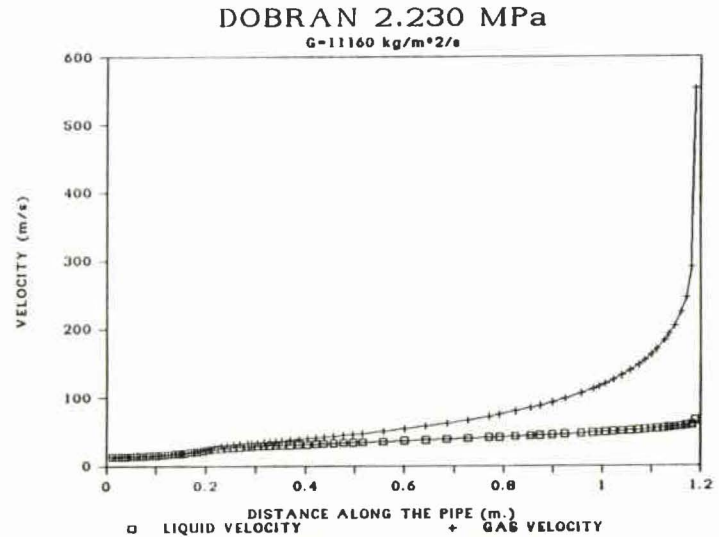


Fig. 5.21(c): Dobran Simulation 2.23 MPa: Velocity:

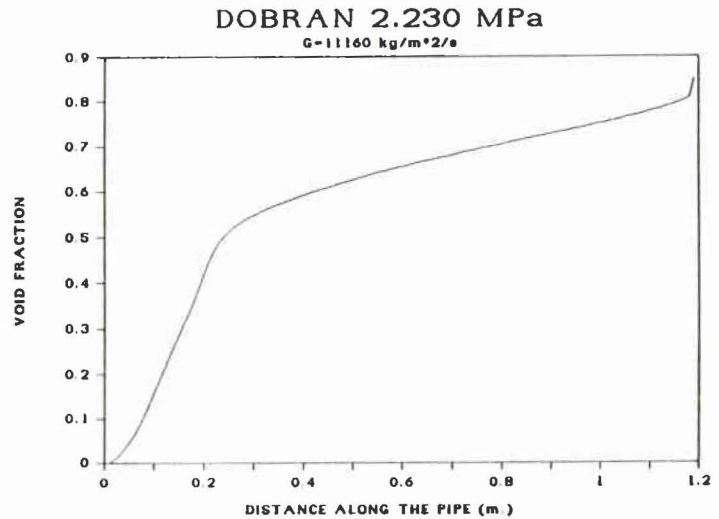


Fig. 5.21(e): Dobran Simulation 2.23 MPa: Void Fraction:

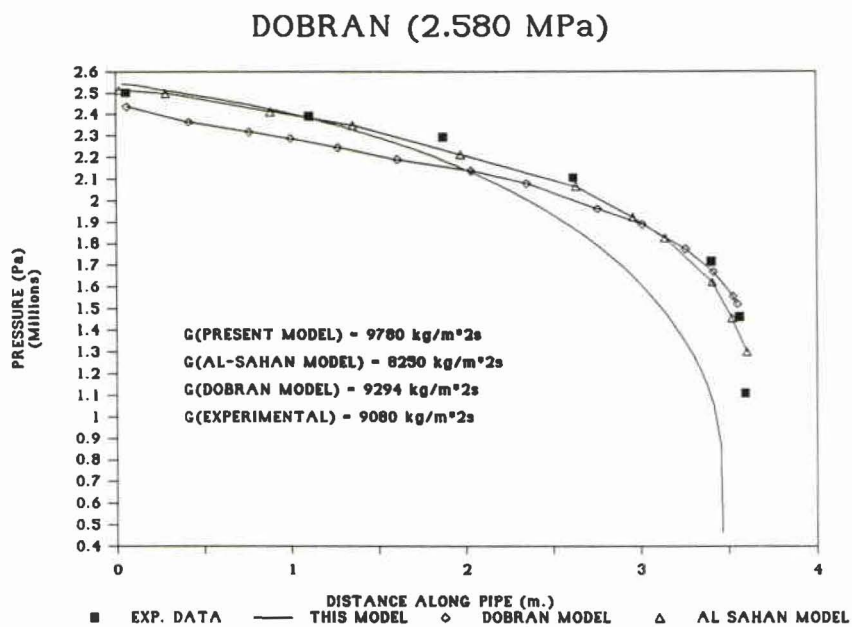


Fig. 5.22(a): Dobran Simulation 2.58 MPa: Pressure:

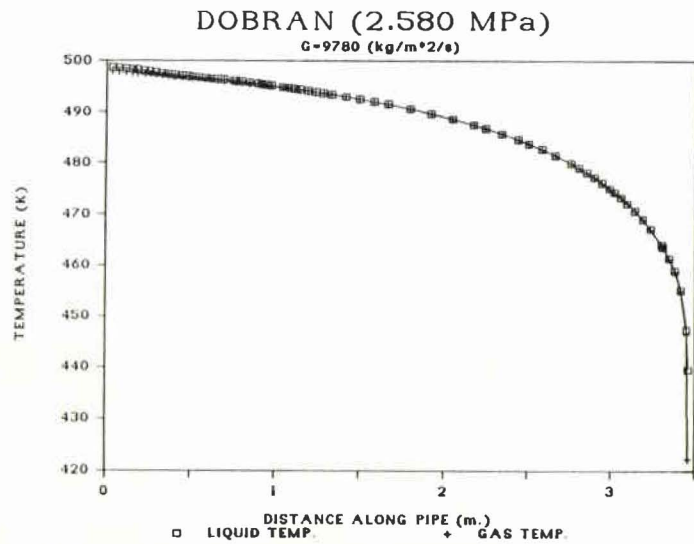


Fig. 5.22(b): Dobran Simulation 2.58 MPa: Temperature:

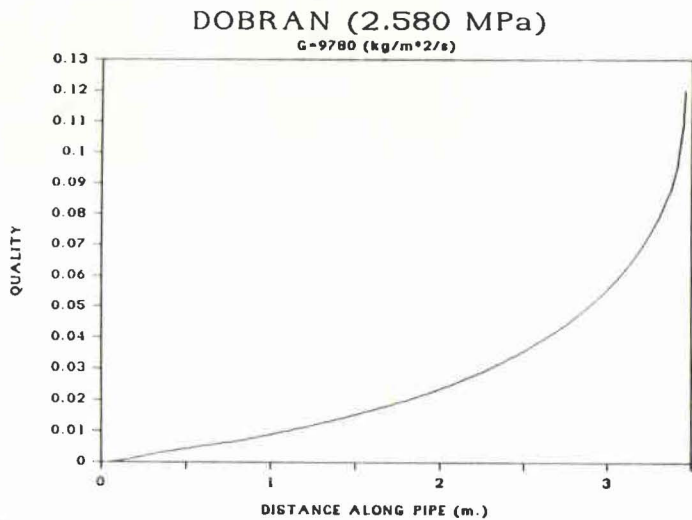


Fig. 5.22(d): Dobran Simulation 2.58 MPa: Quality:

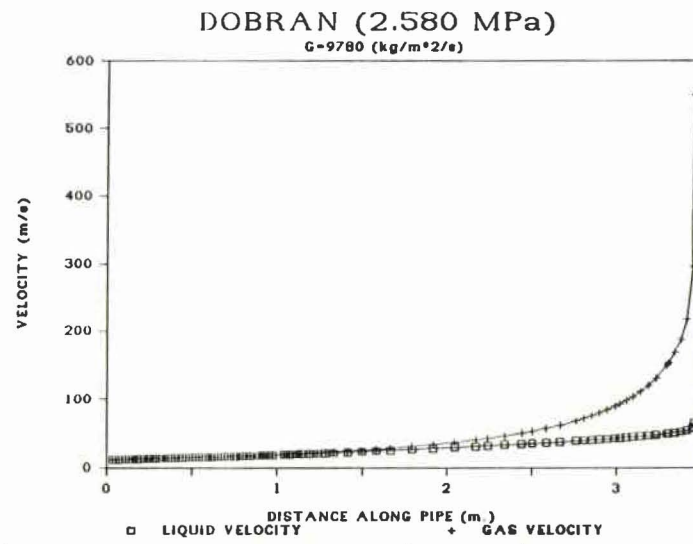


Fig. 5.22(c): Dobran Simulation 2.58 MPa: Velocity:

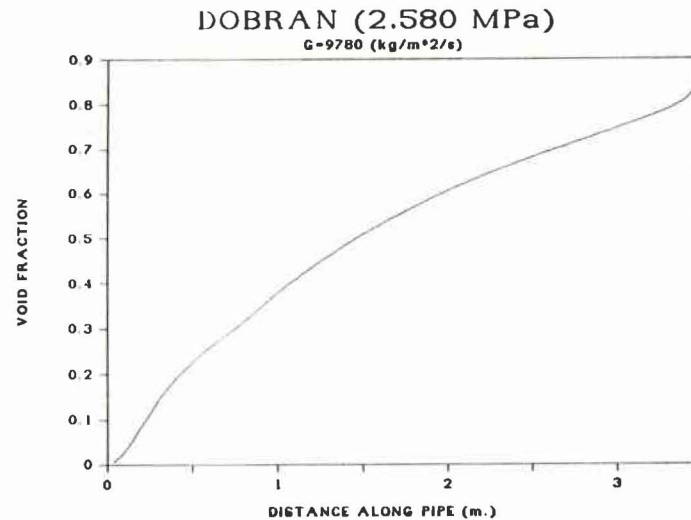


Fig. 5.22(e): Dobran Simulation 2.58 MPa: Void Fraction:

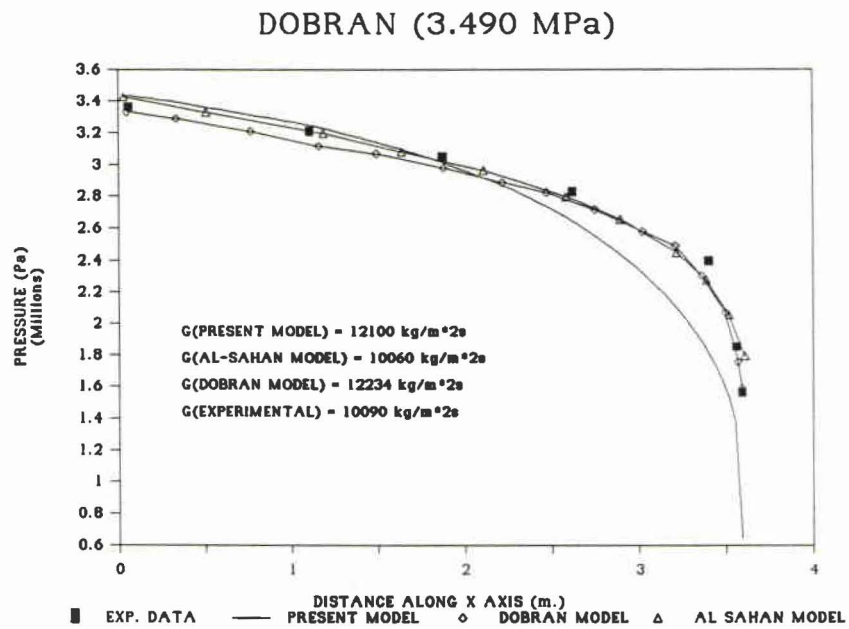
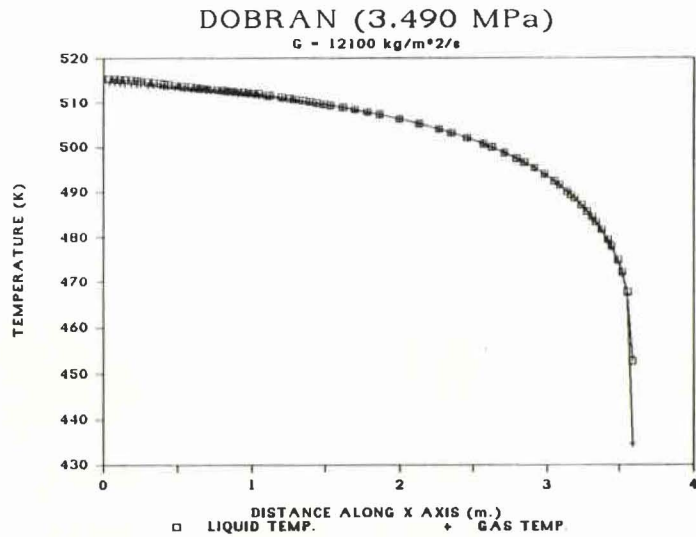
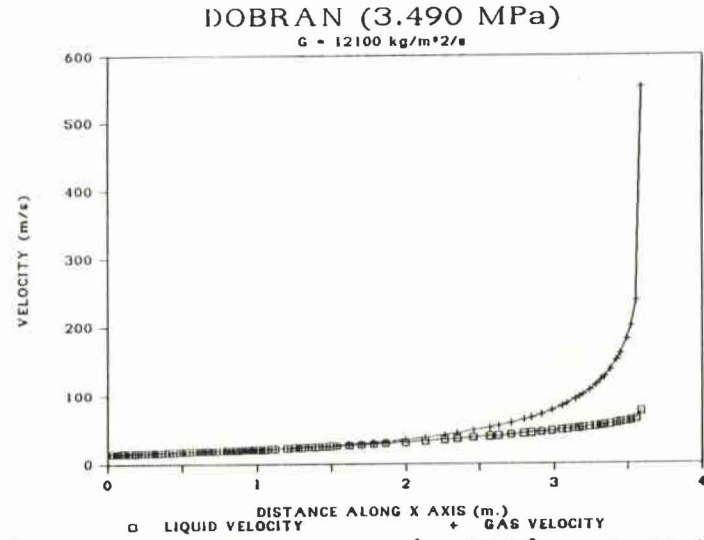


Fig. 5.23(a): Dobran Simulation 3.49 MPa: Pressure:



**Fig. 5.23(b): Dobran Simulation 3.49 MPa:
Temperature:**
DOBRAN (3.490 MPa)
G = 12100 kg/m²/s



**Fig. 5.23(c): Dobran Simulation 3.49 MPa:
Velocity:**
DOBRAN (3.490 MPa)
G = 12100 kg/m²/s

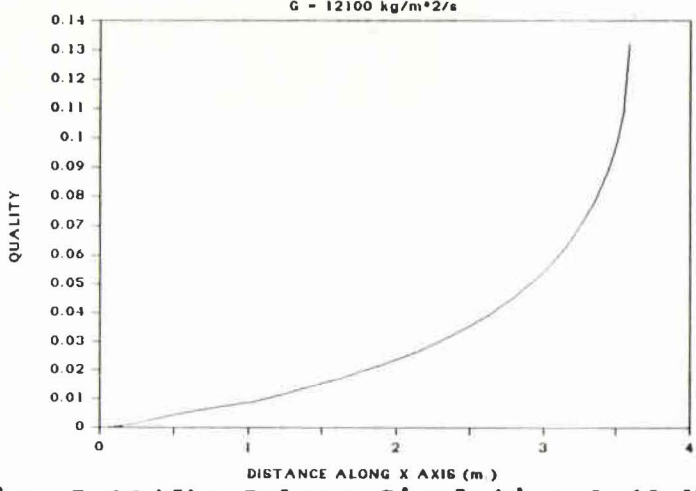


**Fig. 5.23(d): Dobran Simulation 3.49 MPa:
Quality:**

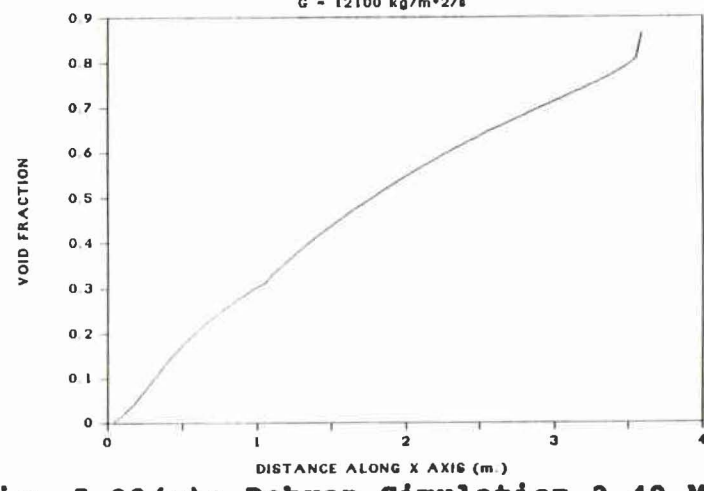


**Fig. 5.23(e): Dobran Simulation 3.49 MPa:
Void Fraction:**

5.2.3 Richter Test Case:

The Richter test case from Sozzi and Sutherland (1975) data shows a very good agreement between the simulations but the general model has a sharper pressure gradient. In the higher pressure experimental runs, this has been noticeable in the experimental data plots. Because of this, the present model would seem to agree well with expected results.

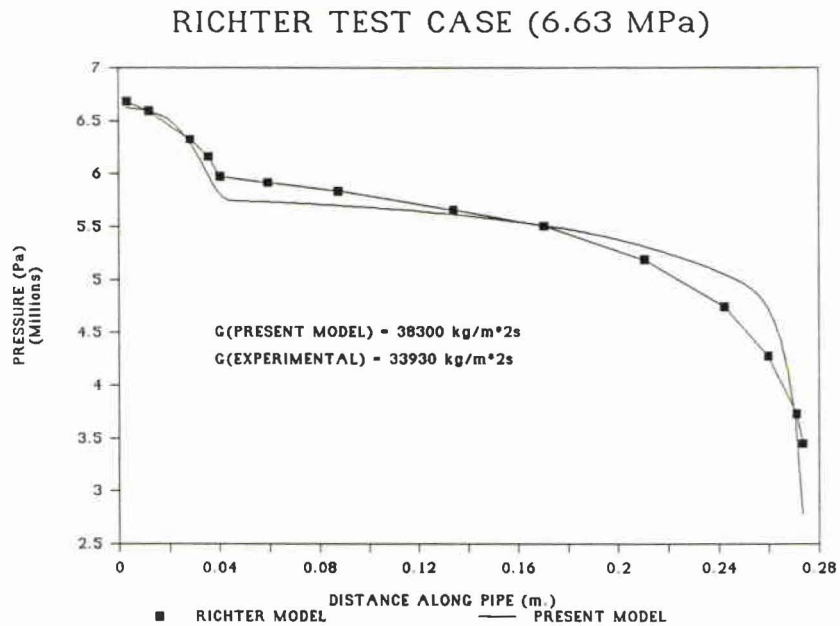


Fig. 5.24(a): Richter Simulation 6.63 MPa: Pressure:

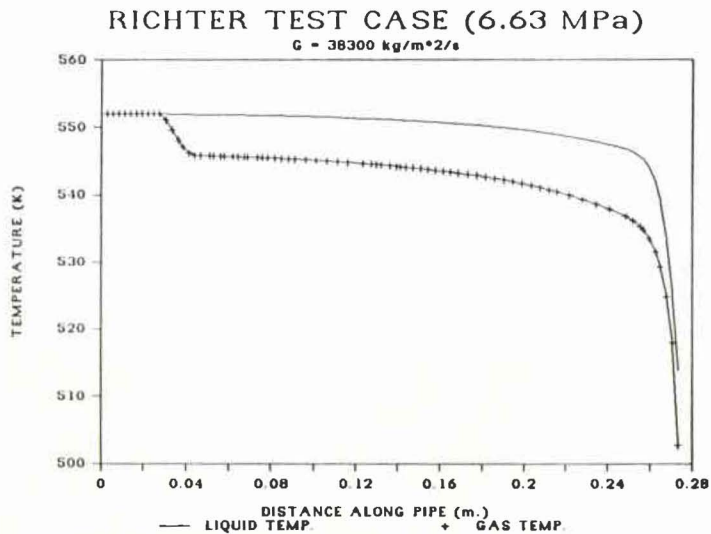


Fig. 5.24(b): Richter Simulation 6.63 MPa: Temperature:

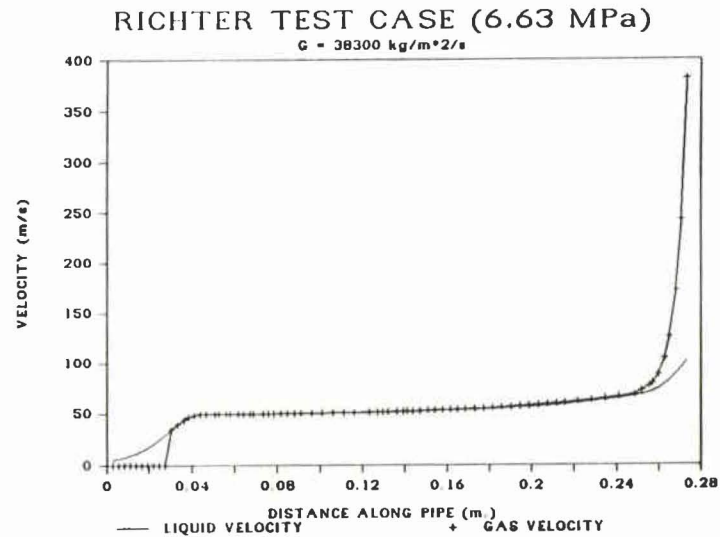


Fig. 5.24(c): Richter Simulation 6.63 MPa: Velocity:

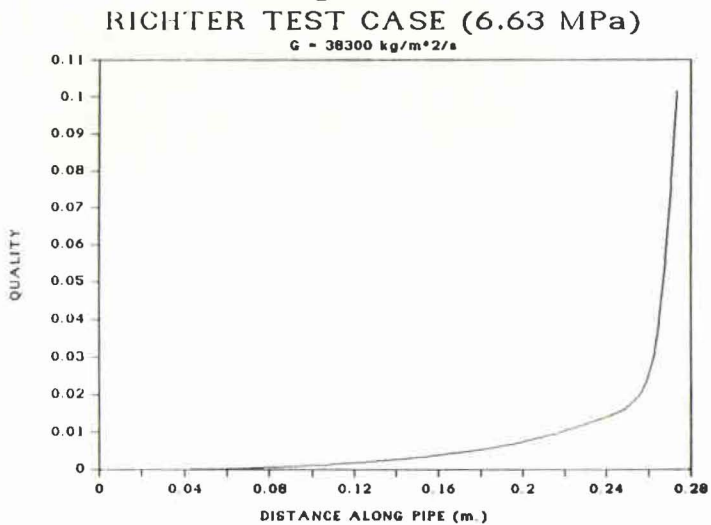


Fig. 5.24(d): Richter Simulation 6.63 MPa: Quality:

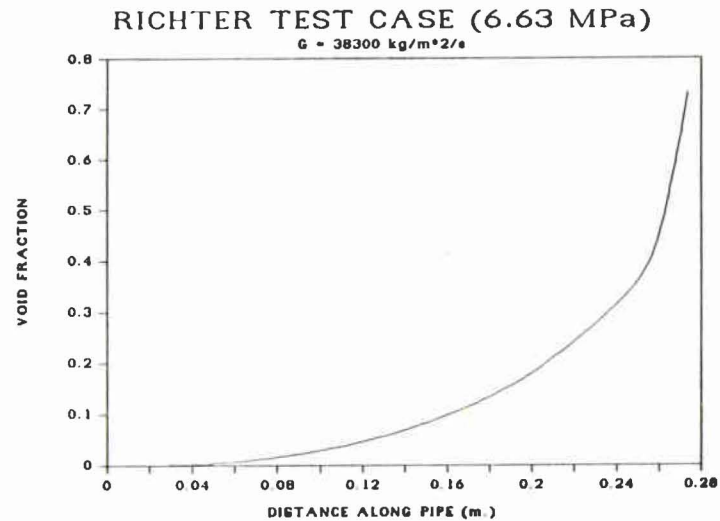


Fig. 5.24(e): Richter Simulation 6.63 MPa: Void Fraction:

5.2.4 Celata et al. Orifice Data:

Data by Celata et al. (1983) was from very small orifices with a very small length to exit diameter ratio of approximately .8. As with Dobran's data, exact geometry could not be found, but in this case a good estimate was made from a diagram in the literature. The orifice was essentially a rounded hole in a cap with a diameter of .00125 m. and a length of .001 m. In the experiments, a so-called metastable region of flow formed just after the exit and extended out about .002 m. before the flow began to expand radially. This was noted in all test cases.

An attempt was made to simulate the orifice for the .950 MPa case which had an experimental critical mass flux of 28485 kg/m²/s. The simulated mass flux estimate was 51000 kg/m²/s which is unsatisfactory. A second run was made with the orifice geometry modified to include a straight section of simulated pipe approximately .002 m. in length. Due to the very high mass flow rates and the extremely small diameter of the orifice, it was postulated that the distance taken for the pressure inside the extended jet to equalize with atmospheric pressure would be on the order of 2 mm, i.e. the depressurization wave would take a certain period to reach the center of the flow. In that time the flow would move a certain distance. In other words, the flow is literally under pressure for an extended distance. In most experimental cases this would not amount to any significant distance, but, in the orifice test cases it does. Using this new geometry, the mass flux estimate was 31000 kg/m²/s which is within less than 10% error. Although this is an unusual case, it

does demonstrate the utility of the general model for the prediction of mass fluxes for very small length to diameter ratios.

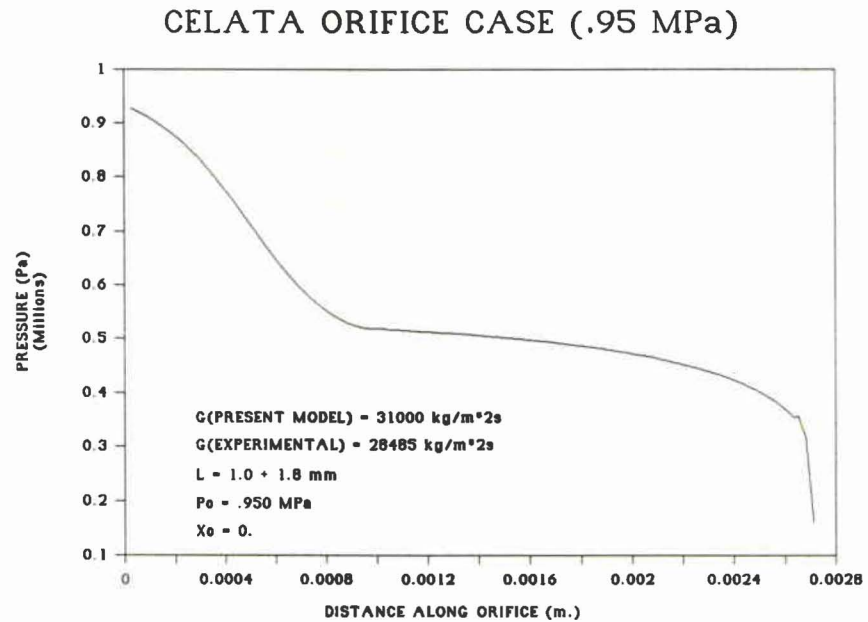


**Fig. 5.25(a): Celata Orifice Simulation .950 MPa:
Pressure:**

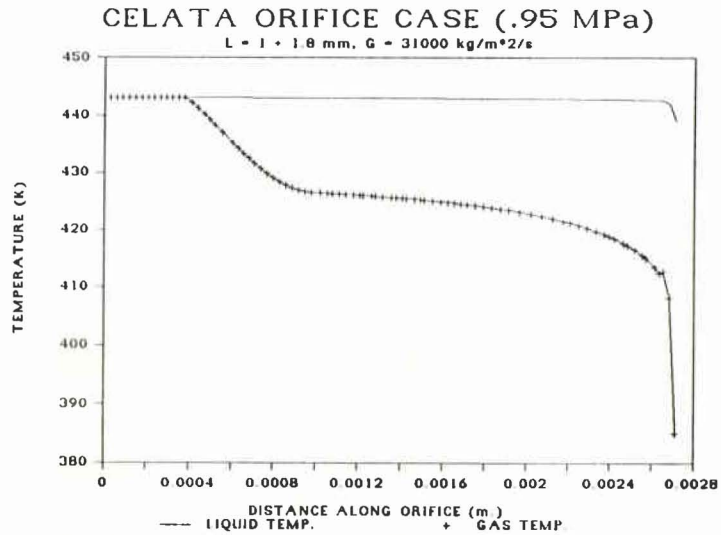


Fig. 5.25(b): Celata Simulation .950 MPa: Temperature:

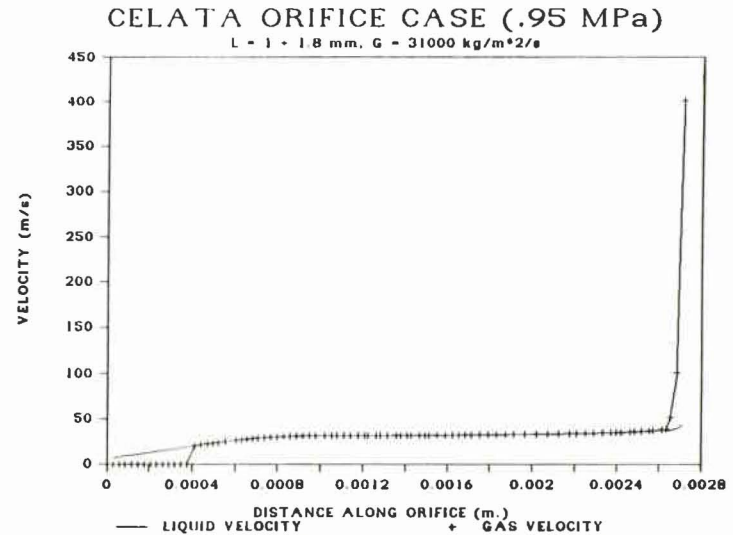


Fig. 5.25(c): Celata Simulation .950 MPa: Velocity:

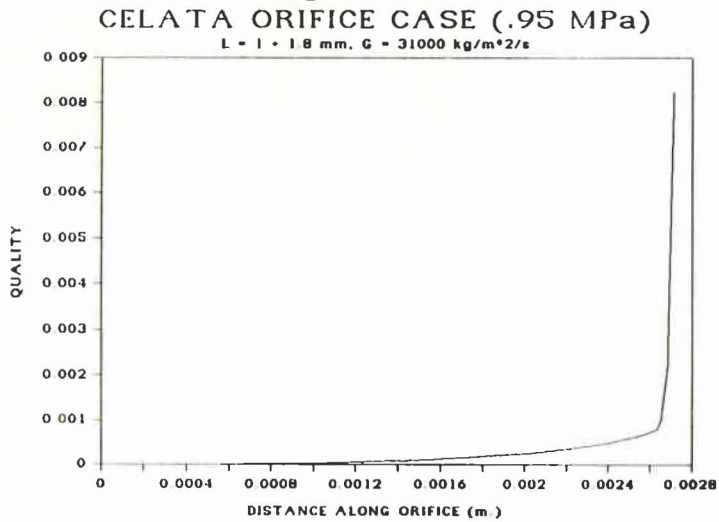


Fig. 5.25(d): Celata Simulation .950 MPa: Quality:

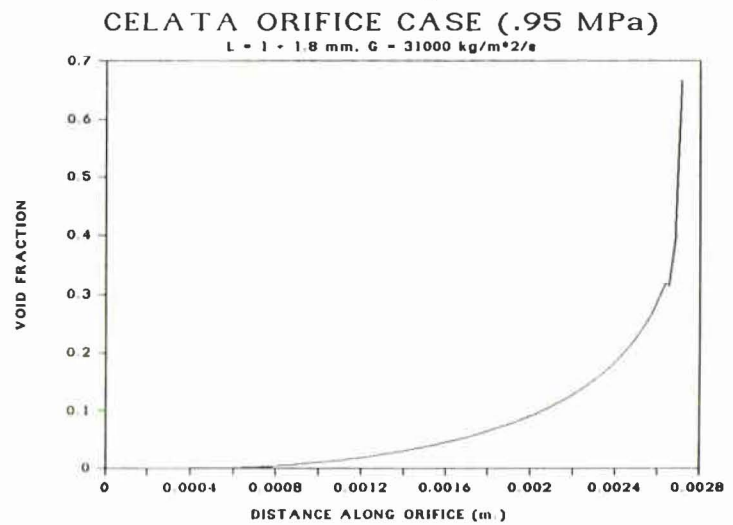


Fig. 5.25(e): Celata Simulation .950 MPa: Void Fraction:

5.2.5 Mass Flux Data:

The mass flux data is largely the most important result from a calculation. Although the other primary variables are of interest, only the mass flux would be needed for computation in most applications. A table of the simulation results is shown below:

Table 5.3: Chart of Mass Flux Data:

<u>PRESS.</u> (MPa)	<u>EXP. MASS</u> <u>FLUX</u> (kg/m ² s)	<u>SOURCE</u>	<u>THEOR. MASS</u> <u>FLUX</u> (kg/m ² s)	<u>% ERROR</u>
.196	2426	AL-SAHAN	2240	-7.7
.300	2943	AL-SAHAN	2675	-9.1
.479	3364	AL-SAHAN	3380	.48
.703	4205	AL-SAHAN	4400	4.6
.950	28485	CELATA	31000	8.9
1.00	5175	AL-SAHAN	5700	10.1
2.23	11155	DOBRAN	11160	.05
2.58	9080	DOBRAN	9780	7.7
3.49	10090	DOBRAN	12100	19.9
6.63	33930	RICHTER	38300	12.8

With one exception, the error varies from -9% to +14%. Considering the range of data points and the fact that no parameter was used to fit the data, the results are impressive. An interesting observation was that the model tends to overpredict for higher pressures and underpredict for lower pressures. This is an almost linear trend and can be seen in the plot of the data (Fig. 5.26).

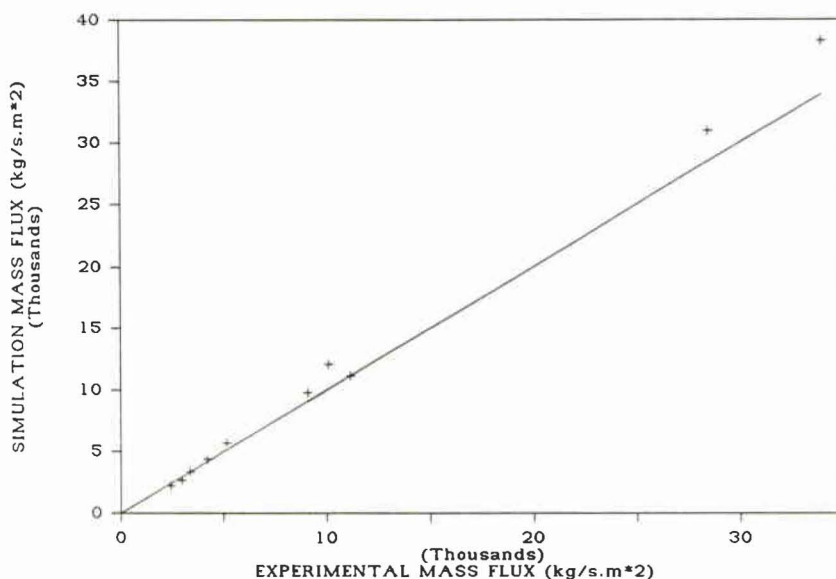


Fig. 5.26: Comparison of Experimental Data:

If more data points were used, it is possible that a corrector might be found but this defeats the reason for holding the initial nucleation values constant. The only parameters that can readily affect the simulation are N , d_0 and the flow regime transition points. Basically, the situation in nucleation theory is that; if one knows one of N , d_0 and pressure difference due to surface tension, one can guess a second to calculate the third. There does not seem to be any correlation interrelating the three with the possible exception of Al-Sahan's empirical curve fit. The most logical choice, therefore, is to use the flow regime transition points according to relative phase velocities. Only one flow regime map has a theoretical basis so that it can be used for different fluids. This work by Taitel and Dukler (1976) does not have sufficient accuracy to be of use particularly at the churn to annular flow transition equation which is not clearly defined.

Because the transition from bubble flow is generally accepted at a void fraction of .3, the use of the map would not likely result in any major benefits.

CHAPTER 6

CONCLUSIONS

The primary conclusions are:

1. A study of a general two fluid model for critical flow has been performed and recommendations as to the best available forms of the equations, terms, and correlations have been made. These include:

- the use of the full vapour energy conservation equation rather than an energy balance at the interface;

- the use of a seventh dependent equation to calculate bubble diameter from changes in void fraction and quality and a variable bubble number density;

- the use of full interfacial momentum transfer terms with transfer and sinks;

- the use in the churn flow regime of linear interpolation for interfacial area, exponential interpolation for the interfacial drag coefficient and for the heat transfer parameter used to calculate the heat transfer coefficient;

In general, continuous forms of the parameters are preferable for the mathematical stability of the calculations even if not strictly adhering to empirical correlations.

2. The comparison of simulations produced by this model against experimental data points shows generally good agreement considering the range of data checked and the fact that no empirical parameter was used to fit the data. The mass flux values, with one exception, are within $\pm 13\%$ of the experimental values.

CHAPTER 7
FUTURE WORK

There is considerable work that can be done to improve the model. Correlations for churn flow are needed for the three interfacial variables. The virtual mass term needs to have more clearly accepted forms for its constants and the initial bubble diameter and density must be experimentally checked further as there is almost no data on the subject. Two dimensional effects such as void fraction and velocity distribution need to be quantified as well.

CHAPTER 8
BIBLIOGRAPHY

Abdollahian, D., Healzer, J., Janssen, E., Amos, C.,
"Critical-Flow Data Review and Analysis", EPRI Report
NP-2192, 1982

Al-Sahan, M. A., "On the Development of the Flow Regimes and
the Formulation of a Mechanistic Non-Equilibrium Model for
Critical Two-Phase Flow", PhD Thesis, University of Toronto,
1988

Ardron, K. H., Furness, R. A., "A Study of the Critical Flow
Models Used in Reactor Blowdown Analysis", Nucl. Eng. and
Design, Vol. 39, pp 257-266, 1976

Ardron, K. H., Ackerman., M. C., "Studies of the Critical
Flow of Subcooled Water in a Pipe", CSNI Specialist Meeting
on Transient Two-Phase Flow, Paris, 1978

Banerjee, S., Chan, A. M. C., "Separated Flow Models -I:
Analysis of the Averaged Local Instantaneous Formulations",
Int. J. Multiphase Flow, Vol. 6, pp 1-24, 1980

Bergles, A. E., Collier, J. G., Delhaye, J. M., Hewitt, G.
F., Mayinger, F., Two-Phase Flow and Heat Transfer in the
Power and Process Industries, Hemisphere Pub. Corp., London,
1981

Bilicki, Z., Kestin, J., "Two-Phase Flow in a Vertical Pipe
and the Phenomenon of Choking: Homogeneous Diffusion Model
I", Int. J. Multiphase Flow, Vol. 9, pp 269-288, 1983

Bouré, J. A., "On a Unified Presentation of the Non-Equilibrium Two-Phase Flow Models", The Winter Meeting of the ASME, Houston, pp 1-9, 1975

Carey, G. F., Oden, J. T., Finite Elements: Computational Aspects, Vol. 3, Prentice-Hall, New Jersey, 1984

Celata, G. P., Cumo, M., Farello, G. E., Incalterra, G. C., Naviglio, A., "Thermodynamic Disequilibrium in the Critical Flow of Subcooled Liquids", Nucl. Tech., Vol. 60, pp 137-142, 1983

Chang, J. S., Donveski, B., Groenveld, D. C., "Examination of Correlations for Interfacial Parameter in the Bubbly, Slug and Churn Flow Regimes", To be published, 1988

Collier, J. G., Convective Boiling and Condensation, McGraw Hill, Toronto, 1972

Collins, R. L., "Choked Expansion of Subcooled Water and the I.H.E. Flow Model", J. Heat Transfer, Vol. 100, pp 275-280, 1978

Cook, T. L., Harlow, F. H., "Virtual Mass in Multiphase Flow", Int. J. Multiphase Flow, Vol. 6, pp 691-696, 1984

Dobran, F., "Non-Equilibrium Modelling of Two-Phase Critical Flow in Tubes", J. Heat Transfer, Vol. 109, pp 731-738, 1987

Dostie, M., Mercadier, Y., "Choking Criteria for One-Dimensional Critical Multiphase Flow in Ducts and Open Channels", 13th Annual Reactor Simulation Symposium, CNS and AECL, pp 50-68, 1987

Drew, D., Cheng, L., Lahey, R. T. Jr., "The Analysis of Virtual Mass Effects in Two-Phase Flow", Int. J. Multiphase Flow, Vol. 5, pp 233-242, 1979

Edwards, A. R., "Conduction Controlled Flashing of a Fluid and the Prediction of Critical Flow Rates in a One-Dimensional System", United Kingdom Atomic Energy Authority Report AHSB (S) r147, 1968

Elias, E., Chambré, P. L., "A Mechanistic Non-Equilibrium Model for Two-Phase Critical Flow", Int. J. Multiphase Flow, Vol. 10, pp 21-40, 1984

Fauske, H., "Critical Two-Phase, Steam-Water Flows", Proc. Heat Transfer and Fluid Mechanics Institute, Stanford Univ. Press, pp 79-89, 1961

Fauske, H., "Contribution to the Theory of Two-Phase, One-Component Critical Flow", ANL-6633, 1962

Gerald, C. F., Applied Numerical Analysis, Addison-Wesley, Massachusetts, 1980

Henry, R. E., Fauske, H. K., McComas, S. T., "Two-Phase Critical Flow at Low Qualities, Parts I and II", Nucl. Sci. and Eng., Vol. 41 pp 79-98, 1970(a)

Henry, R. E., "The Two-Phase Critical Discharge of Initially Saturated or Subcooled Liquids", Nucl. Sci. and Eng., Vol. 41, pp 336-342, 1970(b)

Henry, R. E., Fauske, H. K., "The Two-Phase Critical Flow of One-Component Mixtures in Nozzles, Orifices and Short Tubes", J. Heat Transfer, Vol. 93, pp 179-187, 1971

Henry, R. E., "Calculational Techniques for Two-Phase Critical Flow", EPRI Workshop on Basic Two-Phase Flow Modelling, Tampa, pp 415-435, 1979

Hirt, C. W., Romero, N. C., "Application of a Drift-Flux Model to Flashing in Straight Pipes", LA-6005-MS, NR-DRSK-001, 1975

Hsu, Y., Graham, R. W., Transport Processes in Boiling and Two-Phase Systems, McGraw Hill, Toronto, 1976

Hutcherson, M. N., Henry, R. E., Wollersheim, D. E., "Two-Phase Vessel Blowdown of an Initially Saturated Liquid Part I: Experimental", J. Heat Transfer, Vol. 105, pp 687-699, 1983

Isbin, H., "Some Observations on the Status of Two-Phase Critical Flow Models", Int. J. Multiphase Flow, Vol. 6, pp 1-24, 1980

Ishii, M., Thermo-Fluid Dynamic Theory of Two-Phase Flow, Eyrolles, Paris, 1975

Ishii, M., Chawla, T. C., "Local Drag Laws in Dispersed Two-Phase Flow", NUREG/CR-1230 and ANL-179-105, 1979

Ishii, M., Zuber, N., "Drag Coefficient and Relative Velocity in Bubbly, Droplet, or Particulate Flows", AIChE J., Vol. 25, pp 843-855, 1979

Jackson, R., Davidson, B. J., "An Equation Set for Non-Equilibrium Two-Phase Flow and an Analysis of Some

Aspects of Choking, Acoustic Propagation and Losses in Low Pressure Wet Steam", Int. J. Multiphase Flow, Vol. 9, pp 491-450, 1983

Kazimi, M. S., No, H. C., "On the Formulation of the Virtual Mass Term in Two Fluid Models", Nucl. Eng. and Design, Vol. 95, pp 163-170, 1986

Kelly, J. E., Kazimi, M. S., "Interfacial Exchange Relations for Two-Fluid Vapour-Liquid Flow: A simplified Regime-Map Approach", Nucl. Science and Eng., Vol. 81, pp 305-318, 1982

Kroeger, P. G., "Application of a Non-Equilibrium Drift Flux Model to Two-Phase Blowdown Experiments", BNL-NUREG-21506-R, 1976

Lahey, R. T. Jr., Cheng, L. Y., Drew, D. A., Flaherty, J. E., "The Effect of Virtual Mass on Numerical Stability of Accelerating Two-Phase Flows", Int. J. Multiphase Flow, Vol. 6, pp 281-294, 1979

Levy, S., "Prediction of Two-Phase Critical Flow Rate", J. Heat Transfer, Trans. ASME, Vol. 87, pp 53-58, 1965

Lyczkowski, R. W., Gidaspow, D., Solbrig, C. W., Hughes, E. D., "Characteristics and Stability Analyses of Transient One-Dimensional Two-Phase Flow Equations and Their Finite Difference Approximations", Nucl. Science and Eng., Vol. 66, pp 378-396, 1978

Malnes, D, "Critical Two-Phase Flow Based on Non-Equilibrium Effects", The Winter Annual Meeting of the ASME, Houston Texas, pp 11-17, 1975

Miller, R. S., "Photographic Observations of Bubble Formation in Flashing Nozzle Flow", J. Heat Transfer, Vol. 107, pp 750-755, 1985

Moody, F. J., "Maximum Flow Rate of a Single Component Two-Phase Mixture", J. Heat Transfer, Trans. ASME, Vol. 86, pp 134-143, 1965

Moody, F. J., "Maximum Two-Phase Vessel Blowdown from Pipes", J. Heat Transfer, Trans. ASME, Vol. 87, pp 285-295, 1966

Moody, F. J., "Maximum Discharge Rate of Liquid-Vapour Mixtures from Vessels", ASME Symposium on Non-Equilibrium Two-Phase Flows, R. T. Lahey and G. B. Wallis Ed. pp 27-36, 1975

No, H. C., Kazimi, M. S., "Effects of Virtual Mass on the Mathematical Characteristics and Numerical Stability of the Two-Fluid Model", Nucl. Science and Eng., Vol. 89, pp 197-206, 1985

Plesset, H. S., Zwick, S. A., "The Growth of Vapour Bubbles in Superheated Liquids", J. Applied Physics, Vol. 25, pp 493-500, 1954

Reocreux, M. L., "Experimental Study of Steam-Water Choked Flow", Proc. of CSNI Specialists Meeting, Toronto, 1976

Richter, H. J., "Separated Two-Phase Flow Model: Application to Critical Two-Phase Flow", EPRI Report NP-1800, 1981

Richter, H. J., "Separated Two-Phase Flow Model: Application to Critical Two-Phase Flow", Int. J. Multiphase Flow, Vol. 9, pp 511-530, 1983

Rivard, W. C., Torrey, M. B., "Numerical Calculation of Flashing from Long Pipes Using a Two-Field Model", LA-NUREG-6330-MS, 1975

Rivard, W. C., Torrey, M. B., "K-FIX: A Computer Program for Transient Two-Dimensional Two-Fluid Flow", LA-NUREG-6623 NRC-4, 1976

Rohatgi, V. S., Reshotko, E., "Non-Equilibrium One-Dimensional Two-Phase Flow in Variable Area Channels", The Winter Meeting of the ASME, Houston, Texas, pp 47-54, 1975

Rowe, P. N., Henwood, C. A., "Drag Forces in a Hydraulic Model of a Fluidized Bed, Part I", Trans. Inst. of Chem. Eng., Vol. 39, pp 43-54, 1961

Saha, P., "A Review of Two-Phase Steam-Water Critical Flow Models with Emphasis on Thermal Non-Equilibrium", NUREG/CR-0417, 1978

Shoukri, M., Judd, R. L., "Nucleation Site Activation in Saturated Boiling", J. Heat Transfer, Vol. 97, pp 1-6, 1975

Solbrig, C. W., McFadden, J. H., Lyczkowski, R. W., Hughes, E. D., "Heat Transfer and Friction Correlations Required to Describe Steam-Water Behavior in Nuclear Safety Studies", AIChE Symposium Series, Vol. 174, pp 100-128, 1978

Sozzi, G. L., Sutherland, W. A., "Critical Flow of Saturated and Subcooled Water at High Pressure", The Winter Meeting of the ASME, Houston, Texas, pp 19-25, 1975

Streeter, V., Wylie, E., Fluid Mechanics, McGraw Hill, New York, 1979

Taitel, Y., Dukler., A. E., "A Model for Predicting Flow Regime Transitions in Horizontal and Near Horizontal Gas-Liquid Flow", AIChE Symposium Series No. 174, Vol. 77, pp 83-91, 1976

Trapp, J. A., Ransom, V. H., "A Choked-Flow Calculations Criterion for Non-Homogeneous Non-Equilibrium Two-Phase Flows", Int. J. Multiphase Flow, Vol. 8, pp 669-681, 1982

Travis, J. R., Hirt, C. W., Rivard, W. C., "Multidimensional Effects in Critical Two-Phase Flow", Nucl. Science and Eng., Vol. 68, pp 338-348, 1978

Wallis, G. B., One-Dimensional Two-Phase Flow, McGraw Hill, Toronto, 1969

Wallis, G. B., "Critical Two-Phase Flow", Int. J. Multiphase Flow, Vol. 6, pp 97-112, 1980

CHAPTER 9
APPENDIX A
DEVELOPMENT STAGES

The final form of this model was quite different from the starting point and there are some observations relevant to the development of future models. Initially, the program consisted of several of the simple models used to calculate and produce plots of mass flux versus pressure with constant stagnation quality or stagnation quality with constant stagnation pressure. The models used were the HEM, the Fauske slip model, the Moody slip model and the various forms of the Henry-Fauske model for different entrance geometries and lengths.

This program allowed one to gain an understanding and insight into critical flow simulation and the importance of several computational errors, the most significant of which was the necessary use of very high accuracy correlations for the thermodynamic properties. The problem can be reduced to the fact that, for low qualities, the model equations magnify greatly the error in the thermodynamic properties. The original correlations used had error in the range of $\pm 5\%$. This relatively small error could be enlarged to the point of producing negative square roots. More advanced correlations developed by K. Kanavan at Ontario Hydro, based on the International Steam Tables and the Helmholtz potential with an accuracy of better than $.01\%$, were incorporated and the numerical error decreased dramatically. The comparison of the worst case follows:

Fig. A.1: Comparison of Errors in Simple Model Calculations

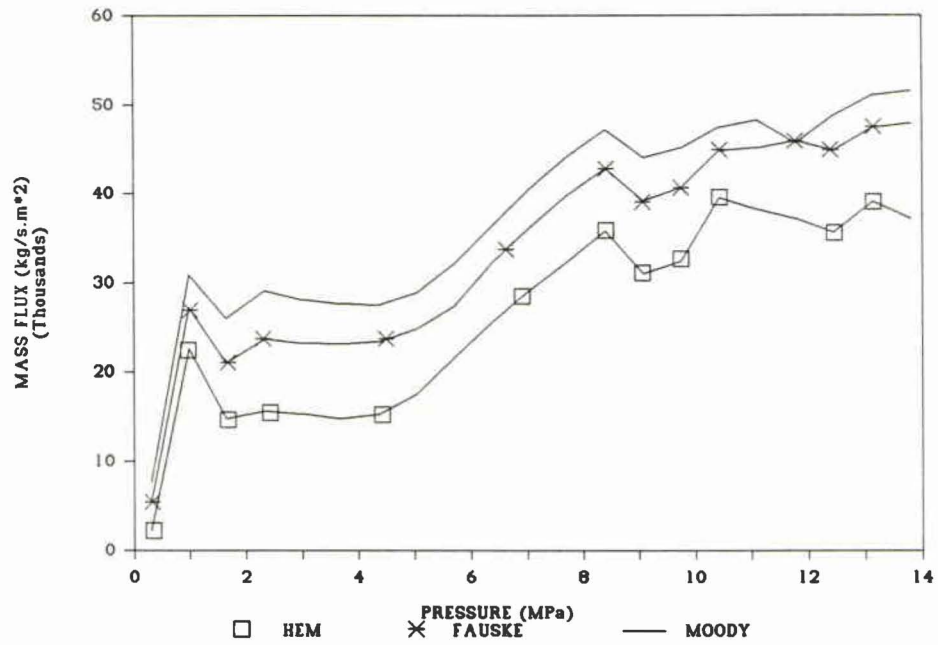


Fig. A.1 (a): Simple Property Correlations:

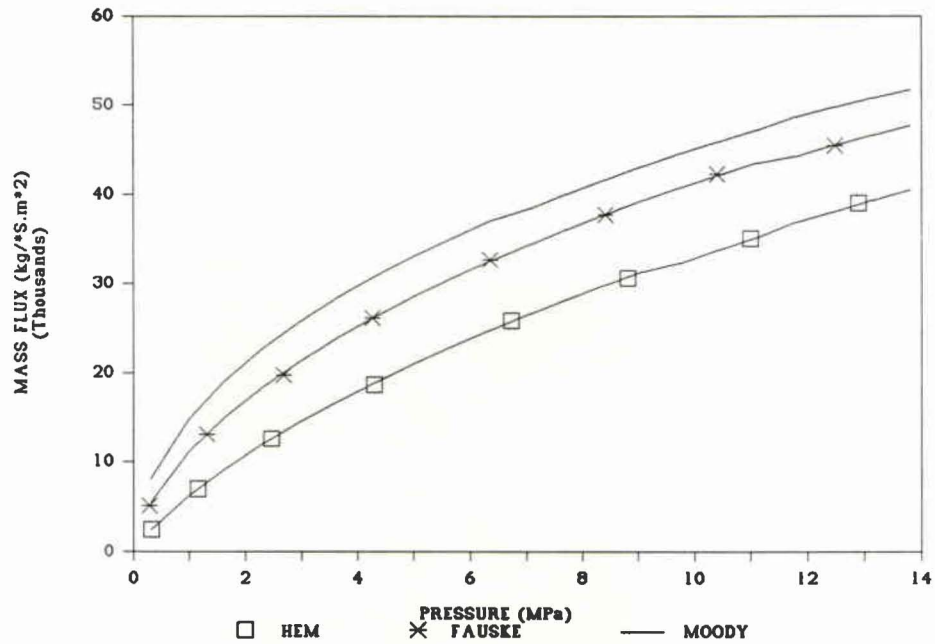


Fig. A.1 (b): Kanavan Property Correlations:

This demonstrates very effectively that, at least for the simple models with subtraction of two similar quantities, high accuracy property calculation subroutines should be used.

The next model to be implemented in a program was the Richter model. Originally the intention was to combine the five models together in one program and use it for predicting experimental results with the five models producing a range of predicted mass fluxes. Since the model was a full two fluid code, it gave valuable experience in understanding the intricacies and limitations of the existing models. Again thermodynamic properties caused much in the way of problems. It is important to note a few of these. The first problem of major importance was the ability of the correlations to predict properties in the superheated liquid range. This is crucial to the assumption of thermodynamic non-equilibrium. Devising a program in which the liquid is intended to be above saturation temperature, using the values at saturation simply will not work. Secondly, a rather important assumption is that the properties of the gas are at saturation and that the derivative of specific volume with respect to distance can be calculated using the derivative of specific volume with respect to pressure at saturation:

$$\frac{\partial v_c}{\partial z} = \left(\frac{\partial v_c}{\partial P} \right)_{sat} \left(\frac{\partial P}{\partial z} \right) \quad (A.1)$$

This is fine for the gaseous phase and for the liquid, the derivative of enthalpy is handled directly as a variable and transformed to a derivative of liquid temperature. There is, however, a term for which this is not the case. The derivative of specific volume of the liquid with respect to distance is required. In order to approximate this, since

the liquid is not at saturation, the same simplification that was used for the gas is used. The derivative must be at saturation. If it is calculated from superheated volumes, the result is an initially small but steady error which, although mathematically not an error, makes the results physically meaningless. The question is then, for saturation to be used, which quantity temperature or pressure is used to determine saturation point. If the saturation temperature corresponding to the pressure is used, the results are unstable. The only stable solution occurs when the saturation pressure corresponding to the superheated temperature is the state utilized. This effect was noted only in the final model but has a profound effect on the stability of the calculations.

After a final working, somewhat correct version of the Richter model had been debugged, the decision to examine the effects of the various parameters in the general one dimensional model was made.

Some research has been done on the simulation of behavior of a liquid in a depressurized tank including investigation of the foaming phenomenon and prediction of void fraction at the entrance to the outlet pipe configuration. It was hoped that a combined program using the model, a relatively simple tank model and system geometry input section will in the future be developed to provide a packaged program to simulate emergency relief valve systems in the chemical industry and header LOCA's in CANDU reactor design.

CHAPTER 10
APPENDIX B:
TEST SECTION GEOMETRY

The various pipe geometries for the different experiments are shown here. Accurate cross sectional profiles are crucial to program simulation and the accuracy of the mass flux results. As an example, a rounded entrance produces a significant change in the simulation results even if it only affects a length portion of one diameter out of a total length of almost three hundred diameters.

10.1 Al-Sahan Pipe Geometry:

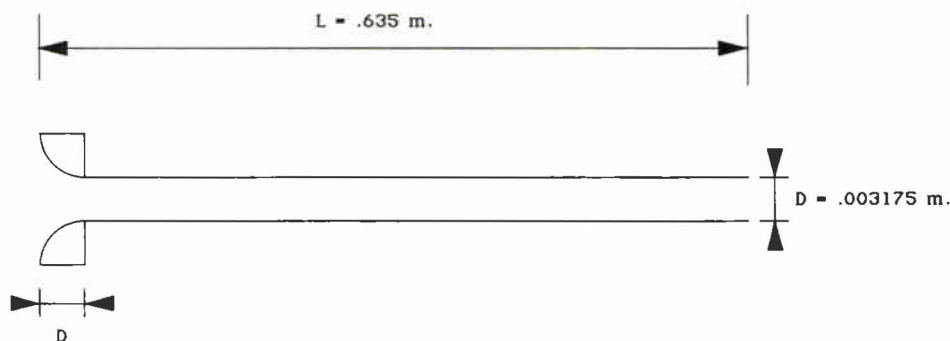
The configuration of the experimental apparatus was the same for all the tests. It consisted of a stainless steel pipe with diameter .003175 m. and length .635 m. It was modelled as perfectly straight with constant cross section.

Inlet conditions were stagnation pressures from .196 to 1.00 MPa at saturation with zero quality. The measured quantities included experimental and predicted critical mass flux and both experimental axial pressure distribution and theoretical pressure profile from Al-Sahan's model. Table B.1 shows mass flux data and Figure B.1 shows the pipe geometry.

Table B.1: Al-Sahan Test Mass Flux Data:

<u>PRESSURE</u> (MPa)	<u>EXP. MASS</u> <u>FLUX</u> (kg/m ² s)	<u>AL-SAHAN</u> <u>MASS FLUX</u> (kg/m ² s)	<u>THIS MODEL</u> <u>MASS FLUX</u> (kg/m ² s)
.196	2426	2425	2240
.300	2943	2810	2675
.479	3364	3364	3380
.703	4205	4205	4400
1.00	5175	5175	5700

SKETCH OF AL-SAHAN EXPERIMENTAL GEOMETRY



ROUNDED ENTRANCE WITH RADIUS OF CURVATURE EQUAL TO DIAMETER
 STRAIGHT LENGTH OF PIPE AFTER ENTRANCE (CONSTANT DIAMETER)

Fig. B.1: Al-Sahan Test Section Geometry:**10.2 Dobran Pipe Geometry:**

The exact Dobran test geometry was very difficult to determine. The original data had been published by Celata et al. at a conference but only the abstract was available. The geometry was indicated to be a straight pipe with rounded entrance. Data from two test section lengths was examined (1.21 m. and 3.60 m.). The program assumed a circularly rounded section with quarter round profile with a radius of approximately one diameter and a

straight pipe after that. The fact that the exact geometry was not available may explain some of the inaccuracy in the present model results.

Both experimental critical mass flux and axial pressure distribution were available, as were simulation pressure profiles from Dobran's and Al-Sahan's models which were taken from Al-Sahan's thesis and theoretical mass fluxes from both models from Al-Sahan's thesis and Dobran's paper. The inlet conditions were just at saturation with zero quality and stagnation pressures of 2.23 MPa for the short pipe and 2.58 and 3.49 MPa for the longer test section. Table B.2 shows the mass flux data and lengths and Figure B.2 shows the test section geometries.

Table B.2: Dobran Test Mass Flux Data:

<u>PRESS.</u> (MPa)	<u>LENGTH</u> (m.)	<u>EXP. \underline{G}_C</u>	<u>DOBRAN</u> \underline{G}_C	<u>AL-SAHAN</u> \underline{G}_C	<u>THIS</u> <u>MODEL \underline{G}_C</u>
2.23	1.21	11155	10230	10425	11160
2.58	3.60	9080	9294	8250	9780
3.49	3.60	10090	12234	10060	12100

* Note all mass fluxes in kg/m²s

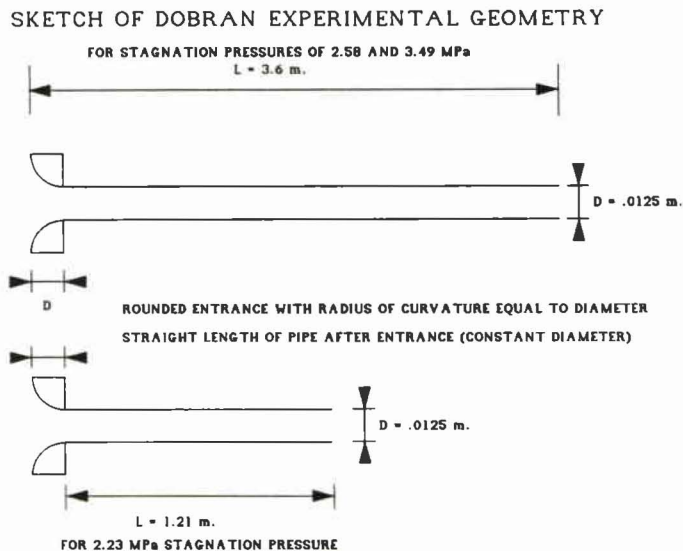


Fig. B.2: Dobran Test Section Geometry:

10.3 Richter Test Case Geometry:

The Richter test case was taken from a paper by Sozzi and Sutherland (1975) with a diagram of the geometry in the Richter report (1981). It consisted of a circularly rounded entrance slightly flattened and a straight section. The total length was .2745 m. and the exit diameter was .0127 m. The cross sectional profile was taken from the Richter simulation program directly (see Figure B.3).

Only a simulation of the axial distribution of the pressure and other primary variables and the experimental and theoretical critical mass fluxes were available. The inlet conditions were slightly subcooled with a stagnation pressure of 6.63 MPa and a temperature of 278.93 C. or 3.22 C. subcooled corresponding to a quality of -0.0004 . The experimental critical mass flux was 33,930 kg/m²s and Richter's model predicted a value of 32,240 kg/m²s and this model predicted a value of 38,300 kg/m²s. Figure B.3 shows the test section geometry.

SKETCH OF SOZZI AND SUTHERLAND EXPERIMENTAL GEOMETRY

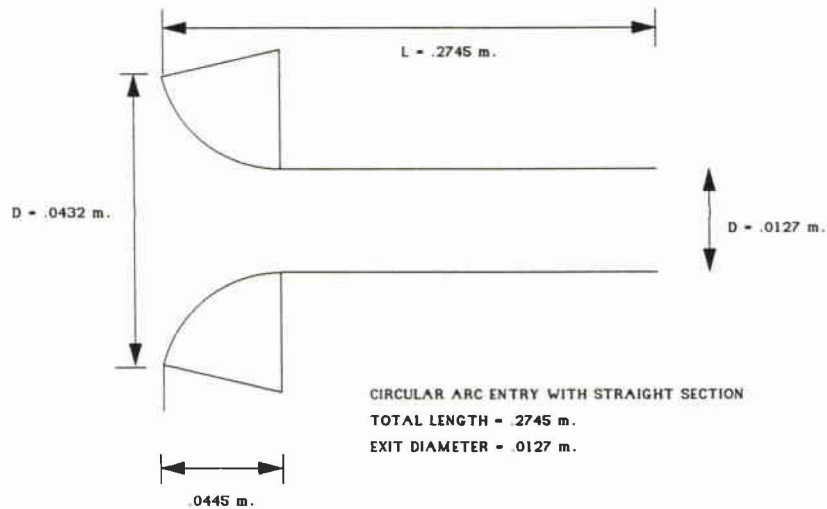
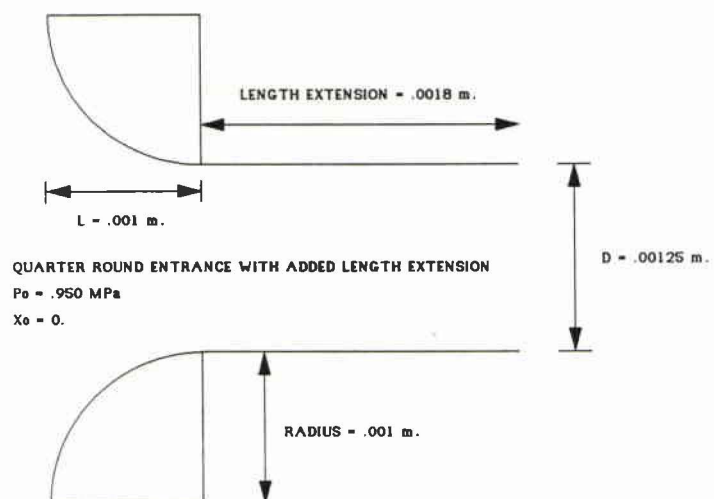


Fig. B.3: Richter Test Section Geometry:

10.4 Celata Experimental Orifice Geometry:

The orifice test case comes from work by Celata et al. (1983). The geometry is described as a rounded entrance orifice with length to exit diameter ratio of .8. In this program, the entrance was modelled as a quarter round profile with radius equal to the length of the orifice (.001 m.). Again an exact cross sectional profile was not given in the paper. The inlet conditions are .950 MPa stagnation pressure and zero quality at saturation. The only data available was for the experimental mass flux of $28485 \text{ kg/m}^2\text{s}$ and experimental data for the length extension of the flow of approximately 1.8 mm. The critical mass flux predicted by this model was $31000 \text{ kg/m}^2\text{s}$. Figure B.4 shows the orifice geometry.

SKETCH OF CELATA ET AL ORIFICE GEOMETRY

**Fig. B.4: Celata Test Section Geometry:**